DEVELOPMENT OF A TWO-DIMENSIONAL STATIC NEUTRONICS MODEL OF THE PEBBLE BED MODULAR REACTOR CORE FOR FLOWNEX

Ramazan Sonat Şen
B.Sc. Eng (Nuclear)

Thesis submitted in partial fulfilment of the requirements for the degree
Magister in Engineering
School of Mechanical and Materials Engineering
at the
North-West University

Supervisor: Professor G.P. Greyvenstein
Co-supervisor: Professor O.K. Kadiroğlu
Potchefstroom, 2005

Abstract

High temperature gas cooled reactors have a special importance in the future of nuclear technology. Due to their high thermal capacity, high burn-up and thermodynamic efficiency, a decrease in the electricity generation cost is expected. New generation high temperature reactors are designed to be inherently safe. The most efficient way of hydrogen production, IS process, requires very high temperatures. Very High Temperature Gas Cooled Reactors (VHTR) of the future are considered as the heat source for hydrogen production.

Two fuel types are used in high temperature reactors, namely pebble and prismatic block fuels. The South African Pebble Bed Modular Reactor (PBMR) is a promising design to be built in the near future. A very important aspect of the design of a High Temperature Gas Cooled Reactor (HTR) is to predict the neutronics of the reactor, as this determines the fission heat release. This thesis deals with the development of a model for the prediction of neutronics behaviour of the PBMR core which will be used in conjunction with a thermal hydraulic code for the design of the PBMR.

Acknowledgements

To Gülru, my wife, thank you for all your love, understanding and patience through very hard times. Thank you for always listening; your loving words and smiles gives me strength.

I would like to thank my supervisors, Professor Gideon Greyvenstein and Professor Osman Kemal Kadiroğlu, for their helpful cooperation and guidance.

I would also like to thank all the members of Hacettepe University Nuclear Engineering Department for allowing me to use their resources.

My fellow post-graduate students and friends, thank you for your help, jokes and lessons we learned from each other. I thank the University for the environment and resources they made available to help us further our studies.

Ramazan Sonat Şen

Table of Contents

List of Figures

List of Tables

List of Acronyms

AVR	Arbeitgemeinschaft Verscuhsreaktor
DLOFC	Depressurized Loss of Forced Cooling
ENDF	Evaluated Nuclear Data File
ENDL	Evaluated Nuclear Data Library
GT-MHR	Gas Turbine Modular High Temperature Reactor
HTR	High Temperature Gas Cooled Reactor
HTTR	High Temperature Test Reactor
JENDL	Japanese Evaluated Nuclear Data Library
LWR	Light Water Reactor
MCNP	Monte Carlo N-Particle Transport Code
MEDUL	Multiple Recycling
MGC	Macroscopic Group Constant
MGD	Multigroup Diffusion
MHTR	Modular High Temperature Reactor
MOCCA	Modular Core Calculation
NR	Narrow Resonance
NRIM	Narrow Resonance Infinite Mass
ORNL	Oak Ridge National Laboratory
OTTO	Once Through Then Out
PBMR	Pebble Bed modular Reactor
SCALE	Standardised Computer Analysis for Licensing Evaluation
THTR	Thorium High Temperature Reactor
VSOP	Very Superior Old Programs

List of Symbols

Roman Letters (Lower Case)

Symbol	Units	Description
k	-	Reactor multiplication factor
m	kg	Mass
r	-	Space coordinate
t	s	Time
v	m/s	Velocity

Roman Letters (Upper Case)

Symbol	Units	Description
B	-	Buckling
D	-	Diffusion coefficient
E	eV	Energy
G	-	Total number of energy groups
J	n/cm^2s	Neutron current
N	$\#/cm^3$	Number density
S	#	Neutron source
T	K	Temperature
E_0	eV	Resonance energy

Subscripts and Superscripts

Symbol	Description
a	absorption
f	fission
g	number of group
s	scattering
t	total
tr	transport
R	removal

Greek Letters

Symbol	Units	Description
α	-	Alpha particle
χ	-	Fission spectrum
ϕ	n/cm^2s	Scalar neutron flux
γ	-	Gamma particle
Γ_γ	-	Natural line width
Γ_n	-	Natural line width for resonance scattering

Γ_p	-	Natural line width for potential scattering
ν	#	Average number of neutrons released in a fission reaction
Ω	-	Unit vector in the direction of the neutron motion
ψ	-	Shape function
σ	barn	Microscopic cross-section
Σ	cm^{-1}	Macroscopic cross-section
σ_0	barn	Total cross-section at the resonance energy for the unbroadened cross-section

Chapter 1. Introduction

1.1. Introduction

Approximately 93.5 percent of South Africa's electricity is produced by coal-fired power plants. An additional 4.5 percent is provided by a large nuclear power plant with two reactors at Koeberg near Cape Town. The percentage of hydroelectric power generation is only 1.5% and there are no more economic hydro sites in South Africa that could be developed to deliver significant amounts of power. In addition, because the natural gas resources of South Africa are limited, natural gas is not a viable option for power generation on a large scale (PBMR, 2003).

South Africa can produce cheap electricity from coal due to abundant resources. Coal rich areas are located far from the densely populated and industrial areas where the electricity load is high; therefore long power lines are needed to transport power. This results in high capital and transportation cost as well as high transmission losses.

The electricity demand in the mornings and evenings significantly increases due to cooking and hot water requirements. In addition to daily electricity demand fluctuations, short, sharp electricity demand peaks occur during winter, which are difficult to accommodate with the existing large thermal power stations since there is no heating source other than electricity.

Although the demand for power in South Africa is currently lower than the capacity, the predictions for the growth in the electricity demand show that it will be necessary to add new power plants to the current capacity in the near future. In addition to electricity demand growth, ESKOM's older power stations will reach the end of their design lives after 2025 (PBMR, 2003). South Africa will need to access and use all its natural resources to produce the additional demand for electricity that it will need by 2025. Therefore ESKOM has to look at new power generation options to provide the future electricity demand. These options include nuclear and renewable energy sources.

Renewable energy systems use resources that are constantly replaced and are usually less polluting. Examples of renewable energy systems include solar, wind, and geothermal energy (getting energy from the heat in the earth). Renewable energy systems can be considered as non-continuous electricity production systems, since they need wind or sun light to produce electricity. Therefore they can not be the only source to cover the electricity demand for future

but they can be used in conjunction with other sources.

Nuclear power plants convert fission energy to electricity. The conventional nuclear power plants are relatively large in terms of energy capacity which brings a large increment to the overall capacity. Furthermore, due to their high capital cost and long construction period, these power plants do not meet the requirements of South Africa.

A new concept that has received increasing attention in the past 30 years and which is currently being investigated by ESKOM, is the High Temperature Gas Cooled Reactor (HTR). Due to their relatively small size of about $300MW_{th}$, HTRs are characterised as inherently safe, modular reactors. Higher power can be realised by several, parallel working modular reactors on site. HTRs have relatively low capital cost of \$1000/kW installed capacity and a short construction period of 24 months. This reduces financing costs, thus improving the overall generation cost of approximately 25 ¢/kWh (PBMR, 2003).

The modular concept and inherently safe character has many advantages when compared to large thermal or nuclear power plants. They can be placed near to the areas of demand since their emergency planning zone is small. They have fast load following capability and they can be added to current capacity with small increments which means addition or subtraction of one power station will not affect the grid to the same extent as in the case of large power stations.

For these reasons ESKOM decided to develop a prototype HTR known as a Pebble Bed Modular Reactor (PBMR). The PBMR concept has short construction period, low operating cost and fast load following capabilities. The fundamental concept of the design of the PBMR is aimed at achieving a plant that has no physical process that could cause radiation-induced hazards outside the site boundary. The reactor core is elongated and the volume-to-surface ratio is much lower than the minimum leakage rate cores. Increasing the surface of the core is not good for neutron economy but it must be done to make the reactor inherently safe. The inherently safe feature is achieved in the PBMR by demonstrating that the integrated heat loss from the reactor vessel exceeds the decay heat production in the accident condition, and that the peak temperature reached in the core during the transient is below the demonstrated fuel degradation point and far below the temperature at which the physical structure is affected. This is intended to prevent any prospect of a core meltdown accident. Heat removal from the vessel is to be achieved by passive means.

A very important aspect with the design of HTRs is to predict the neutronics of the reactor, as this determines the fission heat release. The neutronics behaviour of an HTR is different than that of water cooled reactors. In HTRs, the fuel design brings a double heterogeneity that has to be taken into account and the coolant does not act as a moderator in the same way as in the case of water cooled reactors.

This thesis deals with the development of a mathematical model for the prediction of neutronics in the PBMR, which will be used in conjunction with a thermal hydraulic code for the design of the PBMR.

1.2. History of High Temperature Gas Cooled Reactors

Natural uranium, graphite moderated reactors were developed in the US during World War II for the conversion of ^{238}U to ^{239}Pu for military purposes. These reactors became the starting point of the nuclear industry in several nations, especially in Great Britain and France, which at the time lacked the facilities for producing the enriched uranium necessary to fuel reactors of the light water type production reactors.

HTRs are very different from the light and heavy water type reactors. The use of helium as coolant and graphite as structural material allows much higher coolant temperature compared to the other types of reactors. The coolant temperature in HTRs varies between 800 and 950 °C and the hot helium can be used directly in a gas turbine to drive an electrical generator, thus eliminating the need for an intermediate steam cycle. There are many advantages to such a system. Gas turbines and their associated cycle components are more compact than comparable steam cycle equipment. The most important advantage of HTRs is their very high thermal efficiencies in the order of 40 to 45 percent, compared to 33 to 38 percent for steam producing nuclear power plants.

Furthermore, the temperature of the rejected heat is so high that this energy can be used itself in a number of practical applications, such as the desalination of seawater (Sen et al., 2003), leading to an overall efficiency of the HTR system as high as 50 percent. Besides producing electricity, the HTR can provide high temperature heat required in many applications, such as gasification of the coal and hydrogen production (Kugeler et al., 2003).

The development of helium cooled high temperature reactors started in Great Britain with the

DRAGON project as a common project of several European countries (Kugeler et al., 2003). At the same time in the United States the development of the HTR with tubular type fuel elements had been initiated with the Peach Bottom Reactor. In Germany HTR technology started with pebble shaped fuel elements and the AVR (Arbeitgemeinschaft Versuchsreaktor) research reactor in 1965. It was operated successfully for 20 years. The THTR (Thorium High Temperature Reactor) were put into operation in 1985. This plant was connected to the grid for only three years before it was shutdown in 1988. Despite all difficulties during construction and start-up of this plant, the design data of the power plant was fully achieved; operation was finished because of financial and political reasons after the accident in Chernobyl (Kugeler et al., 2003). Table 1-1 gives an overview on some data of the HTR plants that have been built and operated until now.

Table 1-1: Overview of HTR Plants which have been built and operated until now (Kugeler et al, 2003: 1-9).

Plant	Thermal Power	Electrical Power	Fuel Element	Site	Operation	Status
AVR	46 MW	15 MW	Pebble shaped fuel elements	Jülich/Germany	1965 - 1988	Decommissioning in preparation
DRAGON	20 MW	-	Tubular fuel elements	Winfrith/Great Britain	1966 - 1975	Safe enclosure
Peach Bottom	115 MW	40 MW	Tubular fuel elements	Susquehanna/ USA	1965 - 1988	Safe enclosure
THTR	750 MW	308 MW	Pebble shaped fuel elements	Schmehausen/ Germany	1985 - 1988	Safe enclosure
Fort St. Vrain	852 MW	342 MW	Block type fuel elements	Platteville/USA	1976 - 1989	Partly decommissioned

The fuel used in a pebble bed reactor (Figure 1-1 and Figure 1-2) is very different from the well-known fuel pellets in Light Water Reactors (LWR). Three layers of pyrolytic carbon, silicon carbon and again pyrolytic carbon protect the fuel itself. The coated particle was one of the main inventions in the development of HTR technology. These very small particles are embedded in graphite and this system allows high operating temperatures. Under normal operating conditions the fuel temperature is about 1300°C and under accident conditions up to 1600°C well below the temperature for release of significant quantities of fission products.

There are two types of fuel elements used in HTR technology: (a) prismatic (block type) fuel elements and (b) spherical fuel elements, which are used in pebble bed type reactors. The design of the fuel elements of the HTRs, regardless of the fuel type, is more complex than the design of fuel elements of the other reactors since the fuel contains coated particles which are embedded

in a graphite matrix.

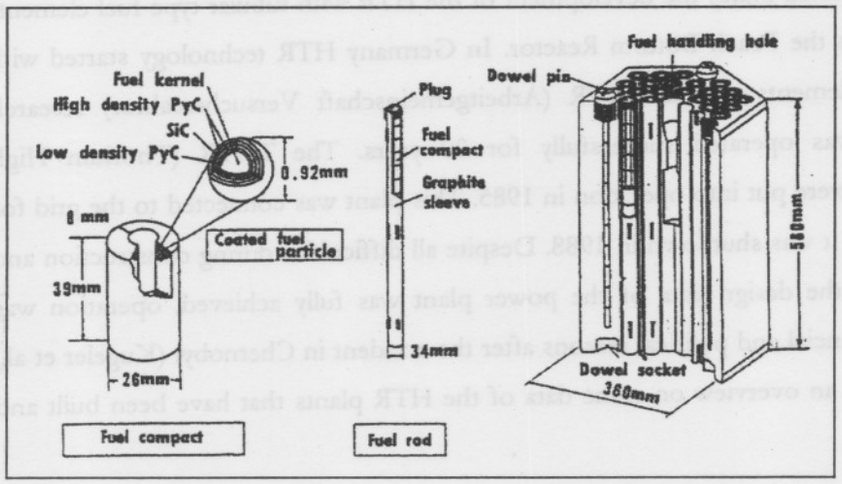

Figure 1-1: Prismatic Fuel Elements (Japanese Design) (Kugeler et al., 2003: 1-2).

In the prismatic or block-type HTR the coated particles are loaded in cylindrical fuel compacts that are inserted in prismatic graphite fuel elements, as shown in Figure 1-1. These elements contain other holes for control rods, flow of coolant gas, and rods with burnable poison. This reactor type has been initiated by the United States, United Kingdom, and more recently by Japan, France and Russia. Predecessors (with tubular fuel) of the prismatic type are the Peach Bottom and Dragon reactors built in the sixties, and decommissioned in the seventies. The next power reactor, Fort St. Vrain, has operated from 1976 to 1989. Recently, in 1998, the Japanese test reactor HTTR reached first criticality. The United States, Russia, Japan and France have joined in a project for weapon-grade plutonium burning in the GT-MHR, based on the conceptual design of the MHTGR.

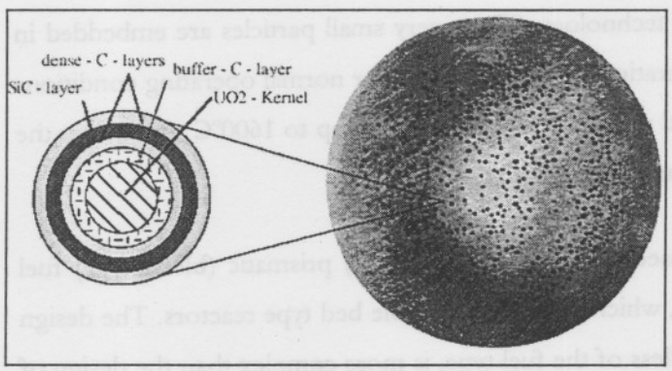

Figure 1-2: Spherical Fuel Elements (Kugeler et al., 2003: 4-1).

In the pebble bed type HTR the coated particles are embedded in spherical graphite elements the size of a tennis ball, as shown in Figure 1-2. Such a pebble typically contains around 15000 coated particles embedded in a graphite matrix of 5 cm diameter. This fuel zone is protected by a layer of graphite, which gives the pebble a total diameter of 6 cm. A randomly packed bed of these spheres in the core cavity of the reactor forms the core. The coolant flows through the bed, normally from top to bottom. Depending on the size of the core, control rods are inserted directly into the bed, or into the reflector encircling the bed. This reactor type has been developed and tested in Germany, first with the AVR test reactor and later with the THTR power reactor. China has a test reactor; South Africa is aiming to build of a series of power reactors, the PBMR, in the near future.

In the last few years HTR technology received significant attention from many scientific and technical organisations around the world. This is due to intrinsic safety characteristics of these reactors. The safety characteristics of HTR, independent from the fuel type (prismatic or spherical), related with the design aspects are as follows:

- no melting of the fuel elements (use of ceramic fuel materials),
- fission product retention in accident conditions (use of coated particles),
- very strong negative temperature coefficient,
- effective and inert coolant medium (use of helium),
- high temperatures of coolant (use of ceramic structural materials in the core),
- low power density,
- self-acting decay heat removal.

Some new concepts of HTR have been developed during the last few years, and some are in the stage of detailed engineering. The modular HTR and HTR-100 have been designed on the basis of AVR technology. China constructed a 10 MW-HTR in 1995 and the reactor has begun operation in 2002. The technology of this reactor is based on the AVR experience. Japan has put into operation a 30 MW HTTR plant achieving first criticality in 1998. This reactor uses a block type tubular fuel element. Together with Russia, France, USA and Japan develop the GAC-600 (GT-MHR), a 600 MW_{th} gas turbine plant, which will be used to burn plutonium.

In 1996 the South African electricity utility, ESKOM, bought the pebble bed reactor technology licence from HTR (a joint of venture of Siemens and ABB) in order to develop HTR technology

into a viable and safe source of power. In PBMR a steel pressure vessel replaced the concrete pressure vessel, and control rods are inserted in the side reflectors instead of the core to prevent the damage to fuel. The annular core design has implemented in the PBMR concept, the fuel elements are inside an annular core which contains a central graphite column as central reflector.

1.3. Prediction of Neutronics Behaviour of a Nuclear Reactor

The design of a reactor core depends on nuclear considerations as much as thermal-fluid considerations. The reason for this is that the design of the core must be done in such a way that it should produce the desired thermal power without exceeding the temperature limitations on core components that might lead to fuel failure.

Such thermal limitations constitute the primary factor in determining core size (Katz and Melese, 1984). A critical mass of fissile material can theoretically operate at any power level if sufficient cooling is provided. The efficient cooling also plays a very important role in the detailed fuel element design. Furthermore, the heat transfer and fluid dynamics behaviour of the coolant as it flows through the core will play a role in determining the core lattice design.

After determining the basic fuel element geometry and core volume from thermal-fluid considerations, nuclear analysis of the core should be performed to determine the fissile concentration or loading necessary to allow the core to operate at rated power over the desired life time.

The nuclear analysis of the core is rather closely related to its thermal analysis in other ways as well. The nuclear cross-sections that determine core multiplication are sensitive to temperature (e.g. Doppler Effect). Furthermore the material composition of the core changes depending on the thermal considerations such as the density changes accompanying the addition of heat energy to the coolant (e.g. expansion or vapour formation in LWRs (Kazimi and Todreas, 1993)). On the other hand, since this heat energy is generated by the fission reactions induced by neutron flux in the reactor, the temperature distribution in the core also depends on its neutronics behaviour.

In order to design or analyse a nuclear reactor properly, it is necessary to be able to predict how the neutrons will be distributed throughout the core. This, in general, is a difficult problem for the neutrons move about in a nuclear reactor in a random way as a result of repeated nuclear

collisions.

Since the neutron plays the central role in the chain reaction in the analysis of fission reactors, the key problem of the reactor theory is to determine the distribution of neutrons in a reactor core. The neutron density is proportional to the rate at which the fission reactions occur and hence proportional to the core power density. The neutron density is also the key to the subsequent thermal and mechanical analysis of the reactor.

The power produced during the course of a reactor accident is one of the most important factors determining the degree of damage that may result to the plant. The rate at which power is produced is closely linked to the critical state of the reactor and therefore the multiplication factor, k. One of the most important factors affecting criticality is the reactor temperature. Several parameters entering into the value of k are temperature dependent, and changes in temperature necessarily lead to changes in k.

Modelling and simulation of a reactor core including thermal hydraulic and neutronic behaviour under different operating conditions have become an important part of the research and development phase of the design process. The neutronic behaviour of a reactor core can be very accurately predicted by means of current software codes. The most common codes can be used either in the neutronic analysis or in the thermal hydraulic analysis of a reactor core and few of them can be used in both types of analyses.

FLOWNEX is a general purpose thermal-fluid network analysis code. It solves the flow, pressure and temperature distribution in large unstructured thermal-fluid networks and provides essential information on the interaction between network components and the behaviour of the complex systems. FLOWNEX is now capable to perform a transient thermal simulation of PBMR core including the power conversion cycle. The effects of power changes during a transient are performed by a basic point kinetics model.

The point kinetics and internal heat generation simulation model in FLOWNEX consists of twelve coupled differential equations. The first seven of these are known as the point kinetics equations (Rousseau, 1999). In the point kinetics approach the global reactor behaviour is simulated dynamically as a single point having certain weighted average properties that may be assumed to be constant over time. This approximation is valid when: (a) the reactor is sufficiently small so that it is well coupled and (b) the space and time variables are separable. The

latter assumption means the neutron flux shape changes during a transient is negligible. If the flux shape is not altered during the transient the results of the point model are sufficiently accurate as far as neutron kinetics is concerned. This is not valid for the postulated ejection of the control rod with highest reactivity worth. Such a strongly localised perturbation in the core composition would certainly cause a considerable deviation from the spatial shape factor $\psi(r)$ and invalidate the point kinetics model.

One of the most important safety questions concerning reactor analysis involves the reactor kinetic behaviour following the postulated ejection of the control rod with highest reactivity worth (Lewis, 1977). Such a strongly localised perturbation in the core composition would certainly cause a considerable deviation from the spatial shape factor and would invalidate the point kinetics model.

Furthermore, HTR cores are quite large from a neutronic point of view, being as much as 200 diffusion lengths in diameter (Duderstadt, 1976: 367). The neutronic behaviour in such cores tends to be loosely coupled from point to point. This means that a change in the flux or power density at one point in the core will not be felt at other points until an appreciable time delay. Therefore, the point kinetics equations are incapable of predicting the detailed behaviour of reactor transients initiated by rapid local changes in reactivity; more precisely, the neutron flux changes rapidly on a time scale of the order of the effective neutron lifetime.

One possible approach to predict the spatial dependence of neutron flux in such a transient is solving the time-dependent multigroup neutron diffusion equation and precursor equations. The aim of this study is to develop a basic neutronic model of PBMR core which will form the basis to a more sophisticated space-time kinetic model.

1.4. Objective of Study

The objective of this study is to develop a computer routine for the prediction of neutron flux and ultimately the fission heat release in the pebble reactor that will take both axial and radial variations in the reactor into account. The study will therefore comprise of setting an accurate and reliable model to predict and simulate the neutronic behaviour of PBMR core under different operating conditions and nuclear design specifications.

1.5. Layout of Thesis

The next chapter gives a basic description of the reactor physics with the current status of the codes and a review of the previous work in this field. The physical meanings of the approximations and assumptions that are used in this study will be discussed in some detail in this chapter.

In Chapter 3, cross-sections and cross-section libraries are discussed to make sure that the importance of the cross-sections in reactor analysis is well understood. The generation of macrogroup constants and the methodology and approximations used in the fast and thermal spectrum calculations are given at the end of this chapter.

The results of the neutron energy spectrum calculations and the procedure followed to generate the macroscopic group constants are presented in Chapter 4.

Chapter 5 gives a brief discussion on the finite difference method followed by the application of this method to multigroup diffusion equations. The results of the multigroup calculations and the verification of these results with other Monte Carlo and diffusion codes for the neutronic analysis of the PBMR core with different nuclear specifications are also given in this chapter.

The results of the model and the comparison and verification of the results with using other diffusion codes is given in Chapter 6. Different conditions and nuclear specifications of a pebble bed reactor are used in the calculations. The results of PBMR system simulation under different operating conditions is tabulated in this chapter.

In the last chapter the most important results and findings from the previous chapters will be discussed. Conclusions on the applicability of the model will be made and some of the shortcomings will be identified. Recommendations will be made for future work and the improvement of results.

Chapter 2. Literature Survey

2.1. Introduction

The high temperature reactor (HTR) has a tradition that extends back to the 1940s, when the first ideas about this reactor type took shape. Since then, nuclear reactors using gas (helium or carbon dioxide) as a core coolant have been built and operated successfully, as mentioned in the previous chapter. Although these types of reactors have achieved only limited use to date, there is a recent renewal of interest in many countries for this reactor type. In South Africa the PBMR project (Nicholls, 1997) is approaching the construction phase of the plant. China (Xu and Zuo, 2002; Zhang and Yu, 2002) and Japan (Yamashita et al., 1996) each recently commissioned a small HTR test reactor, the HTR-10 and HTTR respectively. The United States, Russia, France and Japan have joined in a project for weapon-grade plutonium burning in the GTMHR (Kiryushin et al., 1997).

Above all other possible advantages of the HTR stands its potential to operate as an inherently safe reactor. The concept of "inherently safe" can be interpreted as the impossibility of the reactor to reach a state where radioactive fission products are set free above predefined levels. This implies the usage of passive safety measures, i.e. measures that rely on natural processes to limit core temperatures in situations where all other active control fails, and that do not require human action. Characteristic features in this sense are the fuel configuration, the low power density (some ten to 20 times lower than in light water reactors) and the high specific heat capacity of the graphite that serves as moderator and construction material.

The fuel is dispersed in billions of particles (~0.5 mm diameter), each having several high-density coatings on them. One of the layers, made of tough silicon carbide, serves as a miniature pressure vessel that can retain fission products up to temperatures of 1600 °C. This characteristic affords a considerable margin of operating safety. The coated particles are embedded into graphite fuel elements, where the graphite functions as moderator. The elements are placed into a metal pressure vessel in which they are surrounded by a shield of graphite blocks that functions as a reflector and moderator. Unlike light water reactors, the working fluid in a HTR does not combine the functions of coolant and moderator. The helium coolant is both chemically and nuclear inert and does not interfere in the neutron moderation process. Furthermore, the heat transfer and transport are uniform and well defined because helium does not experience a phase

change.

The reactor type discussed in this thesis will be the pebble bed HTR. The fuel elements of a pebble bed HTR are tennis ball size graphite spheres which are called as pebbles, each containing about 15 000 coated particles. They are packed into the core as a bed of 100 000s of pebbles. In addition, unfuelled graphite pebbles may be loaded into the core to shape its power and temperature distribution by spacing out the hot fuel pebbles. In order to maintain criticality, pebbles are added to the top of the bed and discharged at the bottom during operation. If the burn-up of a discharged pebble has not reached the desired level, it can be returned to the top of the pebble bed. This way of on-line fuelling ensures that the excess reactivity is minimal. Typical operation temperatures are 900 °C for the helium working fluid exiting the core, while entering it at around 500 °C

2.2. Pebble Bed Modular Reactor Project

The fundamental design concept is aimed at achieving a plant lacking any physical process that could cause an internally induced and/or externally induced radiation hazard outside the site boundary. This is principally achieved in the PBMR by demonstrating that the system stabilises itself neutronically and thermal-hydraulically by appropriate inherent feedback mechanisms. Neutronic self-stabilisation is enhanced by the small excess reactivity margin and by strong negative temperature coefficient of reactivity (Doppler and moderator). The thermal hydraulic stabilisation is provided by relatively low power density (~3.2 MW/m^3), such that the integrated heat loss from the reactor exceeds the decay heat production in a total control rod withdrawal followed by a de-pressurized loss of forced cooling.

The use of helium as coolant and the high temperature integrity of the fuel and structural graphite allow the use of high primary coolant temperatures (900 °C) that yield high thermal efficiencies. The use of a closed cycle gas turbine is supported with these high temperatures. It enables the increase of the efficiency over a steam plant, thus reducing the output specific capital cost. Furthermore, the user requirement specifying unrestricted load-following operation within the power range 100-40-100 percent directly implies the use of a gas turbine. In an indirect steam cycle this requirement cannot be met due to the inherent thermal-dynamic characteristics of a two-loop steam cycle layout.

2.2.1. Safety aspects of the PBMR

The PBMR is characterised by a series of inherent safety properties, differentiating it from other reactor types. Due to these characteristics PBMR does not require the typical nuclear safety systems which actively guard the plant. These safety characteristics are summarised below.

- The use of graphite as a fuel element cladding/moderator and core structural material/reflector means that a core melt situation can be ruled out, because of the large difference between the normal, average operating temperature (1100 °C) and the maximum tolerable temperature (2800 °C).
- The large thermal inertia enhanced by the big volume of graphite used in the core and reflector ensure slow temperature transients.
- The low power density (~3.2 MW/m^3), coupled to small particles of fuel, and the good thermal conductivity of graphite ensures that the fuel element temperature does not exceed 1600 °C even in the event of direct cooling failure. Fission product release due to the failure of fuel particles occurs at much higher temperatures. Decay heat can be removed solely by means of conduction and radiation.
- Use of the single phase medium helium as a coolant in a graphitic environment is another safety feature. Helium is chemically inert and does not react with graphite or the metallic core components. Furthermore the neutron absorption cross-section is very small, thus in a depressurised loss of forced cooling (DLOFC) event there is no reactivity increase.
- The use of coated particles in the fuel elements results in low levels of contamination in the primary circuit, thus ensuring low radiation doses to the operating personnel.
- Regarding the neutron physics, a strong negative temperature coefficient prevails over the entire temperature range of the reactor due to presence of the large amount of fertile material, U-238. Large power excursions can be ruled out due to the self stabilising effect.
- The continuous fuelling concept has the advantage of keeping the level of excess reactivity as low as possible. Adding single fuel spheres has a small effect on reactivity and could be compensated for by simply not adding anymore fuel should higher temperatures be experienced on the PCU side than expected.

2.2.2. Plant Overview

The future of new nuclear power plant construction will depend in large part on the ability of designers to reduce capital and maintenance costs. One of the methods proposed is to improve the modularity of designs in which the basic plant modules are built in a factory in modules and shipped to the site for assembly. This approach improves overall quality, reduces site field work and rework, and speeds the construction of the plant further reducing the time to operation. The advantage of modularity is also that it takes advantage of the economies of production, not necessarily relying on the economies of scale to reduce costs. Another advantage of modularity is that it can reduce maintenance costs and downtime since modules, if properly designed, allow for a replacement rather than online repair strategy.

PBMRs are designed to produce approximately 110MW each which means that 30 000 average homes could be sustained by one such reactor. More than one PBMR can be located in a facility with a common control centre due to its modular design to build energy parks. Modularity in design allows sequential construction of modules, so more modules can be added to meet the industrial and domestic needs for electricity in an area.

The 250 MW_{th} conceptual design presented in Table 2-1 offers a very high degree of inherent and passive safety that precludes severe core damage and core disarray accidents, without reliance on operator action or powered equipment.

Table 2-1: PBMR overall plant performance data (Mulder, 1999).

Description	Rating
Reactor core thermal output (MW_{th}) (maximum nominal)	250
Net electrical power output (MW_e) (maximum nominal)	110
Thermal hydraulic cycle efficiency (%)	47.3
Net plant efficiency (%)	44.7
Core inlet temperature (°C)	560
Core outlet temperature (°C)	900
Helium mass flow rate through core (kg/s)	142
Nominal pressure at core inlet (bar)	70
Pressure drop over core (bar)	1.05
Pressure drop over reactor (bar)	1.74
Average core power density (MW/m^3)	3.2
Brayton cycle pressure ratio	2.7
Compressor efficiency (%)	87
Turbine for compressor efficiency (%)	89
Power turbine efficiency (%)	90
Alternator efficiency (%)	97
Ramping capability "up-down" between 0 → 100 % power load (%/min)	10
Step function, % of current power between 0 → 100 % power level (%/min)	10
Load rejection (%)	100

2.3. Neutron Reactions

The neutron-nuclei reactions of present interest fall mainly into three general categories; scattering, capture and fission.

The net result is the exchange of energy between a neutron and a nucleus in scattering reactions. In elastic scattering, the energy exchanged between the neutron and the nucleus is entirely kinetic in nature. In inelastic scattering, part of the kinetic energy of the neutron is transferred to the nucleus as internal (potential) energy. Elastic scattering is possible in all energies, but inelastic scattering can occur only when the neutron energy is large enough to produce an exited state of the nucleus.

Except in most instances of elastic scattering, the first stage in a neutron-nucleus interaction is usually the absorption of the neutron by the nucleus to form a compound nucleus in an excited (high energy) state. In inelastic scattering, the compound nucleus almost immediately expels a neutron of lower energy, leaving an excited state of the original nucleus. Instead of expelling a neutron, a compound nucleus formed by the absorption of a neutron can change by emitting its excess energy as γ-radiation; this process is referred to as *radiative capture*.

The third important interaction between neutron and nuclei is fission, or more precisely nuclear fission. When fission takes place, the excited compound nucleus formed after absorption of a

neutron breaks up into two lighter nuclei, called fission fragments. ^{233}U, ^{235}U, ^{239}Pu, which will undergo fission with neutrons are called fissile nuclides. ^{232}Th and ^{238}U can be converted into the fissile species; they are called fertile nuclides.

The description of the interaction of neutrons with atomic nuclei can be made quantitative by means of the concept of "cross-sections". If a given material is exposed to the action of neutrons, the rate at which any particular nuclear reaction occurs depends upon the number and nature of the nuclei in the specified material. The cross-section of a target nucleus for any given reaction is a measure of the probability of a particular neutron-nucleus interaction and is a property of the nucleus and of the energy of the incident neutron.

2.4. Neutron Cross-Section Libraries

All reactor physics and shielding calculations need data for neutron-induced reactions. This data must cover the whole range of incident neutron energies used in the calculation. In addition, these nuclear data libraries must contain all materials present in the system. The experimental data usually comes from different sources and have to be first compiled in a suitable form acceptable by computer codes (Massimo, 1975:12-17). Various sets of nuclear data have been in use at different laboratories (CINDA, 2002). By the early 1970s there was a great tendency towards standardisation, based on the utilisation of the evaluated nuclear data file (ENDF), which allows an easy exchange of information between various laboratories.

2.4.1. ENDF/B Format

The Evaluated Nuclear Data File (ENDF) system was developed for the storage and retrieval of evaluated nuclear data to be used for applications of nuclear technology. These applications control many features of the system including the choice of materials to be included, the data used, the formats used, and the testing required before a library is released.

The ENDF system is logically divided into formats and procedures. Formats describe how the data are arranged in the libraries and give the formulas needed to reconstruct physical quantities such as cross-sections and angular distributions from the parameters in the library. Procedures are the more restrictive rules that specify what data types must be included, which format can be used in particular circumstances, and so on (ENDF-102, 2001).

The ENDF/B library maintained at the National Nuclear Data Center (NNDC) contains the recommended evaluation for each material. Each material is as complete as possible; however, completeness depends on the intended application. For example, when a user is interested in performing a reactor physics calculation or in doing a shielding analysis, evaluated data are needed for all neutron-induced reactions, covering the full range of incident neutron energies, for each material in the system that it is being analysed. The user also expects that the file will contain information such as the angular and energy distributions for secondary neutrons. For another calculation, the user may only need a minor isotope for determining activation, and would then be satisfied by an evaluation that contains only reaction cross-sections.

ENDF/B data sets are revised or replaced only after extensive review and testing. This allows them to be used as standard reference data during the lifetime of the particular ENDF/B version.

Once the evaluated data sets have been prepared in ENDF format, they can be converted to forms appropriate for testing and actual applications using processing codes. Processing codes that generate group-averaged cross-sections for use in neutronics calculations from the ENDF library have been written. These codes include such functions as resonance reconstruction, Doppler broadening, multigroup averaging, and/or rearrangement into specified interface formats (MacFarlane and Muir, 1994).

The existing codes for neutron calculations require libraries which are different from one another and from ENDF/B. Therefore processing codes are needed in order to generate suitable libraries from ENDF/B for neutronics calculation. The fine group libraries and the energy structures of most common libraries listed in Table 2-2 must be produced and regularly updated starting from cross-section sets of the type of ENDF/B.

Table 2-2: Nuclear Data Libraries Energy Structures (Massimo, 1975:91).

Library	Energy Range (eV)	No. of Groups
MUPO	1E7 – 0.0025	43
†GAM – I	1E7 – 0.414	68
‡GATHER – I	2.1 – 0	96
GAM – II	1.49E7 – 0.414	99
GATHER – II	2.38 – 0.001	101
THERMOS	0.683 – 0	≤ 30
MICROX	Like GAM-II – GATHER-II plus ultra fine grid resonance range	
WIMS	1E7 – 0	69
APOLLO	1E7 – 0	186 or 99

The nuclear data centres in USA, Europe, Japan, Russia and China have been evolving computerised nuclear data files in ENDF/B format (ENDF-102, 2001) in the last 40 years to satisfy the nuclear data needs of nuclear energy development. These data files cannot be directly used in neutronic codes that are used to perform reactor physics calculations. To use the best nuclear data in application calculations, it is imperative to correctly process the basic evaluated nuclear data files into usable format compatible with neutronic codes.

The recently released basic evaluated nuclear data files, such as ENDF/B-VI, JENDL3.1, BROND-2, and CENDL-2, are not directly used as input to neutronics but are converted to pre-processed files which are post-processed into multigroup files which are then cast into specially formatted working libraries that are compatible with neutronic codes. This procedure will not be applied in this thesis but it will be left for future work.

2.4.2. GAM-I Library

GAM-I library is available in 68 energy groups ranging from 10^7 eV to 0.414 eV with a constant group lethargy difference of 0.25. GAM-I library has been extracted from the basic nuclear data sets ENDF/B-V and JEF-I and it contains 181 materials. For the complete list of those materials, please refer to Appendix A. . The GAM-I library contains the data of different sources which are given in Table 2-3. The library contains cross-sections of 116 fission products (see Appendix A.).

GAM-I library contains the fundamental cross-section data for each isotope such as absorption, fission, etc. as well as the group-to-group scattering, inelastic scattering and (n, 2n) cross-sections

† Nuclear data library that is used in fast energy range.
‡ Nuclear data library that is used in thermal energy range.

and the resonance data for the resonance materials which are required in the calculation of resonance integrals.

Table 2-3: Sources in GAM-I Library.

GAM Id No.	Description		
6	Th-232	Mat 4902	JEF-I
7	Pa-233	Mat 1391	ENDFB-V
8	U-233	Mat 4923	JEF-I
9	U-234	Mat 4924	JEF-I
10	U-235	Mat 4925	JEF-I
11	U-236	Mat 4926	JEF-I
12	U-238	Mat 4928	JEF-I
13	Np-239	Mat 4939	JEF-I
14	Pu-239	Mat 1264	ENDFB-IV
15	Pu-240	Mat 4940	JEF-I
16	Pu-241	Mat 4941	JEF-I
17	Pu-242	Mat 1342	ENDFB-V

2.4.3. GATHER-I Library

GATHER-I thermal source library is available in 96 energy groups ranging from 2.1 eV to 0 eV. The library is subdivided into two parts: (a) the absorbers with identification numbers being the same as the GAM-I library. (b) The scatterers with identification numbers consisting of four digits. A complete table of the materials are presented in Appendix A.

The library contains the fundamental cross-sections such as absorption, scattering, etc. for all materials and for the scattering nuclides scattering kernels have formerly been prepared with application of different scattering laws and for different temperatures.

2.5. Diffusion Theory and Its Solutions

As neutrons move within a medium, which may be gaseous, liquid or solid, they collide with the nuclei of the atoms in the medium. In a collision, a neutron may be absorbed by the nucleus or it may be scattered, elastically or inelastically. Absorption may result in a loss of the neutron or in an increase in the number of neutrons by fission. The fission neutrons will usually have different energies and move in different directions than the incident neutrons. Furthermore, as a consequence of scattering, there will generally be a change in the position, energy and direction of motion of the neutron. The interaction of neutrons with nuclei in a medium thus results in the transfer (transport) of the neutrons from one location to another.

The distribution of neutron in space, energy and time can be expressed in a straightforward manner by means of the transport equation (Duderstadt, 1976:103-149). It is sometimes called "the Boltzman equation" because of its similarity to an expression derived by L. Boltzmann (about 1870) in connection with the kinetic theory of gases.

2.5.1. Transport Equation

The general time, position and angle dependent form of the transport equation is

$$\frac{\partial N(r,E,\Omega,t)}{\partial t} = -\Omega\nabla N(r,E,\Omega,t)v - \Sigma_t N(r,E,\Omega,t)v + \int\Sigma_s(E'\to E,\Omega'\to\Omega)N(r,E',\Omega',t)v'dE'd\Omega + S \quad . \tag{2.1}$$

where

v = neutron velocity corresponding to energy E,

N = neutron angular density,

Σ_t = total neutron cross-sections (generally function of r and E),

S = neutron source,

r = space coordinate,

Ω = unit vector in the direction of the neutron motion,

E =energy,

t = time,

$\Sigma_s\left(E'\to E,\Omega'\to\Omega\right)$ = scattering cross-section from E',Ω' into E,Ω.

This equation represents a neutron balance in a volume dV for the neutrons having energy between E and $E+dE$ and flight direction in the solid angle $d\Omega$ around Ω. For more detailed information on transport equation, please refer to Appendix B.

Since neutrons of a given energy and moving in a specified direction may result from scattering collisions, by neutrons with energies and directions over a wide range, integration of the scattering terms must be carried out over all initial energies and directions of motion.

Consequently, the transport equation is an integrodifferential equation which has been solved exactly in only a few very simple cases.

One of the simple approximations to transport theory that has been widely used is the diffusion theory approximation. It is given this name because it involves a relationship similar to the familiar Fick's law that applies to diffusion in gases and solutions.

2.5.2. Diffusion Equation

Diffusion theory is a simple model of neutron transport in the study of nuclear reactor theory. This model is certainly sufficient to introduce most of the important concepts of reactor analysis. It can even be used on occasion to provide useful qualitative information such as in preliminary survey design studies (Duderstadt, 1976).

While deriving the diffusion model from transport equation the angular flux is assumed to be weakly dependent on angle (in fact, linearly anisotropic) so that the diffusion approximation is valid. Usually this assumption is reasonably well satisfied in large power reactors provided one take care to modify the analysis a bit in the vicinity of strong absorbers, interfaces, and boundaries to account for transport effects (Massimo, 1975).

The diffusion approximation is actually a consequence of different approximations: (a) the angular flux can be adequately represented by linear anisotropic angular dependence, (b) isotropic sources, and (c) the neutron current density changes slowly on a time-scale compared to the mean collision time. The derivation of multigroup diffusion equation from transport equation is given in Appendix C.

The neutrons produced by fission have a range of high energies, up to about 10 MeV. In a nuclear reactor, these neutrons are slowed down by scattering collisions with atomic nuclei until they are thermalised. In the thermal region, below about 1 eV, the neutrons exchanged energy with the moderator atoms, so that upscattering, in which the neutrons gain energy, as well as the common down-scattering, can occur. As a result of the various interactions, the neutron energies in a reactor core range from about 10 MeV to 0.001 eV or less.

2.5.3. Multigroup Diffusion Equation

The energy dependence of the neutron flux in a reactor core can be discretised over the energy range of neutrons. Thus the neutron energy variable E is discretised into energy intervals or groups. The division of the neutron energy range into G groups is illustrated in Figure 2-1 below.

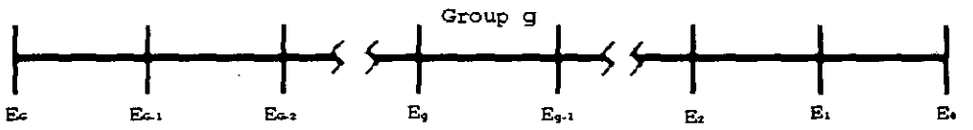

Figure 2-1: Division of neutron energies into G groups.

The maximum energy in the range of interest is represented by E_0 and the minimum is E_G. The group with the highest energy designated the first group, i.e. $g = 1$, and the value of g increases with decreasing neutron energy. If a neutron introduced into a group g' by fission or by scattering, it will pass during moderation into a group g, where $g > g'$, i.e. at lower energy. In the thermal energy region, a certain amount of upscattering may also occur, i.e. $g < g'$.

The steady-state neutron balance equation for the group g is

$$\nabla \cdot D_g \nabla \phi_g - \Sigma_g^t(x,y)\phi_g(x,y) + \sum_{g=1}^{G} \Sigma_{g' \to g}^S(x,y)\phi_g(x,y) + F_g(x,y) = 0, \qquad (2.2)$$

where "del operator" (∇) in Cartesian coordinates is given by

$$\nabla = \frac{\partial}{\partial x} i + \frac{\partial}{\partial y} j + \frac{\partial}{\partial z} k,$$

and the "Laplacian operator" (∇^2) in Cartesian coordinates is given by

$$\nabla^2 = \nabla \cdot \nabla = \frac{\partial^2}{\partial x^2} + \frac{\partial^2}{\partial y^2} + \frac{\partial^2}{\partial z^2}.$$

The source term in equation (2.2) is given by

$$F_g(x,y)=\frac{1}{k}\chi_g(x,y)\sum_{g'=1}^{G}\nu_{g'}\Sigma_{g'}^{f}(x,y)\phi_{g'}(x,y)+S_g(x,y). \tag{2.3}$$

The complete set of multigroup equations consist of G equations of this form with $g=1,2,3,...,G$. These equations are coupled since the flux ϕ_g in group g is dependent on the values of $\phi_{g'}$ in other groups.

The other strategies for solving the multigroup diffusion equations and the numerical methods behind them are presented in chapter five and Appendix C. and Appendix D.

2.5.4. Methodology Used in the Thesis

For the purpose of reactor analysis, the steady-state distribution of the neutron flux in energy and space is required. This energy distribution can be obtained to a good approximation, by considering a fairly large number of energy groups.

In actual calculations the complexity is reduced in two steps: (1) the reactor system is divided into regions in which the composition can be assumed to be constant. The group constants are then essentially independent of the space coordinates in each region. With these simplifications the group fluxes can be determined by solving the multigroup equations. This is called the 'fine group' calculations. (2) Several energy groups are combined into a single 'macrogroup'. Macrogroup of few-group cross-sections and diffusion coefficients, evaluated from the microgroup cross-sections, when combined with the appropriate neutron fluxes, give good approximation to the rates of neutron interactions.

The few-group constants can now be used in the determination of the spatial distribution of the neutron flux. The few-group constants will only be constants if the neutron flux in the multigroup diffusion equations is of the separable form in which case they reduce to group averages over the neutron flux energy spectrum $\varphi(E)$,

$$\phi(r,E)=\psi(r)\varphi(E).$$

The physics which are important in various energy ranges in the multigroup diffusion calculations are given in Table 2-4. In this study inelastic downscattering and certain types of

resonance absorption are not treated in the slowing down calculations.

Table 2-4: Physics important in various energy ranges.

Energy Range	Description
$10^5 - 10^7$ eV (fast)	No upscattering Downscattering (elastic and inelastic) Resonance absorption Fission sources
$1 - 10^5$ eV (fast)	No upscattering Downscattering (elastic) Resonance absorption
0 – 1 eV (thermal)	Upscattering Downscattering

For the treatment of the spatial distribution of the neutron flux the finite difference method is used to solve the multigroup diffusion equations in two-dimensions. The geometry that is used in thermal hydraulic analysis using a thermal hydraulic code forms the basis of the space dependent calculations. Diffusion calculations are done with a suitable boundary condition in each node that has already been generated by the thermal hydraulic code for the thermal hydraulic calculations.

The output of the module contains the neutron flux in the core as well as the heat generation due to the fission reaction induced by neutrons and therefore the power profile in two dimensions while it requires the temperature profile throughout the core and the nuclear design specifications as input.

2.6. Current Status of "Codes"

The procedure of HTR core design calculations can be subdivided into three parts: (a) generation of working data libraries by processing the evaluated nuclear data files like ENDF/B, (b) establishing a reactor model using the methods of homogenisation and condensation, and (c) performing steady-state neutronics, burn-up, thermodynamics and thermalhydraulics reactor calculations in 1D or 2D geometric approximations.

2.6.1. Cross-section Data Processing Codes

These codes not only select the cross-section data of interest and prepare them in a form suitable for input to reactor design codes, but also interpolate existing data to fill in any gaps which may exist, as well as apply various theoretical models (such as optical model of nuclear structure) to

generate cross-section data in those regimes in which no data exist. These library codes also generate differential scattering cross-sections, resonance integrals, and thermal energy scattering kernels.

The differential scattering cross-sections for elastic scattering are usually generated as a sequence of terms in a Legendre polynomial expansion. By way of contrast, inelastic scattering and (n, 2n) processes are usually assumed to be isotropic in the laboratory system and calculated using available data on the appropriate nuclear states or a theoretical model of the nucleus.

In the regime in which the resonances are isolated and measured, this can be accomplished using the standard techniques (such as NR, NRIM approximations). Various nuclear models can be used to generate resonance parameters for the energy range in which the resonances are still isolated but not measured. The most difficult area to treat is the energy range in which the resonances are not only unresolved but overlap so appreciably that they cannot be considered independently. It is also necessary to account for heterogeneous effects, temperature effects, and overlap of resonances of different materials (Duderstadt, 1976:315-375).

The most widely used system for nuclear data libraries generation is the NJOY package. The principal advantage of NJOY is its most general purpose applicability and comprehensive capability to process data in the recent ENDF/B-VI format. In particular, it is able to produce thermal scattering laws and cross-sections for the most common moderating materials at the some selected temperatures. NJOY calculates the cross-sections for moderators in two ways (Gillette et Al., 1999): (a) free gas theory, and (b) calculation of the scattering matrix from the $S(\alpha,\beta)$ matrixes supplied in the ENDF/B-VI library.

At the Oak Ridge National Laboratory (ORNL), a new version of the AMPX cross-section processing system (AMPX – 2000) has been developed to process the full range of ENDF formats used to describe the physics associated neutron, gamma and neutron-gamma interactions up to 20 MeV (Dunn and Greene, 2002).

The NJOY code system and AMPX-2000 are the only complete software packages and that are used to process data for all versions of ENDF/B data through Version IV. AMPX-2000 can be used to generate a variety of multigroup or continuous energy (point) cross-section libraries that can be used to perform nuclear analysis.

2.6.2. Static Design Codes

Static design codes are used to obtain the global spatial dependence of the neutron flux throughout the reactor core. This information is required for accurate predictions of the fuel loading, power distributions, temperature dependence of reactivity, excess reactivity, shutdown margins, shielding requirements, and other quantities.

These codes are usually few-group diffusion or transport codes, which are usually used to determine multiplication factor (eigenvalue) and flux distribution in the system of interest. Before such a calculation can be performed the heterogeneities in the core must be homogenised. Multigroup diffusion codes are usually adequate for a wide class of problems, including the determination of the overall flux and power distribution, the effects of fuel zoning, reactivity predictions, and so on. Such codes can also be used to calculate temperature and power coefficients of reactivity. This is usually performed by merely calculating the core multiplication for several different core temperatures or power levels.

Another powerful approach for predicting the neutron density in the reactor core is given by the Monte Carlo method, which replaces a deterministic problem by an analogous one consisting of a game to be played many times. These numerical calculations, which make use of statistical variables, can be used to simulate the physical phenomena actually happening in a reactor where the neutrons have stochastic behaviour. A high number of neutron histories are simulated on the computer, every interesting event is recorded and statistical averages are calculated. Random numbers are used to decide at which place collisions occur and of which type they are (absorption, scattering, etc.).

The result of a Monte Carlo method is a statistical variable and its accuracy roughly inversely proportional to the square root of number of events. This means that number of variables which can be calculated by this method should be relatively small in order not to increase the computational effort (Massimo, 1975: 18-42).

2.6.2.1. The HTR-2000 Code System

The aim of the generation of this code system is the generation of a tool for detailed monitoring of the AVR reactor (Wolf et al., 1990). In HTR-2000 code system a 3D diffusion approximation is used for the calculation of global neutron flux distribution and it is coupled with a 3D finite-

difference thermodynamics and thermalhydraulics module. Burn-up calculations can be performed for 50 isotopes. Heavy metal, fission products, structural and absorber isotopes are treated separately. The partial load and startup transient simulations are allowed with the use of explicit calculations of short-lived species like Pa-233, Np-239, I-135 and Xe-135.

The HTR-2000 code system can now be used for all pebble bed HTR designs and allows a comprehensive analysis of all questions in quasi-stationary reactor core design (Wolf et al., 1990).

2.6.2.2. The V.S.O.P. System

Very Superior Old Programs (V.S.O.P.) was developed at KFA. It is a modular code package for simulation of nuclear reactors and fuel cycles. The basic modules are the GAM-1, ZUT, THERMOS, CITATION and FEVER codes. These codes were updated and adapted according to special requirements of high temperature, heavy water and light water reactors (Teuchert et al., 1994).

Different fuel element types are taken into account and for all of them burn-up and spectrums calculations can be performed. The global neutron flux distribution calculation is performed by using the diffusion code CITATION in 2D geometry. Temperature distribution and pressure drop are calculated in 2D geometry using the THERMIX code. For burn-up calculation a modified version of FEVER code is used in which the reactor is treated in 2D pattern and up to 42 fission products are managed explicitly. The combination of neutronics, thermalhydraulics, thermodynamics and burn-up simulates the mutual coupling between fuel flow and nuclear burn-up. Thus monitoring the reactor life from the initial core loading up to equilibrium conditions is possible.

Besides the simulation of these in-core events, VSOP follows the fuel outside the reactor through decay storage, reprocessing plant and refabrication. The life history of all fuel is accompanied by a cost routine that finally gives information on fuel cycle costs.

2.6.2.3. The ZIRKUS Code System

The INTERATOM programme system ZIRKUS is used for nuclear and thermalhydraulic design calculations of pebble bed cores. Once through (OTTO) and multiple recycling (MEDUL) loading schemes may be applied. The system is able to follow the reactor life from

initial loading up to equilibrium core. The ZIRKUS system has been validated by comparison with experiments and other accepted code systems. It was successfully used in the frame of the HTR-Modul power plant conceptual licensing procedure (Wolf et al., 1990).

2.6.2.4. The MOCCA System

The modular code system MOCCA (Modular Core Calculation) was developed as an efficient tool for commercial HTR core design. The cross-section data libraries based on JEF-1 data sets in 86 energy group structure which allows improved modelling of the low-energy resonances of Pu and Hf isotopes (Wolf et al., 1980). The MOCCA system was extensively used in the design calculations for the HTR-100, HTR-500 and GHR.

2.6.2.5. The SCALE Code System*

The history of the Standardized Computer Analyses for Licensing Evaluation (SCALE) code system dates back to 1969 when the current Computational Physics and Engineering Division at Oak Ridge National Laboratory (ORNL) began providing the transportation package certification staff at the U.S. Atomic Energy Commission with computational support in the use of the new KENO code for performing criticality safety assessments with the statistical Monte Carlo method.

The SCALE code system contains different modules that allow a complete licensing analysis of a nuclear reactor. The control modules were designed to provide the system analysis capability. The CSAS and CSAS6 modules are the criticality control modules designed for the calculation of the neutron multiplication factor of a system. Eight sequences in CSAS enable general analysis of a 1D system model using XSDRNPM or a 3D system model using KENO V.a. The CSAS6 control module provides two sequences for analysing 3D models using KENO-VI for more complex geometries or fuel systems with hexagonal arrays. The SAS1 and SAS3 modules provide general 1D deterministic and 3D Monte Carlo analysis capabilities. The HTAS1 module is the only heat transfer control module and uses the various capabilities of the HEATING code to perform different sequences of steady-state and transient analysis that enable the normal and accident conditions of a transportation package to be evaluated (NUREG/CR-0200, 1998).

* The detailed information and history of the code system can be found at the web site: http://www.ornl.gov/scale.

The SCALE system has a wide range of capabilities. The SCALE modules used for preparing problem-dependent cross-section libraries and performing criticality safety analyses are well established. Applications extend well beyond cask analysis to the areas of fuel reprocessing and handling facilities, storage facilities, and critical experiment design and analysis as well as selected reactor applications.

2.6.2.6. The MCNP Code System

A general Monte Carlo N-Particle Transport Code (MCNP) is a general purpose, continuous-energy, generalised geometry, time-dependent, coupled neutron/photon/electron Monte Carlo transport code. It can be used in several transport modes; neutron only, photon only, electron only, combined neutron/photon transport where the photons are produced by neutron interactions, neutron/photon/electron, photon/electron, or electron/photon. The neutron energy regime is from 10^{-11} MeV to 20 MeV, and the photon and electron regimes are from 1 keV to 1000 MeV. The capability to calculate k_{eff} eigenvalues for fissile systems is also a standard feature of MCNP (LA-12625-M, 1997).

MCNP uses continuous energy nuclear and atomic data libraries. The primary sources of nuclear data are evaluations from the ENDF system and the Evaluated Nuclear Data Library (ENDL). Evaluated data are processed into a format appropriate for MCNP by codes such as NJOY.

Nuclear data tables exist for neutron interactions, neutron induced photons, photon interactions, neutron dosimetry or activation, and thermal particle scattering. Photon and electron data is atomic rather than nuclear in nature. Each data table available to MCNP is listed on a directory file, XSDIR.

Over 500 neutron interaction tables are available for approximately 100 different isotopes and elements. Multiple tables for a single isotope are provided primarily because data has been derived from different evaluations, but also because of different temperature regimes and different processing tolerances. More neutron interaction tables are constantly being added as new and revised evaluations become available. Neutron-induced photon production data are given as part of the neutron interaction tables when such data are included in the evaluations (LA-12625-M, 1997).

Cross-sections for nearly 2000 dosimetry or activation reactions involving over 400 target nuclei

in ground and excited states are part of the MCNP data package (LA-12625-M, 1997). These cross-sections can be used as energy-dependent response functions in MCNP to determine reaction rates but can not be used as transport cross-sections.

The geometry of MCNP treats an arbitrary three-dimensional configuration of user-defined materials in geometric cells bounded by first- and second-degree surfaces and fourth-degree elliptical tori (LA-12625-M, 1997). The cells are defined by the intersections, unions, and complements of the regions bounded by the surfaces. Surfaces are defined by supplying coefficients to the analytic surface equations or, for certain types of surfaces, known points on the surfaces. MCNP has a more general geometry than is available in most combinatorial geometry codes. In addition, the geometry-plotting capability in MCNP helps the user check for geometry errors. MCNP treats geometric cells in a Cartesian coordinate system. The particular Cartesian coordinate system used is arbitrary and user defined, but the right-handed system is often chosen.

2.7. Summary and Conclusion

In this chapter an overview of the PBMR project was presented, in view of its current status. An introduction to reactor physics was given without going into detail, along with the current status of the codes. The methodology that is used in this study was presented briefly.

The neutron cross-section libraries play an important role in the nuclear reactor calculations. The ENDF/B data files contain the basic nuclear data, which are either directly accessed by current codes or the required data for each material of interest is gathered with an appropriate spectrum from these files to construct a new cross-section library. The GAM and GATHER libraries are constructed for the HTRs from ENDF/B and JEF data formats. These cross-section libraries are used and verified many times for HTR analysis.

The current nuclear reactor analysis codes are actually well established for nuclear reactor analysis. The multigroup diffusion codes are accurate enough even for licensing calculations of a nuclear reactor. Furthermore, the diffusion approximation requires less computation time then more accurate Monte Carlo calculations and direct solution of transport equation.

Chapter 3. Neutron Spectrum Calculations

3.1. Introduction

The primary objective in the design and operation of a nuclear reactor is the utilisation of the energy or radiation released by a controlled chain reaction of nuclear fission events maintained within the reactor core. However, there are other possible nuclear reactions a neutron can undergo that do not lead to fission. One such reaction involves the capture of the neutron by a nucleus which then emits a gamma ray rather than fission. Another possible reaction involves the neutron simply bouncing or scattering off of a nucleus. Such processes remove neutrons from the reactor and tend to inhibit the chain reaction.

In order to understand and design a fission chain reaction system, development of the fundamental concepts involved in predicting the distribution of neutrons in a nuclear reactor should be considered. Essentially, two different subjects should be considered: (a) the determination of the probabilities of occurrence of various neutron-nuclear reactions and (b) the derivation and solution of an equation that uses these probabilities to determine neutron density and fission reaction rate in a nuclear reactor.

This chapter presents the nuclear reactions that are of interest in a nuclear reactor analysis. The cross-sections of these reactions and the calculation procedure of these cross-sections are reviewed in this chapter. The methodology is established to determine the neutron density in a nuclear reactor. Although the mathematical models and the approximations used in the analysis are presented in this chapter, the procedure and the results of the analysis will be given in the next chapter.

3.2. Nuclear Reactions

There are essentially two types of nuclear reactions of importance in the study of nuclear reactors: (a) spontaneous disintegrations of nuclei and (b) reactions resulting from the collision between nuclei and/or nuclear particles.

3.2.1. Radioactive Decay

Certain nuclei are unstable in the sense that they may spontaneously undergo a transformation

into a different nuclide, usually accompanied by the emission of energetic particles. Such a spontaneous nuclear transformation is referred to as *radioactive decay*. The three most common types of radioactive decay found in naturally occurring nuclides include alpha decay, in which the nucleus emits helium nucleus ${}_2^4He$; beta decay, which corresponds to the conversion of a neutron in the nucleus into a proton, generally accompanied by the emission of an electron and a neutrino; and gamma decay, the transition of a nucleus from one excited state to a lower excited state with the accompanying emission of a photon (Knoll, 1979).

3.2.2. Absorption Reactions

The most important absorption reactions from the nuclear reactor standpoint are radiative capture and fission. There are, however, a few neutron absorption reactions of different types which are of interest. In considering neutron absorption reaction it is convenient to distinguish between reactions of slow neutrons and of fast neutrons.

Slow Neutrons: Capture of the neutron by target nucleus followed by

- The emission of gamma radiation (n,γ)
- The ejection of an alpha particle (n,α)
- The ejection of a photon (n,p)
- Fission (n,f).

Fast Neutrons: Relatively few reactions of neutrons with atomic nuclei, other than scattering and fission, are important for the study of nuclear reactors. Although many such fast neutron reactions are known, their probabilities are usually so small that they have little effect on reactor operation. (n,α) and (n,p) reactions of nuclei with fast neutrons having energies of 1 MeV or more, frequently occur more readily than the (n,γ) reaction. If neutrons of sufficiently high energies are used, two or more neutrons or protons may be expelled from the compound nucleus. For incident neutrons of about 10 MeV, such reactions as $(n,2n)$ and (n,np) have been observed, and for still higher energies $(n,3n),(n,2np)$, etc. processes are possible (Kugeler et al, 2003: Chapter 2).

3.2.2.1. Radiative Capture

Radiative capture reactions are quite significant for reactor analysis since they remove neutrons from the chain reactions (Duderstadt, 1976). The neutron is retained by the nucleus and new particles are formed in an excited state. Then this compound nucleus subsequently decays by emitting a cascade of high energy gammas.

3.2.2.2. Fission

A target nucleus absorbs a neutron and forms an excited compound nucleus. The excitation energy of the latter is than equal to the binding energy of the neutron plus any kinetic energy that neutron may have had before its capture. As a result of this excess energy, compound nucleus may be considered to undergo a series of oscillations. The excess energy which the compound nucleus must have in order to permit it to deform is called the *critical energy for fission (or fission barrier).* If this energy is available then fission will usually occur. If this amount of energy is not available fission is not possible, at least not at any appreciable rate (Krane, 1998).

The binding energy per nucleon increases with decreasing atomic mass numbers greater then 50 (Duderstadt, 1976: 55). It is possible to produce more stable nucleus and thereby release energy by inducing a heavy nucleus fissioning into two nuclei of intermediate mass number.

To induce nuclear fission one must add a sufficient amount of energy to the heavy nucleus to overcome the fission barrier. One way to overcome this fission barrier is to let the heavy nucleus capture a neutron. Then the binding energy of the added neutron itself would be sufficient to induce fission. This process can occur in certain heavy nuclei such as ^{233}U, ^{235}U, ^{239}Pu, ^{241}Pu with neutrons having very small kinetic energies (thermal neutrons). Such nuclides are called as *fissile* nuclides. With most heavy nucleus additional binding energy provided by a captured neutron is not sufficient to push the nucleus undergo fission. However with adding a dash of kinetic energy to the neutron it would be sufficient to lift the nucleus over the fission barrier to cause fission. Such nuclides referred to as *fissionable*, examples are ^{232}Th, ^{238}U, ^{240}Pu.

A typical nuclear fission reaction spews out a variety of products, including the fissioned nuclei or fission products and several (2 – 3) neutrons as well as numerous gammas, betas, and neutrinos and a very considerable amount of energy (on the order of 200 MeV).

3.2.3. Scattering Reactions

The neutron simply scatters off the nucleus (n,n), although in some cases it may first combine with the nucleus to form a compound nucleus for a short time before being reemitted and will frequently leave the nucleus in an excited form which later decays by gamma emission.

- Inelastic Scattering: the incident neutron is first absorbed by the nucleus to form a compound nucleus. This nucleus then subsequently decays by reemitting a neutron while leaving the final nucleus in an excited state. Such reactions usually occur only for relatively high neutron energies since the neutron kinetic energy must exceed certain threshold energy in order to excite the first excited state of the compound nucleus (Massimo, 1975).
- Elastic Resonance Scattering: a similar compound nucleus reaction involves first the absorption of the incident neutron, followed by the reemission of the neutron with the target nucleus returning to its ground state. In contrast to inelastic scattering, kinetic energy is conserved in elastic events (Massimo, 1975).
- Potential Scattering: the simplest type of nuclear interaction, in which the incident neutron scatters elastically off of the nuclear potential without penetrating the nuclear surface (Massimo, 1975).

3.3. Cross-sections for Neutron Reactions

The nuclear cross-section σ for a specified reaction (at a given energy) is defined as the average number of individual interactions occurring per target nucleus per incident neutron in the beam

$$\sigma = \frac{C}{(N\delta x)I} \quad \text{m}^2, \tag{3.1}$$

where C is the number of individual processes per m^2 per second, δx is thickness of the target in m, N is the number of atoms (or nuclei) per m^3, and I is the monoenergetic beam intensity ($\text{m}^{-2}\text{s}^{-1}$) (Lamarsh, 1983).

The significance of the cross-section may be seen by rearranging the equation into the form

$$(N\delta x)\sigma = \frac{C}{I}. \tag{3.2}$$

If every neutron falling on the target reacted, I would be equal to the number of nuclei taking part in the reaction, hence the right hand side of the equation represents the fraction of the incident neutrons which succeed in reacting with the target nuclei. Thus $(N\delta x)\sigma$ may be regarded as the fraction of the surface capable of undergoing the given reaction, in other words, of 1 m^2 of target surface, $(N\delta x)\sigma$ m^2 is effective.

The cross-section σ for a particular process which applies to a single nucleus is frequently called the "microscopic" cross-section. Since the target nuclei contain N nuclei per m^3, the quantity $N\sigma$ is equivalent to the total cross-section of the nuclei per m^3; this is called "macroscopic" cross-section of the material for the process.

If a target material is an element of atomic weight A on the conventional scale, 1 mole has a mass of 10^3 A kg and contains the Avogadro number N_A (i.e. 6.022×10^{23}) of atoms. If the ordinary (or mass) density of the element is ρ kg/m^3, the number density N is given by

$$N = \frac{10^3 \rho N_A}{A} \quad \text{atoms}/\text{m}^3. \tag{3.3}$$

Hence, the macroscopic cross-section is

$$\Sigma = \frac{10^3 \rho N_A}{A}\sigma \quad m^{-1}. \tag{3.4}$$

For a compound of molecular weight M and density ρ kg/m^3, the number N_i atoms of the i-th kind per m^3 is given by

$$N_i = \frac{10^3 \rho N_A}{M}\nu_i, \tag{3.5}$$

where ν_i is the number of atoms of kind i in a molecule of compound.

The macroscopic cross-section for the compound is expressed by

$$\begin{aligned}\Sigma &= N_1\sigma_1 + N_2\sigma_2 + \ldots + N_i\sigma_i + \ldots \\ &= \frac{10^3 \rho N_A}{M}\left(\nu_1\sigma_1 + \nu_2\sigma_2 + \ldots + \nu_i\sigma_i + \ldots\right).\end{aligned} \tag{3.6}$$

For a homogeneous mixture either of elements or compounds or both, which contains several different nuclear species, the macroscopic cross-section is given by

$$\Sigma = N_1\sigma_1 + N_2\sigma_2 + \ldots + N_i\sigma_i + \ldots . \tag{3.7}$$

The values of $N_1, N_2, etc.$ are dependent upon the composition of the mixture as well as on the atomic (or molecular) weights and densities of the constituents.

3.3.1. Effective Homogeneous Cross-section

A typical PBMR is fuelled with fuel spheres consisting of a fuel free graphite shell or zone of ~0.5 cm thickness and outer diameter of ~6 cm that contains ~5 cm diameter matrix of moderating graphite material with the TRISO coated fuel particles embedded in this fuel matrix. A pile of pebbles can be considered as a double-heterogeneous system. The first heterogeneity is the fuel kernel that is surrounded by coating layers and graphite matrix. The second one is the heterogeneity of the fuel zone and the pebble shell.

The coated particles which are embedded in a graphite matrix can be considered as highly absorbing centres in a graphite medium. Drozdowicz et al. (2001) suggested a theoretical approach to the calculation of the effective cross-section of a heterogeneous system where highly absorbing centres (grains) are embedded in a weakly absorbing material (e.g. a moderator) characterised with the absorption cross-sections Σ_a^2 and Σ_a^1, respectively. The effective absorption cross-section of the heterogeneous system is given by

$$\begin{aligned}\Sigma_a^{eff} &= \left(1-\varphi\right)\Sigma_a^1 + \varphi\tilde{\Sigma}_a^2, \\ \varphi &\equiv \varphi_2.\end{aligned} \tag{3.8}$$

The effective absorption cross-section in the grain, $\tilde{\Sigma}_a^2$ is defined as

$$\tilde{\Sigma}_a^2 = \frac{\Sigma_a^2}{\bar{d}_2\Sigma_d^2}\left(1-e^{-\bar{d}_2\Sigma_d^2}\right), \tag{3.9}$$

where φ is defined as $\varphi = \frac{V_2}{V}$ and V_2 is the total volume of absorber grains in the sample volume V. The average chord length is defined as $\bar{d} = \frac{4V_g}{S_g}$, where V_g and S_g are volume and surface of the grain, respectively. Thermal diffusion cross-section Σ_d^2 is given by $\Sigma_d^2 = \Sigma_a^2 + \Sigma_{tr}^2$.

The agreement between theoretical and experimental results is better or worse depending on the grain size. It is better approximated when the small grains are embedded in a matrix since the theoretical assumption is valid only if the size of grains is smaller than one mean free path (Drozdowicz et al., 2001).

An accurate double heterogeneous cell calculation with enhanced heterogeneity describing the effects on spectrum averaged cross-section is of great importance in certain energy ranges. This is a result of the absorption and scattering collisions within the kernel, coating and matrix material, which is largely different to that of a homogenised material. The self-shielding of coated particles should be accounted for, since it will influence the reaction rates in the kernels, the coatings, and the matrix material.

3.3.2. Coated Particle Grain Structure

At energy ranges with $1/\Sigma_a(E)$ smaller than the mean chord length $\bar{l}$ of a coated particle, the grain structure is of importance in spectrum evaluation. This is due in the resonances and at the lower end of the thermal spectrum. The capability of grain structure effect has been included in the ZUT code (Teuchert, et al., 1994).

The resonance calculation of ZUT code is made for a homogeneous distribution of the resonance absorber in the finite volume of a lump. The transport equation is solved in very fine energy groups over the energy range of each resonance. The calculation also includes the neutrons that are born in the lump, leave it, and are absorbed or scattered down in any other lump of the same configuration. Neutrons which leave the lump and undergo scattering reactions are excluded. Nordheim (Duderstadt, 1976) excludes these neutrons by geometric escape probability

$$P(E)=\frac{P_0(E)(1-C)}{1-(1-\bar{l}\Sigma_a(E)P_0(E))C}. \tag{3.10}$$

in which C is the Dancoff factor and $P_0(E)$ is the probability for a neutron to escape from the lump of its birth. The fuel kernel is the lump for coated particle situation and because of smallness of particles the escape probability $P_0(E)$ is very close to 1. This is also valid for the neutron with energy close to strong resonances. A neutron can pass through the fuel matrix without any collision, reach the boundary of the fuel element, travel to another fuel element make interactions with any coated particles and can be absorbed somewhere between them. Figure 3-1 shows possibilities of escaping from a coated particle. This is a double heterogeneous geometry and it is hard to define a Dancoff factor for this geometry. The ZUT code evaluates escape probability by a numerical method. The details of the method are in Appendix E. and the geometric escape probability is calculated as:

$$P(E)=W_1+W_2(W_3+W_4)+W_2W_5\frac{W_6+W_7}{1-W_8}. \tag{3.11}$$

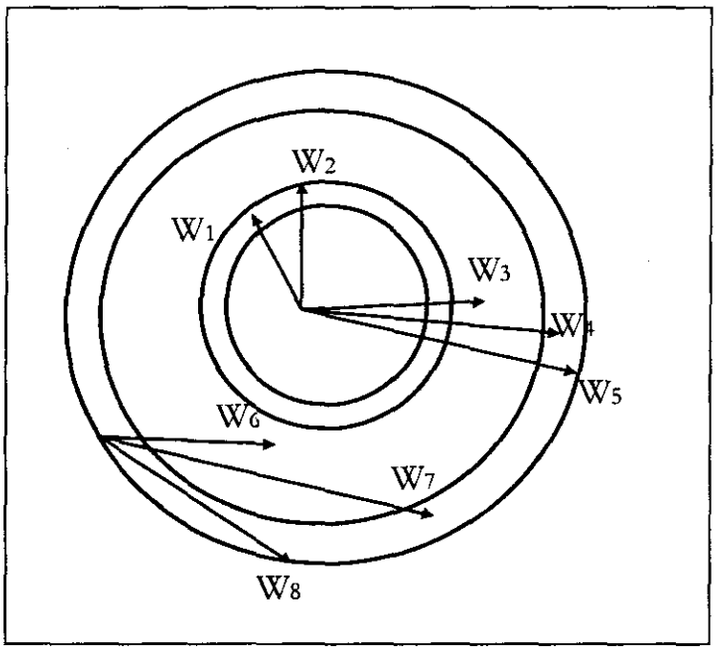

Figure 3-1: Partial escape probabilities.

The definition of the partial escape probabilities W_i are as follows:

W_1: The probability that a neutron born within the absorber zone of a coated particle will have its next interaction in the graphite region of the same coated particle. Apart from the graphite shell a portion of the matrix in between coated particles are included for consideration.

W_2: The probability that a neutron will leave a coated particle and adjoining graphite region without any collision.

W_3: The probability that a neutron, which has left a coated particle, has its next interaction in the graphite region of another coated particle within the same fuel sphere. An average value of all possible positions as to the originating coated particle is possible with this consideration.

W_4: The probability that a neutron as mentioned in W_3 has its next interaction within the fuel free zone of the fuel sphere.

W_5: The probability that a neutron leaves the fuel sphere without any collision.

W_6: The probability that a neutron coming from a neighbouring fuel sphere with random angular distribution of entry has an interaction in the graphite region of a coated particle of that fuel sphere.

W_7: The probability that a neutron as mentioned in W_6 has its interaction in the fuel free zone of the fuel sphere.

W_8: Probability that a neutron leaves the fuel sphere without any collision.

3.4. Generation of Macroscopic Group Constants (MGC)

The basic structure of a reactor calculation model consists of a module to generate the macroscopic group constants, followed by a module to utilise these group constants in a determination of the core multiplication, flux, and power distribution. The power distribution can then be used as the input to a thermal-hydraulics module which solves the equations of heat transfer and fluid flow to determine temperature and coolant density distribution in the core. This latter information is required for the generation of macroscopic group constants; hence feedback to the earlier MGC module (and possible iteration) will be necessary.

Various different types of input data are needed for this sequence of calculations, including the geometry of the core, lattice, and control system, the initial core loading (composition, etc.), inlet coolant conditions, as well as fundamental cross-section data.

Numerous approximations are usually required in order to develop the mathematical models that serve as the basis of reactor design codes (Duderstadt, 1976). Typically, these codes suppress certain independent variables in order to allow a detailed analysis of the process of interest. For example, MGC generation codes usually suppress spatial dependence, either by assuming an infinite medium or an effective buckling mode, in order to facilitate a detailed treatment of the neutron energy. In a similar sense, static design codes employ a rather coarse multigroup structure in order to allow a detailed study of the spatial dependence of the neutron flux. In time-dependent codes one frequently ignores both spatial and energy dependence (Duderstadt, 1976; Massimo, 1975).

There are three basic types of spectral approximations in common use. These are:

- Zero-th order approximation: the equations for $\phi(E)$ strictly apply only in infinite homogenous media and contain no spatial dependence at all.
- First order approximation: "buckling" terms are included in the equations for $\phi(E)$.
- Second order approximation: cross-sections are averaged over a spatially heterogeneous unit cell (e.g. fuel cell).

It is necessary to provide rather careful treatment of the energy dependence of the intragroup flux, because of the extremely complicated energy dependence of microscopic cross-section. For energies above 1 MeV one might approximate $\phi(E)$ by the fission spectrum $\chi(E)$; for intermediate energies, $1\ eV \le E \le 1\ MeV$, $\phi(E)$ behaves very roughly as 1/E; while for energies below 1 eV, $\phi(E)$ might be modelled by a Maxwell-Boltzmann distribution characterising neutrons in thermal equilibrium with the reactor core material at a temperature T (Kugeler et al., 2003: Chapter 2).

The methods used to generate neutron energy spectrum vary depending on the range of the neutron energies of interest. At high energies the main process is neutron slowing down via both

elastic and inelastic scattering. At intermediate energies resonance absorption becomes reasonably important. At low energies up scattering becomes significant as the neutrons have a tendency to approach thermal equilibrium with the reactor core material.

3.4.1. Fast Spectrum Calculations

Most schemes for generating fast group constants first perform a fine multigroup solution of the neutron slowing down equations (usually with P_1 or B_1 approximation) to obtain the fast neutron spectrum and then average microscopic cross-section data over this spectrum to obtain the few-group constants.

In most fast spectrum codes there is an option of specifying the group structure of the few-group constants. In general it is desirable to use the smallest number of coarse groups consistent with the desired accuracy in the corresponding multigroup diffusion equation. Essentially, the necessary group structure depends on the type of calculation of interest such as the core multiplication factor can usually be accomplished with fewer groups than the calculation of power peaking factor in a fuel assembly (Duderstadt, 1976).

The lower cut-off of the fast spectrum is usually chosen high enough, thus the up-scattering out of the thermal groups is negligible. In an HTR, it must be chosen somewhat higher than in an LWR because the higher moderator temperatures in such reactors cause larger up-scattering (Massimo, 1975).

The energy range spanned by the neutron slowing down is extremely large, ranging from 10^7 eV down to 1 eV. In elastic scattering neutron tends to loose a fraction of its initial energy rather than a fixed amount. In neutron slowing down calculations, it is more convenient to use the logarithm of the neutron energy (lethargy) as an independent variable (Duderstadt, 1976). The neutron lethargy is defined as $u \equiv \ln \frac{E_0}{E}$ where E_0 is chosen to be the maximum energy that a neutron can achieve in the problem.

As neutrons slow down from fission energies, they experience a significant probability of being absorbed in the numerous sharp capture resonances which characterise heavy nuclei such as ^{238}U and/or ^{232}Th. Resonance absorption is a very important phenomenon in a nuclear reactor, since it affects reactor multiplication factor, fuel burn-up and breeding performance and reactor

control characteristics.

3.4.1.1. Resonance Absorption

An accurate treatment of resonance absorption is essential to reactor criticality calculations, since it is one of the primary neutron loss mechanisms. In general there will be a depression in the neutron flux at those energies in the vicinity of a strong resonance. The analysis of such flux depressions is of considerable importance in determining multigroup constants.

The most significant resonance absorption in thermal reactors occurs in the lower lying resonances of fertile materials such as 6.67 eV resonance in ^{238}U. This is due to the fact that the asymptotic collision density behaviour is as 1/E (Duderstadt, 1976). Therefore, lower energy neutrons will experience more collisions with absorber nuclei and therefore have higher probability of being absorbed.

The resonance escape probabilities in the neutron slowing down can be calculated by various approximations. The major approximation involves the treatment of absorber scattering integral. This approximation is based on the relative width of the resonance. Both the Narrow Resonance (NR) and the Narrow Resonance Infinite Mass (NRIM) are discussed in some detail in Appendix G.

The NR and NRIM approximations only differ in the way in which scattering from the absorber nuclei is treated. The NR approximation is commonly used for all but the low-lying resonances where the NRIM approximation is more effective. In literature, results of these approximations are compared with the direct numerical calculations of the resonance integrals (Duderstadt, 1976). Although neither approximation seems to yield satisfactory results for the resonances at intermediate energy, when large numbers of resonances are accounted for, the errors tend to average out.

3.4.1.2. Neutron Slowing Down

For the case of fast neutron spectrum calculation in a finite media the spatial dependence of the neutron flux must be considered. Since the effects of anisotropic scattering are usually significant, P_1 or B_1 equations are most commonly used rather than the energy-dependent diffusion equations. The derivation of the lethargy dependent P_1 equations from the transport

equation is presented in Appendix F.

The lethargy dependent P_1 equations are given as (Duderstadt, 1976)

$$\begin{aligned}
&\frac{\partial J}{\partial x}+\Sigma_{ne}(u)\phi(x,u)=-\frac{\partial q_0^H}{\partial u}-\sum_i\frac{\partial q_0^{NH_i}}{\partial u}+S_0(x,u),\\
&\frac{1}{3}\frac{\partial \phi}{\partial x}+\Sigma_{tr}(u)J(x,u)=-\frac{\partial q_1^H}{\partial u}-\sum_i\frac{\partial q_1^{NH_i}}{\partial u}.
\end{aligned} \tag{3.12}$$

The effects of inelastic scattering and fission are included in the source term as

$$S_0(x,u)=\sum_{i=1}^{N}\int_0^u du'\Sigma_{in}^i(u'\to u)\phi(u')+\sum_{i=1}^{N}\chi_i(u)\int_0^\infty du'\nu_i\Sigma_f^i(u')\phi(u')+S_{ext}(u). \tag{3.13}$$

The slowing down densities are given by

$$\begin{aligned}
&\frac{\partial q_0^H}{\partial u}+q_0^H(x,u)=\Sigma_s^H\phi(x,u),\\
&\frac{2}{3}\frac{\partial q_1^H}{\partial u}+q_1^H(x,u)=\frac{4}{9}\Sigma_s^H J(x,u) \qquad \text{(exact treatment of Hydrogeneous medium)},\\
&\lambda_{0i}\frac{\partial q_0^{NH_i}}{\partial u}+q_0^{NH_i}(x,u)=\beta_{0i}\phi(x,u),\\
&\lambda_{1i}\frac{\partial q_0^{NH_i}}{\partial u}+q_1^{NH_i}(x,u)=\beta_{1i}J(x,u) \qquad \begin{pmatrix}\text{approximate treatment of}\\ \text{non-Hydrogeneous medium}\end{pmatrix}.
\end{aligned} \tag{3.14}$$

In most schemes used to generate the fast neutron spectra, elastic scattering is treated using approximate methods which are usually called as continuous slowing down theory. The various approximations are discussed in Appendix F.

The spatial dependence in the P_1 slowing down equations can be treated by assuming the spatial and lethargy dependence of the flux are separable and furthermore the spatial dependence of each of the variables is characterised by a simple buckling mode. The flux can be written in a separable form as

$$\phi(x,u)=\phi(u)\exp(iBx), \tag{3.15}$$

with similar expressions for current, source and slowing down densities. The spatial dependence

is approximated by a single Fourier mode - $\exp(iBx)$. Here the parameter B characterises the leakage in each region of the core. The mathematics behind the treatment of spatial dependence of P_1 slowing down equations and an alternative method – the B_1 method are presented in Appendix F.

Besides providing the fast few-group constants and the fast neutron spectrum, a fast spectrum calculation will provide the rate at which the neutrons slow down to thermal energy range. This rate is needed to complete the determination of few-group constants by generating a thermal spectrum and thermal group constants.

3.4.2. Thermal Spectrum Calculations

The study of thermal neutron behaviour is customarily referred to as neutron thermalisation. Actually, the subject of neutron thermalisation can be classified into two separate problems: (a) the calculation of cross-sections characterising thermal neutron scattering in various materials and (b) the use of these cross-sections in the determination of the energy spectrum characterising low-energy neutrons (e.g. for use in determining thermal group constants for few-group diffusion calculations).

A detailed investigation of neutron energy spectrum below several eV becomes quite complex due to the complicated nature of the neutron scattering process. The energy of thermal neutrons is comparable to the binding energy of the atoms in molecular or crystalline material, and therefore the neutron will lean to interact with a collection of atoms rather than with a single nucleus (Massimo, 1975).

The fact that the kinetic energy of a neutron is comparable to thermal energy of atomic motion means that microscopic cross-sections must be regarded as averages over the thermal distribution of nuclear speeds and hence are temperature dependent. Furthermore, it will be possible for the neutron to gain energy (up-scattering) in a collision with a moving nucleus. This will complicate the numerical solution of the fine structure multigroup equations used to determine thermal spectra.

The energy of a neutron is comparable to the chemical binding energy of the scattering nuclei which means the nucleus will no longer recoil freely and therefore binding becomes significant in determining the energy and angle change in a collision.

Most of the complicated details of thermal neutron cross-section behaviour are of secondary importance in nuclear reactor analysis. Indeed in most large thermal power reactors the neutron energy is well thermalised that rather crude models of the neutron scattering process are sufficient for the generation of thermal group constants (Duderstadt, 1976).

3.4.2.1. Thermal Equilibrium

In thermalisation problems all source neutrons appear as fission neutrons slowing down into the thermal energy range and the absence of up-scattering above the thermal cut-off energy E_c implies that total rate of absorption in the thermal range is equal to the rate at which neutrons slow down into the thermal range.

$$\nu'\Sigma_s(E' \to E)M(E') = \nu\Sigma_s(E \to E')M(E).$$

The principle of detailed balance which is given by the above equation must be satisfied by any neutron cross-section characterising scattering from a system of nuclei in thermal equilibrium at temperature T, where $M(E)$ is the Maxwell-Boltzmann distribution function characterising the energies of particles of an ideal gas at temperature T (Duderstadt, 1976).

By setting the absorption and source terms to zero in the neutron continuity equation in an infinite medium gives the equation

$$\Sigma_s(E)\phi(E) = \int_0^\infty dE'\Sigma_s(E' \to E)\phi(E'). \tag{3.16}$$

The solution to the equation(3.16), regardless of the detailed form of the scattering cross-section, must be the neutron flux characterising neutrons in thermal equilibrium at the same temperature T as the scattering medium.

$$\phi(E) \to \phi_M(E) \equiv \nu n_0 M(E) = \frac{2\pi n_0}{(\pi kT)^{3/2}}\left(\frac{2}{m}\right)^{1/2} E\exp\left(-\frac{E}{kT}\right), \tag{3.17}$$

where n_0 is the neutron number density in the medium and k is the Boltzman constant.

The neutrons will be in thermal equilibrium if there are no mechanisms that tend to introduce

non-equilibrium behaviour. The effects of non-equilibrium perturbations are given in Figure 3-2. In a nuclear reactor core, even for a very thermal reactor the neutron distribution will never be precisely in thermal equilibrium. This is because of one of the following effects:

- presence of absorption,
- presence of sources,
- leakage of neutrons,
- time dependence.

Addition of an absorption term to equation (3.16) will shift the spectrum to higher energies, almost as if its temperature is effectively increased by the addition of absorption. This is known as "absorption heating" of the spectrum.

The opposite effect occurs for the presence of neutron leakage. Since the higher energy neutrons tend to leak more rapidly, the equilibrium spectrum will shift to lower energies, which is called the "diffusion cooling" effect.

The presence of a source term will also perturb the spectrum. With a source corresponding to neutrons slowing down from higher energies, the spectrum will behave as 1/E for energies above several eV.

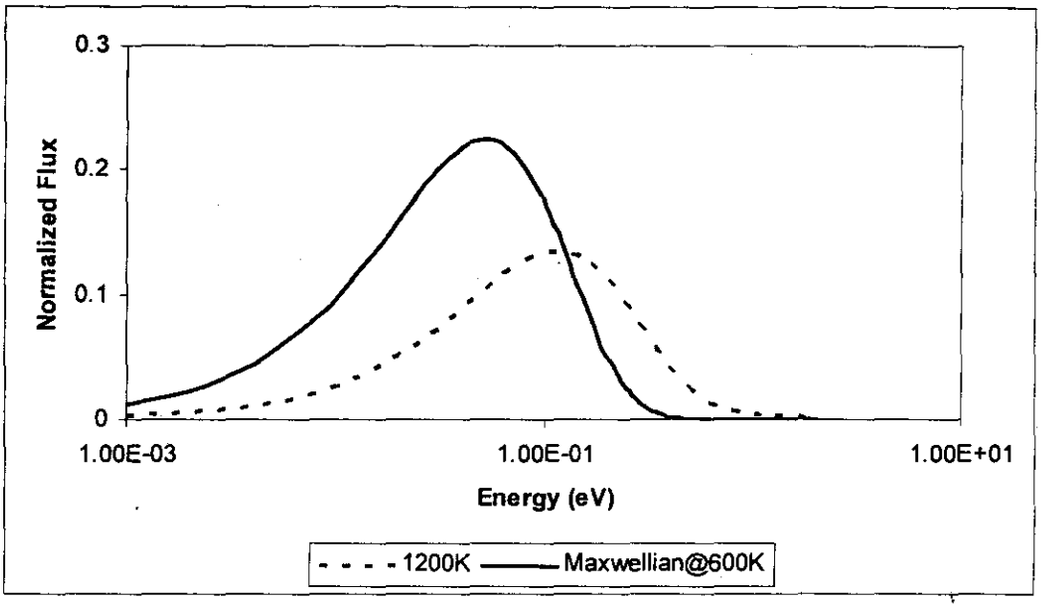

Figure 3-2: Effects of non-equilibrium perturbations on thermal spectrum.

A detailed discussion on the approximate models of the neutron thermalisation process is presented in Appendix H.

3.4.3. Coupling Between Fast and Thermal spectrum Calculations

Down-scattering from the higher energies provides the source term in the thermal range, while thermal neutron induced fissions will raise the fission source in the fast neutron region. The coupling between fast and thermal spectrum regions is sufficiently weak that the calculations of fast and thermal spectra are usually performed separately.

Although the fast and thermal spectrum calculations can be performed separately, fast spectrum calculation generates the P_0 and P_1 slowing down densities to be inserted into the thermal spectrum calculations. All down-scattered neutrons from the fast region are assumed to go into the highest energy thermal group.

3.5. Summary and Conclusion

In this chapter the theory for performing the neutron spectrum calculations and the generation of multigroup constants were discussed. The determination of the intragroup fluxes, i.e. neutron energy spectrum, is the key to the generation of group constants that will yield an accurate few-

group description of nuclear reactor behaviour.

It should be noted that a variety of data is required in order to determine the group constants. For example, basic cross-section data characterising the isotopes occurring in the reactor is required. This is usually provided in the form of fast and thermal libraries which gives these data as fine-group constants.

Next, the information concerning the composition and geometry of the core should be provided. Since the core composition varies throughout the core, it is usually required to generate different group constants for each region of the core in which the composition is significantly different. On a finer scale, the dimensions of the lattice cell for which the group constants are to be generated are necessary. The temperatures of the major components of the cell must be provided as well. The next chapter presents the calculation procedure of the above-mentioned data, and also the results of the spectrum calculations.

Chapter 4. Results of Neutron Spectrum Calculations

4.1. Introduction

This chapter presents the procedure followed in the macroscopic group constants generation based on the theory established in the previous chapter. The results of the spectrum calculations are also presented in this chapter.

4.2. Cross-section Library Processing

For thermal reactor calculations it is necessary to perform detailed spectrum calculations in a high number of energy groups with only a rough approximation of the spatial dependence and then to perform few-group space-dependent calculations with constants calculated by averaging the fine group cross-sections on this spectrum.

Various types of methods and codes are used to perform these multigroup spectrum calculations. All of these codes contain a library in a fine energy structure including cross-sections for all interesting reactions, transfer matrices (the $\Sigma^s_{0,i\to k}, \Sigma^s_{1,i\to k}$ or higher order components of the scattering cross-section), resonance parameters, fission spectra, etc. (Massimo, 1975: Chapter 8).

A working cross-section data library which is generated by processing the evaluated nuclear data files like ENDF/B or JEF is required for neutron calculations. There are various multigroup cross-section data sets available in the literature, as pointed out in the previous chapter, but to process the data available in those libraries one must know the format of data written on those libraries. Since the generation of a new multigroup cross-section set is outside the scope of this thesis and the information required for the other multigroup cross-section libraries is not available in the literature, spectrum calculations are based on the GAM-I and GATHER-I cross-section libraries, which are the most suitable cross-section libraries for the HTR calculations amongst the cross-section libraries available to use in this work.

GAM-I library contains data for 181 different materials and 18 different fission sources. Fast cross-section library reformatting function requires the identification number (see Appendix A.) of each

material of interest as input. Because the library is too large and cross-section data needs to be updated several times when necessary, the data of the materials which are of interest are written to a temporary file to be accessed by the other functions.

Since GATHER-I library is subdivided into two parts as absorbers and scatterers, thermal cross-section library reformatting function requires the id number of the absorbers and the four digit identification number of the scatterer which has been prepared with the lowest temperature (see Appendix A.) as input. The procedure followed in the thermal library reformatting is the same as the one followed in the fast library reformatting.

Absorption cross-sections of some materials of interest gathered from GAM-I and GATHER-I libraries are shown in Figure 4-1 below. The fission cross-sections for ^{238}U and ^{235}U are presented in Figure 4-2. As expected the absorption cross-section is larger in the thermal neutron energy range and the resonances in the epithermal energy range are observed in the ^{238}U data. Fission cross-sections can be separated into three regions; at low energies it is $1/\upsilon$ or nearly so; this is followed by a region of resonances; and, above the resonance region σ_f is smooth. In Figure 4-2, since the cross-sections are not continuous, the three distinct regions to the fission cross-section are not clearly seen.

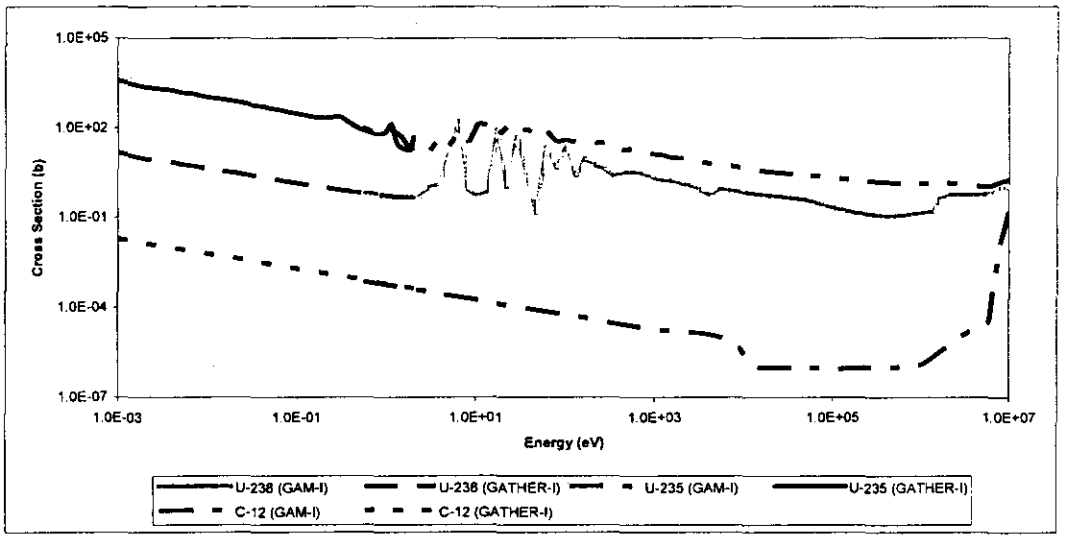

Figure 4-1: Absorption cross-sections of selected materials in complete neutron energy range.

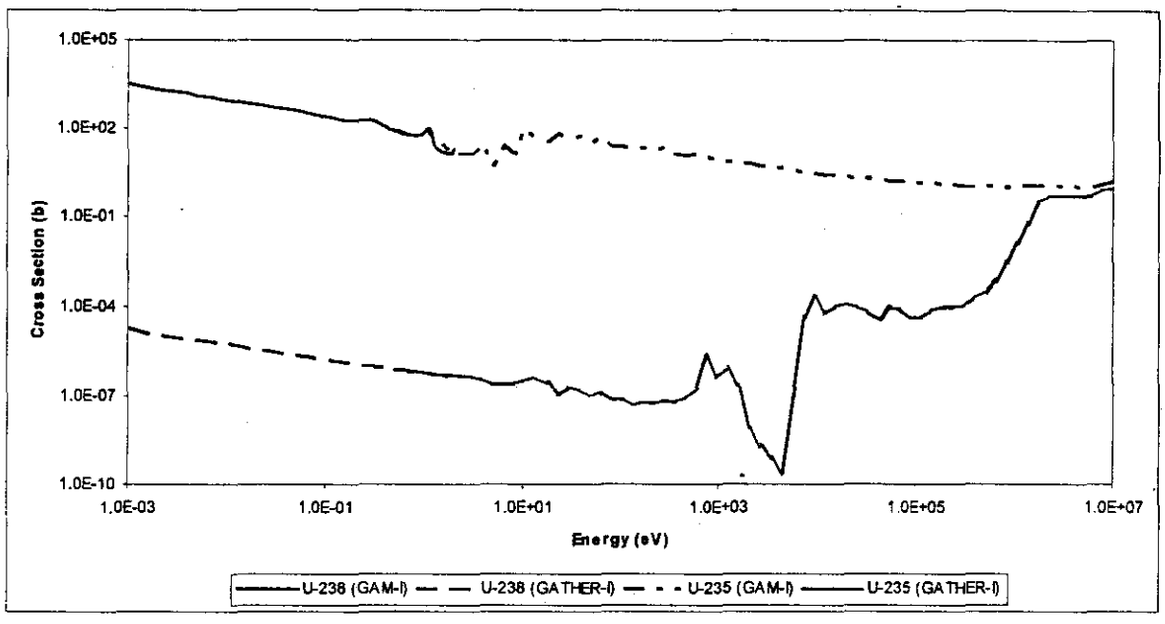

Figure 4-2: Fission cross-sections for U-238 and U-235.

Cross-sections and flux vary greatly as a function of neutron energy. Figure 4-3 shows an illustrative comparison of the variation of neutron flux and absorption cross-section with neutron energy. The fission source neutrons are born with an energy range of 1 to 10 MeV and they slowed down to the thermal energy range with scattering collisions. The absorption cross-section is larger in the thermal neutron energy range, which causes more neutrons to disappear with the capture reactions and lowers the neutron flux in the thermal energy range. The neutron flux is typically depressed at the energies where large resonances are present.

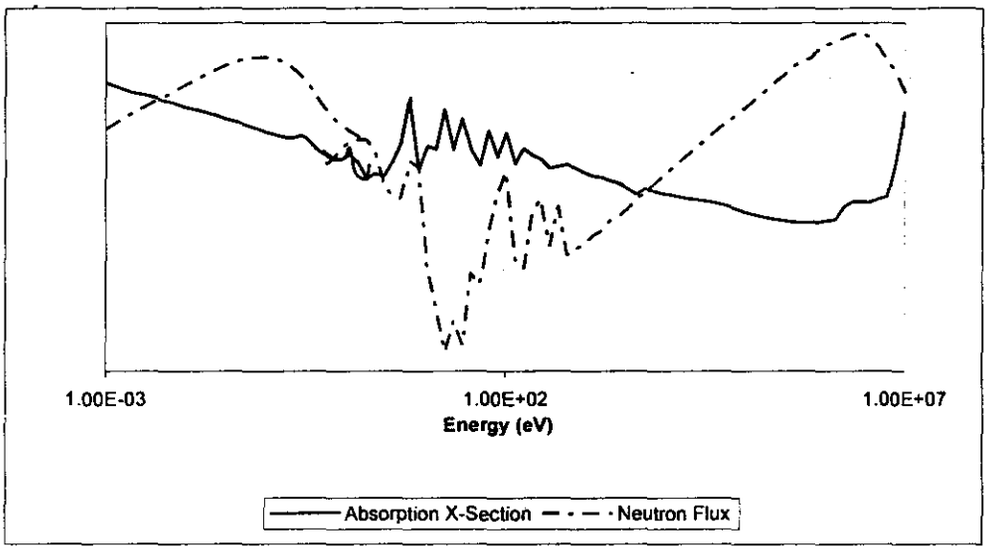

Figure 4-3: Variation of neutron spectrum and absorption cross-section with neutron energy.

4.3. Fuel Homogenisation

The effective cross-section calculation involves double homogenisation of the fuel spheres, which is illustrated in Figure 4-4. First, a homogenisation on grain level is performed and thereafter another one on pebble level. The grain cell has a spherical annular geometry. It consists of the fuel kernel, surrounded by spherical shells of the four coating layers. The volume ratios between the various spherical shells in this grain are the same as in the real pebble bed. The homogenised mixture is treated as the highly absorbing centres embedded in a graphite matrix for the calculation of effective cross-sections for the fuel zone. The pebble cell consists of a fuel zone of 2.5 cm in radius, a pebble shell with an outer radius of 3.0 cm and an outer shell with an outer radius of 3/ (packing fraction) $^{1/3}$ cm. The last shell contains the inter-pebble void and hence its volume depends on the packing fraction of the pebbles.

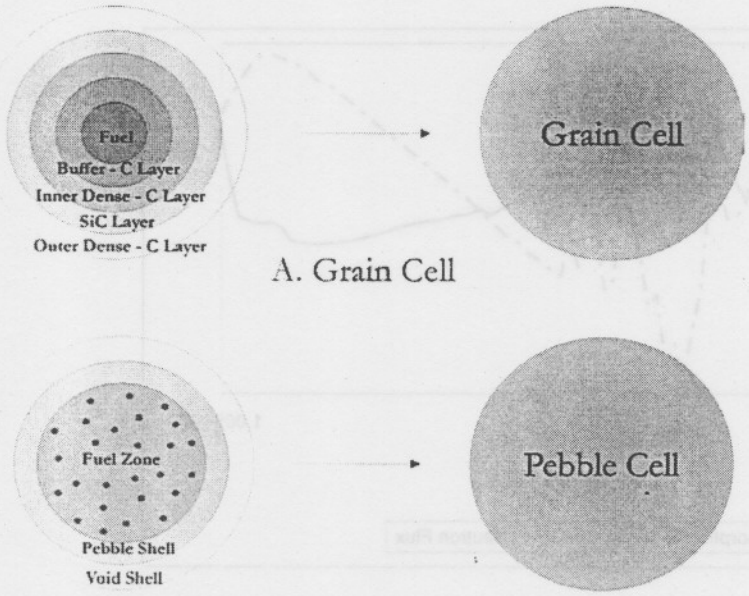

Figure 4-4: Two-step approach of homogenisation.

The homogenisation function calculates the atomic densities of the pebble geometry given in the input. It requires the geometric data of the pebble including the radii and the densities of the coating layers. A typical input data of the fuel pebble is given in Table 4-1, for which the calculated atom densities are given in Table 4-2.

Table 4-1: Fuel design input data.

Description	Value
Pebble radius (cm)	3.0
Fuel zone radius (cm)	2.5
Fuel type	UO2
Fuel theoretical density (g/cm^3)	10.69
Heavy metal loading (g/ball)	9
Fuel enrichment (%)	8
Kernel radius (cm)	455E-04
Graphite matrix density (g/cm^3)	1.75
Graphite shell density (g/cm^3)	1.75
Number of coating layers	4
Location of SiC layer	3
Fuel radius (cm)	250E-04
Coating layer thickness (cm)	
- layer1	95E-04
- layer2	40E-04
- layer3	35E-04
- layer4	35E-04
Coating layer density (g/cm^3)	
- layer1	1.05
- layer2	1.90
- layer3	3.18
- layer4	1.90

Table 4-2: Homogenised atom densities.

One-Region Data	
Isotope	Atom density (atoms/cm*barn)
C	5.536588E-02
U-35	9.833854E-06
U-38	1.130893E-04
O	2.458463E-04
Si	2.680142E-04
Two-Region Data	
Zone 1 – Fuel Zone radius of 2.5 cm	
Isotope	Atom density (atoms/cm*barn)
C	8.524458E-02
U-35	2.785721E-05
U-38	3.203579E-04
O-16	6.964303E-04
Si	7.592271E-04
Zone 1 – Graphite Shell thickness of 0.5 cm	
Isotope	Atom density (atoms/cm*barn)
C	8.774106E-02

The output of the homogenisation function contains the one-region homogenised atom densities for the fast and thermal spectrum calculations and the two-region (i.e. fuel zone and graphite shell)

homogenised atom densities for the calculation of self shielding factors.

4.4. Neutron Spectrum Calculations

The dimensions and the temperature of the spectrum zones are required as input to the fast and thermal spectrum calculation functions. Both functions are allowed for an unlimited number of spectrum zones. Prior to fast and thermal spectrum calculations, temporary files including the cross-section data of the materials of interest, fission spectrum and the resonance integrals data must be generated. Except the resonance data all other required files are created within the calculation procedure.

4.4.1. Fast Spectrum Calculations

The fast spectrum calculation function performs neutron flux evaluation in 68 energy groups ranging from 10^7 eV to 0.414 eV. It assumes the materials are homogeneously distributed and applies the P_1-approximation. Heterogeneous effects can be included with the self shielding factors. Cross-sections of the resolved and unresolved resonances can be included for ^{232}Th and ^{238}U. Resonance cross-section data is obtained from the pre-prepared resonance file for different temperatures of appropriate fuel designs.

4.4.2. Resonance Absorption

For the treatment of resonance integrals the ZUT code of the VSOP calculation system has been used. Resonance integrals for different fuel designs at various temperatures are written to an ASCII file for each fuel design to be accessed by the module. Although this limits the fuel design options, resonance data files for new fuel designs can easily be added to the module by running the ZUT code for the new fuel designs when necessary. The resonance integrals calculated for the 8 percent enriched, 9 gram heavy metal loaded fuels are shown in Table 4-3.

Table 4-3: Resonance integrals calculated with ZUT.

GAM-I	Resonance Integrals			
Group	300 K	600 K	900 K	1200 K
22	-9.296E-05	-8.688E-05	-8.242E-05	-7.888E-05
23	-1.930E-04	-1.818E-04	-1.737E-04	-1.672E-04
24	-3.076E-04	-2.923E-04	-2.808E-04	-2.710E-04
25	-4.375E-04	-4.081E-04	-3.869E-04	-3.695E-04
26	-5.356E-04	-4.730E-04	-4.330E-04	-4.029E-04
27	-5.997E-04	-4.851E-04	-4.198E-04	-3.749E-04
28	-7.436E-04	-5.556E-04	-4.575E-04	-3.947E-04
29	-1.072E-03	-7.815E-04	-6.400E-04	-5.534E-04
30	-1.654E-03	-1.223E-03	-1.016E-03	-8.898E-04
31	-2.647E-03	-2.011E-03	-1.704E-03	-1.516E-03
32	1.327E-01	1.346E-01	1.346E-01	1.351E-01
33	2.169E-01	2.191E-01	2.211E-01	2.219E-01
34	2.804E-01	2.852E-01	2.877E-01	2.893E-01
35	3.546E-01	3.625E-01	3.667E-01	3.695E-01
36	3.230E-01	3.304E-01	3.342E-01	3.367E-01
37	4.614E-01	4.760E-01	4.840E-01	4.894E-01
38	6.308E-01	6.510E-01	6.613E-01	6.677E-01
39	7.136E-01	7.417E-01	7.563E-01	7.656E-01
40	6.976E-01	7.219E-01	7.339E-01	7.415E-01
41	5.255E-01	5.364E-01	5.432E-01	5.465E-01
42	8.439E-01	8.992E-01	9.281E-01	9.480E-01
43	1.205E+00	1.290E+00	1.333E+00	1.364E+00
44	1.811E+00	2.021E+00	2.164E+00	2.271E+00
45	5.645E-01	5.741E-01	5.787E-01	5.816E-01
46	4.480E+00	5.148E+00	5.609E+00	5.964E+00
47	1.057E+00	1.090E+00	1.108E+00	1.120E+00
48	4.305E+00	5.076E+00	5.605E+00	6.009E+00
49	1.883E-02	1.883E-02	1.884E-02	1.884E-02
50	5.896E-01	6.048E-01	6.267E-01	6.622E-01
51	9.591E+00	1.111E+01	1.235E+01	1.338E+01
52	2.153E-01	2.155E-01	2.158E-01	2.160E-01
53	1.617E+01	1.891E+01	2.096E+01	2.262E+01
54	1.080E-01	1.081E-01	1.081E-01	1.081E-01
55	0.000E+00	0.000E+00	0.000E+00	0.000E+00
56	1.840E-01	1.841E-01	1.842E-01	1.843E-01
57	3.235E+01	3.677E+01	3.996E+01	4.231E+01
58	2.557E+00	2.704E+00	2.981E+00	3.436E+00
59	2.335E-01	2.337E-01	2.340E-01	2.342E-01
60	1.131E-01	1.132E-01	1.132E-01	1.132E-01

The ZUT code evaluates the resonance integrals of the isotopes ^{232}Th and ^{238}U. The corresponding absorption cross-sections are added to the background absorption cross-sections of the GAM-I library, which are independent of fuel lumping and temperature.

4.4.3. Thermal Spectrum Calculations

The thermal spectrum function performs direct solution of the infinite medium spectrum equation for 96 energy group ranging from 2.1 eV to 0 eV. It adds a crude spatial treatment in a similar manner to that used in fast spectrum calculation. Thermal leakage is determined by specifying an equivalent geometric buckling B_g^2. Again the additional heterogeneity effects can be included with the self shielding factors. The effect of coated particle grain structure can be included by evaluation of the collision probability for a neutron which travels through a coated particle.

The thermal cross-section library GATHER-I contains data of scattering kernels for different scattering nuclides at different temperatures. The four digit thermal library identification number of the scattering kernel (see Appendix A.) for each scatterer at the lowest temperature must be given in the input. The module uses the scattering kernel at the appropriate temperature for each spectrum zone.

The evaluated neutron fluxes for thermal and fast energy ranges are given in Figure 4-5 to Figure 4-7.

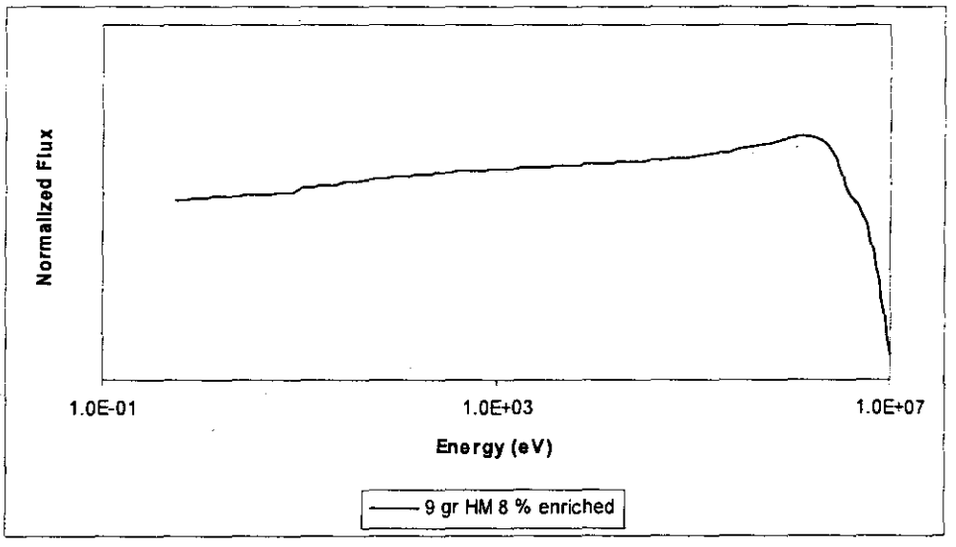

Figure 4-5: Fast neutron spectrum for 8 % enriched fuel.

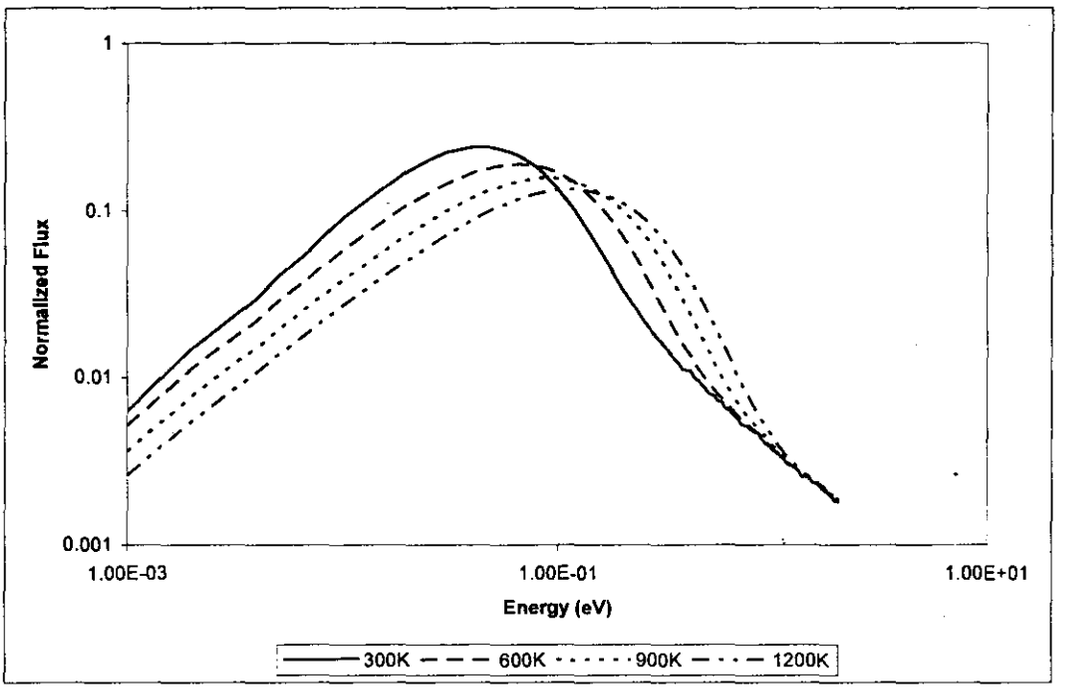

Figure 4-6: Thermal neutron spectrum for 8% enriched fuel at different temperatures.

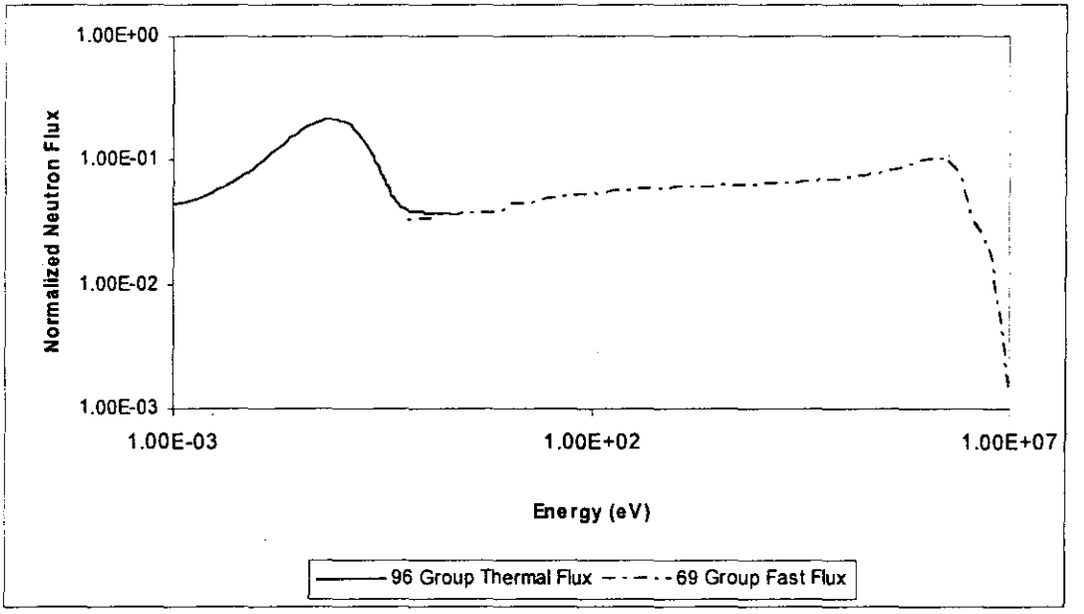

Figure 4-7: Neutron Spectrum for 8% enriched fuel.

In Figure 4-5 the fast spectrum is represented by 69 energy groups. The resonances affect the 1/E shape of the spectrum in the epithermal energy range. The thermal spectrum in Figure 4-6 shows the effects of the non-equilibrium perturbation in the thermal energy range. Due to the increase in the temperature, the spectrum shifts to the higher energies. The spectrum tends to behave like 1/E above several eV due to the presence of the slowing down source.

As seen in Figure 4-7 there is an overlapping in the fast and thermal energy groups. To solve this problem, in the macrogroup constant generation process the overlapped groups can be weighted with the suitable values. A group reduction is performed to show the 1/E behaviour of the neutron spectrum in the epithermal energy range. The energy range where the resonances occur is reduced to three energy group and the 8 group fast flux curve represents the depression of the flux near the resonances.

4.5. Macrogroup Constant Generation

The resulting neutron fluxes of fast and thermal spectrum calculations are applied to form broad group cross-sections for the subsequent diffusion calculation. The number of broad groups should be selected equal or greater than two. In the thermal energy range only one broad group is possible since up-scattering is not included in the energy group collapsing (macrogroup constants preparation).

The fast flux is the source term of the thermal neutrons (by scattering down in energy), while the thermal flux is the source for the fast neutrons by the fission event. So it follows that one would expect to see an abundance or peak of fast neutrons in the fuel region (because that is where fission takes place). They diffuse to the moderator where there is a high probability of slowing down (because of the materials used there for just this reason). Hence one would expect to see peak of thermal neutrons in the moderator. This is illustrated by Figure 4-8 below. The fluxes are generated with fuel balls in an infinite medium of graphite (moderator).

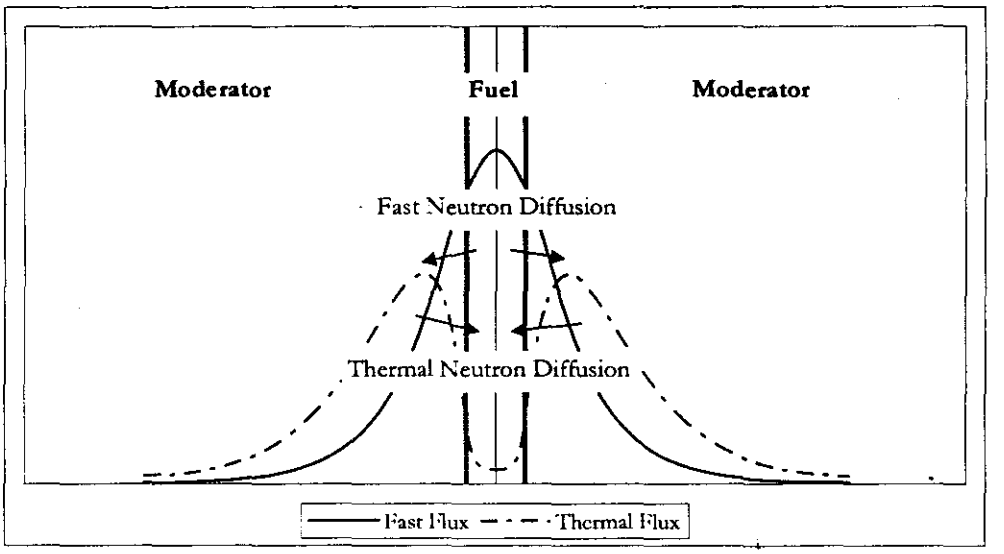

Figure 4-8: Spatial distribution of neutron flux.

The broad group structure (i.e. number of groups and the energy boundaries) must be specified in the input. A four group broad group structure with two epithermal groups is presented in Table 4-4 below.

Table 4-4: Broad group energy structure (four groups).

Description	Desired Energy (eV)	Actual Energy Used (eV)
Fast group	1000000	1000000
First epithermal group	52500	52475.18
Second epithermal group	29	29.02320
Thermal group	1.86	1.855391

The macroscopic group constants generation function first checks the group structure with respect to the group structure of the fine-group cross-section libraries, and then it calculates the appropriate broad group energy boundaries if necessary. After specifying the broad group structure, the ratio of the fission source distribution is calculated for the broad groups to be used in the diffusion calculation. The calculated four-group fission source distribution of U-235 fission spectrum is given in Table 4-5.

Table 4-5: U-235 fission spectrum in four-group.

Description	Fission Source Ratio
Fast group	9.948226E-01
First epithermal group	5.184445E-03
Second epithermal group	6.769019E-08
Thermal group	0.00000E+00

With the knowledge of few-group structures, the calculated neutron flux is then used to generate the few-group constants. For broad group i, with corresponding fine-groups from group g to group $g-1$, the absorption cross-section for broad group i is given by

$$\Sigma_a^i = \frac{\int_{\varepsilon}^{\varepsilon-1} \Sigma_a(u)\phi(u)du}{\int_{\varepsilon}^{\varepsilon-1} \phi(u)du}. \qquad (4.1)$$

After generating the energy averaged few-group constants, a one-dimensional multigroup diffusion calculation in spherical coordinates with white boundary conditions is performed in two regions, i.e. fuel and moderator, for each spectrum zone. This one-dimensional diffusion calculation is based on finite difference solution method which is described in more detail in later chapters (Chapter 5.). The calculated 1D 4-group fluxes are given in Figure 4-9. The fast flux within the fuel region is higher due to the fission source neutrons. Because of the energy loss in the scattering collisions with the moderator nucleus the fast flux decreases in the moderator region, where the slowing down takes place, while the epithermal and thermal fluxes increases. The thermal flux in the fuel region is lower due to higher absorption cross-section of the fuel material.

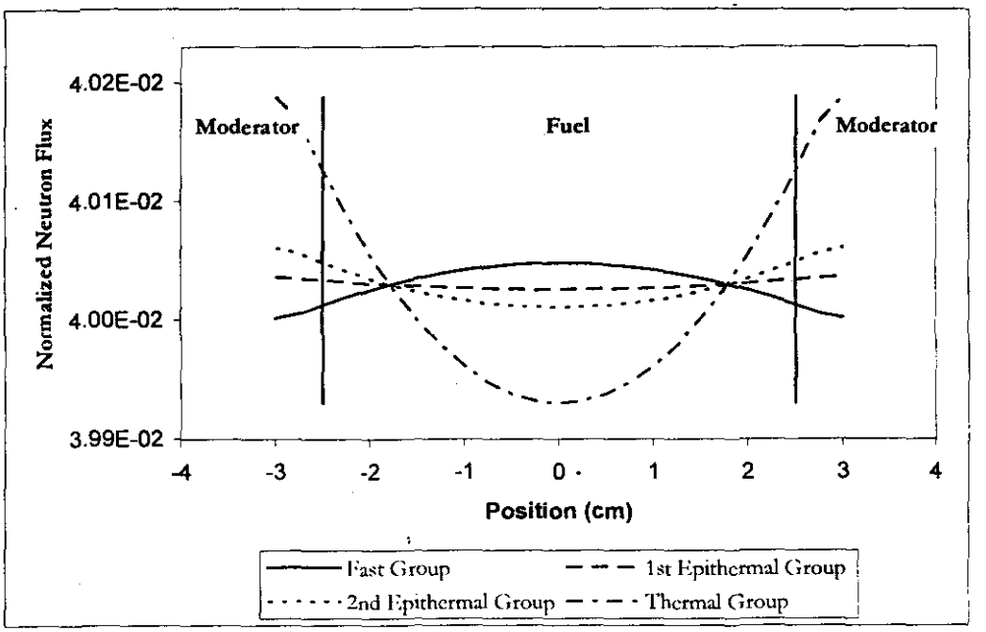

Figure 4-9: One-dimensional 4-group fluxes for 8% enriched fuel.

The spatial averaging is applied to obtain the self-shielding factors which are supplied to the spectrum calculations. The self-shielding factor f_s is defined as

$$f_s \equiv \frac{\bar{\phi}_F}{\bar{\phi}_{\text{hom}}}, \tag{4.2}$$

where, $\bar{\phi}_F$ is the average flux in the fuel and $\bar{\phi}_{\text{hom}}$ is the average flux in the cell and given by

$$\bar{\phi}_{\text{hom}} = \left(\frac{V_F}{V_{Cell}}\right)\bar{\phi}_F + \left(\frac{V_M}{V_{Cell}}\right)\bar{\phi}_M. \tag{4.3}$$

Here, in equation(4.3), V is the volume and subscripts F and M refer to the fuel and moderator respectively.

The self-shielded cross-sections are then used to adjust the fine-group cross-section data used in the spectrum calculation. The broad group values of the self shielding factors are applied to all of the fine

groups in its energy range. The spectrum obtained from these shielded or cell averaged fine group constants is usually much closer to the spectrum in the cell, and averaging the shielded fine group constants over this spectrum provides adequate cell-averaged cross-sections (Duderstadt, 1976: Chapter 10).

Figure 4-10 represents the change in the values of the calculated neutron fluxes due to the self-shielding. Here, the chart (B) is the normalised neutron flux calculated with the self shielded macroscopic cross-sections. Due to the shielding of the homogenized fuel material in the graphite matrix the thermal flux increases in the fuel zone, which means the efficiency of the graphite in coatings and matrix is increased.

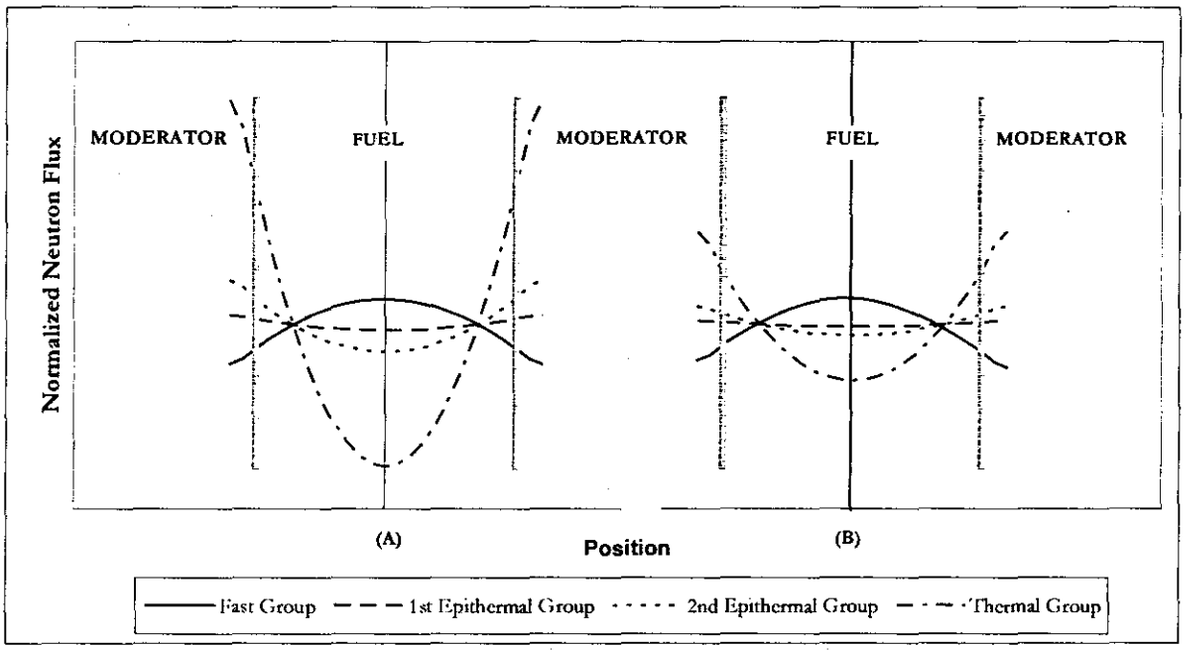

Figure 4-10: Broad group neutron fluxes before and after self shielding calculations.

4.6. Summary and Conclusions

The multigroup diffusion equations are capable of yielding the neutron flux in a nuclear reactor core to a sufficient degree of accuracy for most of the reactor core design problems, provided adequate care is

taken with the determination of the multigroup constants in these equations. The solution of the multigroup diffusion equations is rather straightforward. Most of the effort was expended in the generation of the group constants, for these group constants have to account for the rather complicated energy dependence of the intragroup fluxes used in the averaging basic cross-sections data, as well as for the spatial neutron transport effects arising in core lattices.

Multigroup analysis of a reactor core consists of two principal tasks: (a) generation of the multigroup constants and (b) solution of the multigroup diffusion equations. Generation of the multigroup constants is analysed in the previous chapter and the results are given in this chapter. The next chapter starts with the second task of reactor analysis: solution of the multigroup diffusion equation.

Chapter 5. Criticality and the Flux and Power Distribution Calculations

5.1. Introduction

In the previous chapters it was mentioned that the neutrons produced by fission have a range of high energies, up to about 10 MeV. Neutrons have energies in a reactor core ranging from 10 MeV to 0.001 eV as a result of various interactions. Furthermore, the neutron-nuclear cross-sections depend sensitively on the incident neutron energy. Hence, practical reactor calculations require a more realistic but rather more complicated treatment of the energy dependence than the one-speed diffusion equations.

The previous two chapters presented the generation of few-group constants, which are introduced to the multigroup diffusion equations. Recalling the rather detailed dependence of neutron cross-sections on neutron energy E, it can be expected that so many energy groups would be necessary to adequately describe a nuclear reactor. However, most nuclear reactor calculations achieve sufficient accuracy using only few-group diffusion descriptions.

Whereas a basic introduction to multigroup diffusion equations was given in chapter two, this chapter explains the theory in more detail and explains the solution methodology for these equations. In this chapter a heuristic derivation of the multigroup equations based on the concept of neutron balance is presented, and a more rigorous derivation methodology is presented in Appendix C. Then the common calculation strategies which are useful to solve these sets of coupled partial differential equations will be discussed.

5.2. Multigroup Diffusion Equation

The most straightforward manner in which to arrive at the form of the multigroup diffusion equations is to apply the concept of neutron balance to a given energy group, thereby balancing the ways in which neutrons can enter or leave this group. Consider a typical energy group g as shown in Figure 5-1. Neutron balance for such a group typically reads as follows:

$$\begin{bmatrix}\text{Time rate of}\\ \text{change of}\\ \text{neutrons in}\\ \text{group g}\end{bmatrix} = -\begin{bmatrix}\text{change due}\\ \text{to}\\ \text{leakage}\end{bmatrix} - \begin{bmatrix}\text{absorption}\\ \text{in}\\ \text{group g}\end{bmatrix} + \begin{bmatrix}\text{source}\\ \text{neutrons}\\ \text{appearing}\\ \text{in group g}\end{bmatrix} - \begin{bmatrix}\text{neutrons}\\ \text{scattering}\\ \text{out of}\\ \text{group g}\end{bmatrix} + \begin{bmatrix}\text{neutrons}\\ \text{scattering}\\ \text{into}\\ \text{group g}\end{bmatrix}. \tag{5.1}$$

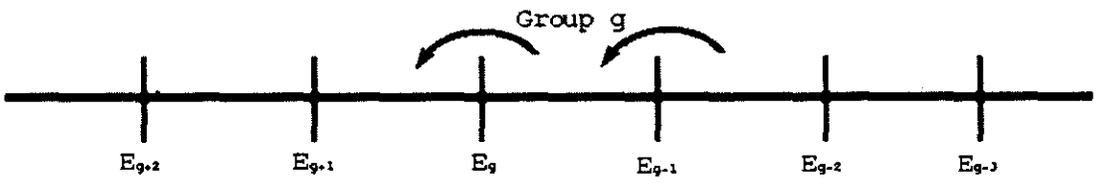

Figure 5-1: Typical energy group g.

A scattering collision can change the neutron energy and hence either remove it from the group g, or if it is initially in another group g', scatter it into energy in the group g. The probability for scattering a neutron from a group g' to the group g is characterised by group-transfer cross-section, $\Sigma_{sg'g}$, which is similar to the differential scattering cross-section $\Sigma_s(E' \to E)$ (Duderstadt, 1976). The cross-section characterising the probability that a neutron will scatter out of the group g is then given by

$$\Sigma_{sg} = \sum_{g'=1}^{G} \Sigma_{sg'g}. \tag{5.2}$$

An absorption cross-section, Σ_{ag} characterising the group g and a source term S_g giving the rate at which source neutrons appear in group g can be defined similarly. Finally, the diffusion coefficient D_g is defined so that the leakage from group g can be written within the diffusion approximation as $\nabla \cdot D_g \nabla \phi_g$. The mathematical presentation of the balance relation, Eq.(5.1), can be obtained with combining all these terms, as

$$\frac{1}{v_g}\frac{\partial \phi_g}{\partial t} = \nabla \cdot D_g \nabla \phi_g - \Sigma_{ag}\phi_g + S_g - \Sigma_{sg}\phi_g + \sum_{g'=1}^{G}\Sigma_{sg'g}\phi_{g'}, \quad g' = 1,2,...,G. \tag{5.3}$$

The source term can be written as

$$S_g = \chi_g \sum_{g'=1}^{G} v_{g'}\Sigma_{fg'}\phi_{g'} + S_g^{ext}, \tag{5.4}$$

where χ_g is the probability that a fission neutron will be born with an energy in group g, while $\Sigma_{fg'}$ is the fission cross-section characterising a group g' and $v_{g'}$ is the average number of neutrons released in a fission reaction induced by a neutron in group g'.

5.3. Strategies for Solving Multigroup Equations

The distribution of the neutron flux in energy and space is required for the purpose of reactor analysis. In actual calculations the complexity is reduced in two steps: (1) the reactor system is divided into regions in which the composition can be assumed to be constant. The group constants are then essentially independent of the space coordinates in each region. With these simplifications the group fluxes can be determined by solving the multigroup equations. This is called the "fine group" calculations. (2) Several energy groups are combined into a single "macrogroup". Macrogroup of few-group cross-sections and diffusion coefficients, evaluated from the microgroup cross-sections, when combined with the appropriate neutron fluxes, give good approximation to the rates of neutron interactions. The few-group constants are now used in the determination of the spatial distribution of the neutron flux.

5.3.1. Separation of Energy and Space Dependence

Few-group constants as defined above are still depend on space and energy. They will be constant only in the case in which the neutron flux is of the separable form

$$\phi(r,E) = \psi(r)\varphi(E). \tag{5.5}$$

In which case they reduce to group averages over the neutron flux energy spectrum $\varphi(E)$. The separation of the treatment of energy and space dependence in multigroup diffusion theory

leads, first to a crude description of the flux spatial dependence to generate a detailed representation of the energy spectrum $\varphi(E)$ suitable for the generation of multigroup constants. These group constants may then be used in a few-group diffusion analysis of the reactor in which the energy dependence of the flux is treated rather coarsely, while more detailed spatial dependence is considered.

These equations are solved by using finite difference methods to discretise the spatial variable and then, following the usual inner-outer iteration strategy, solving for the criticality eigenvalue k_{eff} and the corresponding multigroup flux $\phi_g(r)$. To be more precise, the reactor core is broken up into a spatial grid or mesh, for example, with M mesh cells. Then the multigroup diffusion equation is integrated over a typical cell, and standard sum and difference formulas are used to represent the terms in the equation. Hence the multigroup diffusion equations are replaced by a $M \times G$ set of algebraic equations, that is, a $(M \times G)$ dimension matrix eigenvalue problem,

$$\underline{\underline{M}}\underline{\phi} = \frac{1}{k}\underline{\underline{F}}\underline{\phi}.$$

The elements of the matrices $\underline{\underline{M}}$ and $\underline{\underline{F}}$ are the few-group constants supplied by a macroscopic cross-section module and k is the eigenvalue of the problem. The matrix eigenvalue problem can then be solved by standard power iteration methods (usually accelerated by source extrapolation) (Clark, 1964).

An accurate description of the flux and power distribution in the reactor core using the finite differenced multigroup diffusion equations requires that the mesh spacing be at least comparable to (or less than) the minimum neutron diffusion length in the core (~0.5 cm in a LWR, ~4-5 cm in a HTR). Table 5-1 and Table 5-2 show the mesh point requirements for various reactor types. It has been found that accurate multigroup diffusion calculations of the global power distribution typically require between two and nine energy groups for thermal reactor analysis (Massimo, 1975).

Table 5-1: Mesh point requirements for MGD analysis of various reactor types (continued) (Based on a 3000 MWth core) (Duderstadt, 1976).

Reactor Type	Core Volume (m^3)	Core –Averaged Power Density (W/cm^3)	Characteristic Diffusion Length (cm)	Diameter of Reactor in Diffusion Lengths
PWR	40	75.0	1.8	190
BWR	60	50.0	2.2	178
HTR	430	7.0	12.0	63
LMFBR	5.7	530.0	5.0	36
GCFR	10.7	280.0	6.6	33

Table 5-2: Mesh point requirements for MGD analysis of various reactor types (concluded) (Based on a 3000 MWth core) (Duderstadt, 1976).

Reactor Type	Necessary Number of Mesh Points (one per Diffusion Length)		Number of Groups (Thermal Groups)	Necessary Number of Group – Space Mesh Points (One per Diffusion Length)		
	2D	3D		1D	2D	3D
PWR	36 100	6 859 000	4 (1)	760	144 400	27 436 000
BWR	31 666	5 635 000	4 (1)	712	126 664	22 540 000
HTR	3 947	247 969	7 (4)	441	27 629	1 735 783
LMFBR	1 270	45 270	10 (0)	360	12 700	452 700
GCFR	1 115	37 253	10 (0)	330	11 150	372 530

An alternative approach is to use so-called finite element techniques to calculate the neutron flux at each of a number of ultra coarse-mesh points (Naito et al, 1981). Such finite element methods have been used for some time in performing calculations in mechanical stress analysis, and appear to have considerable potential for multidimensional neutron diffusion calculations.

Other coarse-mesh techniques have been developed that utilise a mesh structure of the order of one mesh point per fuel assembly. However in order to ensure the stability of such techniques, it is usually necessary to alternate between coarse and fine mesh calculation. This latter scheme, known as coarse-mesh rebalancing, also appears to have considerable potential for improved accuracy and accelerating multigroup diffusion calculations (Gregory and Honeck, 1976;Dodds et al, 1975).

There is yet another alternative to a direct multidimensional diffusion calculation that has proven remarkably successful in reactor analysis, namely the so-called flux synthesis method, in which a multidimensional flux is "synthesised" from a combination of one or two dimensional calculations. Most multigroup diffusion codes usually have the capability of computing not only the neutron fluxes $\phi_g(r)$ but also their adjoints $\phi_g^\dagger(r)$ (Cardoso et al, 1996). These quantities are extremely useful in making the perturbation theory estimates of reactivity changes due to the

changes in core composition or configuration.

Although perturbation theory is capable of only limited accuracy, it can provide useful initial guesses for more detailed diffusion calculations. And since one can frequently calculate the adjoint fluxes with only slightly more effort than that involved in simply calculating the fluxes by themselves, many design codes have been developed with perturbation theory options.

5.3.2. Energy Discretisation

An additional simplification of the multigroup equations is achieved by selecting the group spacing such that the neutrons will only scatter to the next lowest group,

$$\sum_{g'=1}^{G} \Sigma_{g'g}^{S} \phi_{g'} = \Sigma_{g-1,g}^{S} \phi_{g-1} + \Sigma_{gg}^{S} \phi_{g}. \tag{5.6}$$

In this case the multigroup equations are directly coupled. Alternative types of multigroup coupling are given in Figure 5-2.

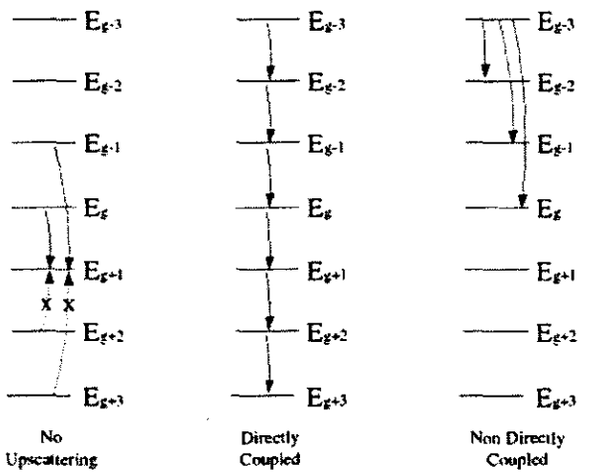

Figure 5-2: Different types of group coupling.

In this case, multigroup equations can be written with ignoring spatial dependence and the presence of an external source as

$$-\nabla\cdot D_g\nabla\phi_g-\Sigma_g^R\phi_g=\sum_{g'=1}^{G}\Sigma_{g'\to g}^S\phi_{g'}+\frac{1}{k}\chi_g\sum_{g'=1}^{G}\nu_{g'}\Sigma_{g'}^f\phi_{g'},$$
$$\text{where}\quad \Sigma_g^R\equiv\Sigma_g^t-\Sigma_{g\to g}^S. \tag{5.7}$$

or in matrix form

$$\begin{pmatrix}-\nabla\cdot D_1\nabla+\Sigma_1^R & 0 & 0 & \cdots\\ -\Sigma_{12}^S & -\nabla\cdot D_2\nabla+\Sigma_2^R & 0 & \cdots\\ -\Sigma_{13}^S & -\Sigma_{23}^S & -\nabla\cdot D_3\nabla+\Sigma_3^R & \cdots\\ \vdots & \vdots & \vdots & \ddots\end{pmatrix}\begin{pmatrix}\phi_1\\ \phi_2\\ \phi_3\\ \vdots\end{pmatrix}$$
$$=\begin{pmatrix}\nu_1\chi_1\Sigma_1^f & \nu_2\chi_1\Sigma_2^f & \nu_3\chi_1\Sigma_3^f & \cdots\\ \nu_1\chi_2\Sigma_1^f & \nu_2\chi_2\Sigma_2^f & \nu_3\chi_2\Sigma_3^f & \cdots\\ \nu_1\chi_3\Sigma_1^f & \nu_2\chi_3\Sigma_2^f & \nu_3\chi_3\Sigma_3^f & \cdots\\ \vdots & \vdots & \vdots & \ddots\end{pmatrix}\begin{pmatrix}\phi_1\\ \phi_2\\ \phi_3\\ \vdots\end{pmatrix}. \tag{5.8}$$

and in closed form

$$\underline{\underline{M}}\,\underline{\phi}=\frac{1}{k}\underline{\underline{F}}\,\underline{\phi}. \tag{5.9}$$

The neglect of upscattering led to a lower triangular form for the "diffusion" matrix $\underline{\underline{M}}$. The fission matrix $\underline{\underline{F}}$ is full, since fission neutrons induced by a neutron absorption in a lower group will appear distributed among the higher energy groups.

In the case of directly coupled groups, $\underline{\underline{M}}$ becomes a simple bidiagonal matrix of the form:

$\underline{\underline{M}}=$ 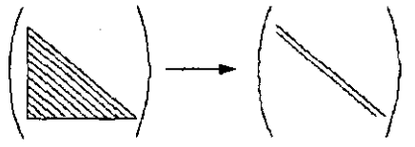

By way of contrast, if several groups assigned to thermal energy range in which upscattering occurs, there will be a full submatrix within $\underline{\underline{M}}$ corresponding to $\Sigma_{g'\to g}^S$ $\Sigma_{g'\to g}^S$ for g' or g in the thermal range.

$$\underline{\underline{M}} = \left(\quad \right)$$

5.3.3. Spatial Discretisation

The geometry of interest discretised into a mesh of cells such as the rectangular grids illustrated in Figure 5-3.

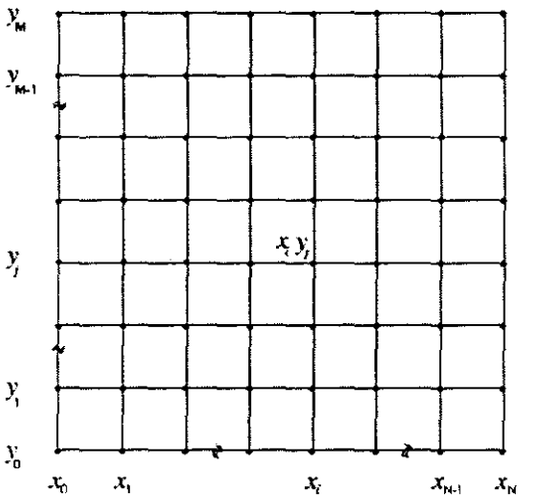

Figure 5-3: Two-dimensional spatial mesh

The most general way to derive difference equations for the mesh is to integrate the diffusion equation over the spatial volume of a given mesh cell. The spatially averaged cell properties are defined as:

$$\begin{aligned}
&\frac{1}{V_i}\int_{V_i} d^3r\phi(r) \equiv \phi_i, \\
&\frac{1}{V_i}\int_{V_i} d^3r\Sigma^a(r)\phi(r) \approx \Sigma_i^a\phi_i, \\
&\frac{1}{V_i}\int_{V_i} d^3r\left[-\nabla\cdot D(r)\nabla\phi\right] \approx L_i\phi_i - \sum_j^J l_{ij}\phi_j, \\
&\frac{1}{V_i}\int_{V_i} d^3rS(r) \equiv S_i.
\end{aligned} \tag{5.10}$$

Here the sum is taken over the adjacent mesh point neighbours, j = 1... J where J = 2, 4, or 6 in1-, 2-, or 3-dimensional Cartesian geometries, while

$$L_i = \sum_{j=1}^{J} l_{ij}, \tag{5.11}$$

where the mesh coupling coefficients l_{ij} are determined by the particular mesh geometry and finite-difference scheme.

The multigroup equations in two-dimensional coordinates can be written as:

$$\begin{aligned}
&\frac{\partial}{\partial x}\left(D_g(x,y)\frac{\partial\phi_g}{\partial x}\right)+\frac{\partial}{\partial y}\left(D_g(x,y)\frac{\partial\phi_g}{\partial y}\right)+\Sigma_g^t(x,y)\phi_g(x,y) \\
&\qquad -\sum_{g'=1}^{G}\Sigma_{g'\to g}^S(x,y)\phi_{g'}(x,y) = \\
&\qquad \frac{1}{k}\chi_g(x,y)\sum_{g'=1}^{G}\nu_{g'}\Sigma_{g'}^f(x,y)\phi_{g'}(x,y)+S_g(x,y).
\end{aligned} \tag{5.12}$$

In Cartesian coordinates, using the simplest approximation schemes for the integrals by expressing them as the value of the integrand evaluated at the mesh point x_i, y_j times the integration interval. To handle the derivative terms, simply using the central difference formula, we have:

$$\left.\frac{\partial^2\phi}{\partial x^2}\right|_{x_i,y_i} \approx \frac{\phi_{i-1,j}-2\phi_{i,j}+\phi_{i+1,j}}{(\Delta x)^2},$$
$$\left.\frac{\partial^2\phi}{\partial y^2}\right|_{x_i,y_i} \approx \frac{\phi_{i,j-1}-2\phi_{i,j}+\phi_{i,j+1}}{(\Delta y)^2}. \tag{5.13}$$

Using the above scheme in two-dimensional grid we find

$$l_{ij} = D_{ij}/\Delta_{ij}^2, \tag{5.14}$$

where $D_{ij}=\frac{1}{2}\left(D_i+D_j\right)$ and Δ_{ij} are defined as the distance between mesh points i,j. Then the general structure of finite-differenced multigroup equations takes the form

$$\left[\Sigma_R^g+\sum_j^J\frac{D_{ij}^g}{\Delta_{ij}^2}\right]\phi_i^g-\sum_j^J\frac{D_{ij}^g}{\Delta_{ij}^2}\phi_j^g-\sum_{g'=1}^{g-1}\Sigma_S^{g'\to g}\phi_i^{g'}=\frac{1}{k}\chi^g\sum_{g'=1}^{G}\nu^{g'}\Sigma_f^{g'}\phi_i^{g'}. \tag{5.15}$$

In addition to the coupling to different energy group fluxes at a given mesh point due to the fission source and scattering, the finite difference equation is coupled to the flux at adjacent spatial mesh points because of the effect of spatial distribution. If the number of groups is G and the number of spatial mesh points is N, we have $G\times N$ simultaneous linear algebraic equations. We have $G\times N$ equations available to determine $G\times N-1$ fluxes and the multiplication factor k_{eff}. This set of equations can be written as a matrix eigenvalue problem as

$$\underline{\underline{M}}\,\underline{\phi}=\frac{1}{k}\underline{\underline{F}}\,\underline{\phi}. \tag{5.16}$$

The general iterative strategy for solving this eigenvalue problem one first makes an initial guess of the source vector $\underline{S}^{(0)}$ and the multiplication eigenvalue $k^{(0)}$. At this point one proceeds to solve the inhomogeneous matrix equation for the flux $\underline{\phi}^{(n+1)}$,

$$\underline{\underline{M}}\,\underline{\phi}^{(n+1)}=\frac{1}{k^{(n)}}\underline{S}^{(n)}. \tag{5.17}$$

This solution involves a number of substeps:

(1) Solving the inhomogeneous diffusion equation characterising each of the energy groups g by solving first for the highest energy group, g=1 (with $\underline{\underline{R}}_0 \equiv 0, \underline{\phi}_0^{(n)} \equiv 0$), and then using $\underline{\phi}_1^{(n+1)}$ to solve for $\underline{\phi}_2^{(n+1)}$ and so on, solving successively down the groups. Noting that the fission source term is a very small value for all but the highest energy group. Depending on the energy group structure selected it can be zero for all other energy groups than the highest energy group, i.e. $\chi_g = 0$ for $g > 1$. Furthermore, the highest energy group obviously has no slowing down source. For a four-group, five-by-four spatial mesh problem, each matrix in the group inhomogeneous equation has $(5\times 4)^2 = 400$ elements, while the flux and source vectors have 20 elements.

$$\underline{\underline{A}}_g \underline{\phi}_g^{(n+1)} = \frac{1}{k^{(n)}} \underline{S}_g^{(n)} + \underline{\underline{R}}_{g-1} \underline{\phi}_{g-1}^{(n)} \equiv \underline{Q}_g^{(n)} \tag{5.18}$$

(2) Having obtained the flux estimate $\underline{\phi}^{(n+1)}$, the next multiplication eigenvalue estimate can now be determined. A variety of schemes can be used to determine the ratio of fission source estimates. One such scheme can be derived by taking the scalar product of the fission source vector $\underline{\underline{F}}\underline{\phi}^{(n+1)}$ with the equation defining the iterative scheme

$$\underline{\underline{M}}\underline{\phi}^{(n+1)} = \frac{1}{k^{(n)}} \underline{\underline{F}}\underline{\phi}^{(n)}, \tag{5.19}$$

and then noting that presumably

$$\underline{\underline{M}}\underline{\phi}^{(n+1)} \approx \frac{1}{k^{(n+1)}} \underline{\underline{F}}\underline{\phi}^{(n+1)}, \tag{5.20}$$

to find

$$k^{(n+1)} = k^{(n)} \frac{\left(\underline{\underline{F}}\underline{\phi}^{(n+1)}, \underline{\underline{F}}\underline{\phi}^{(n+1)}\right)}{\left(\underline{\underline{F}}\underline{\phi}^{(n)}, \underline{\underline{F}}\underline{\phi}^{(n+1)}\right)}. \tag{5.21}$$

(3) At this point the convergence of source iteration can be checked as by comparing

$$\left|\frac{k^{(n+1)}-k^{(n)}}{k^{(n+1)}}\right|<\varepsilon_1, \tag{5.22}$$

or a pointwise criterion

$$\max\left|\frac{S_{gi}^{(n+1)}-S_{gi}^{(n)}}{S_{gi}^{(n+1)}}\right|<\varepsilon_2, \tag{5.23}$$

or both. If the changes in $k^{(n)}$ or the elements $\underline{S}^{(n)}$ or $\underline{\phi}^{(n)}$ are sufficiently small, it can be assumed that the convergence is achieved, and the iteration procedure is ended. If not, a new fission source is calculated and the iteration continues.

5.4. Core Criticality Calculation

For the 2-D multigroup diffusion calculations the pebble bed core is divided into a number of spectrum zones providing a homogenised temperature distribution in each zone. The spectrum calculations are based on the averaged atom densities in these zones. Spectrum calculations are performed (as described in Chapter 4.) in each zone to obtain the broad group cross-sections for the multigroup diffusion calculations.

A schematic representation is given in Figure 5-4. This figure does not represent the exact number and the dimensions of the spectrum zones. The central and side reflector regions are not modelled in the test-case but reflector-core boundaries are treated as reflected boundaries with a given efficiency as input (i.e. albedo boundary conditions). The number of zones can differ vertically and horizontally, which is required in burn-up calculations. The flow velocity of the pebbles in the core differs in the radial direction due to the cone at the bottom of the reactor. This causes different irradiation times for pebbles so that different burn-up for each pass through the core.

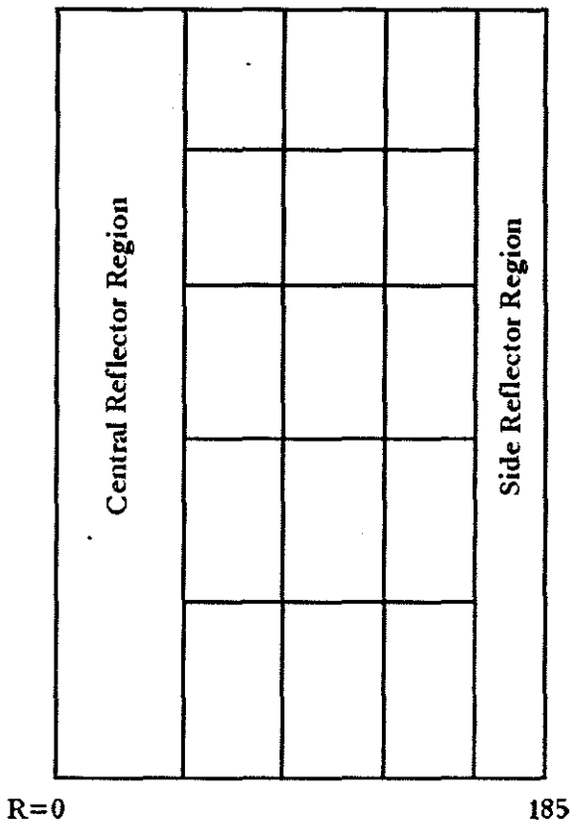

Figure 5-4: Schematic representation of spectrum zones.

The dimensions and the temperature of the each spectrum zone are required as input. For each spectrum zone the material composition should also be supplied in the input.

First core design of PBMR contains graphite pebbles as central reflector. The radius of the central zone with graphite pebbles is approximately 77 cm and there is also a mixing zone that contains both fuel and graphite pebbles, which has a thickness of approximately 33 cm (TECDOC-1198, 2001). The number of fuel pebbles in the mixing zone is approximately equal to the number of graphite pebbles in this zone. Thus, there is a pure fuel pebble zone with 65 cm thickness.

The new design contains a solid graphite column as central reflector. Previously, using graphite spheres as central reflector was considered because of mechanical difficulties, maintenance and replacement of a solid graphite column in the middle of the core. In addition there is not much reliable information about graphite behaviour under irradiation for longer than 20 years. In the new design, central graphite reflector will be replaced with a new one after 20 years of reactor

operation (Koster et al., 2003).

In this work the geometry of the previous design with a central reflector region containing graphite pebbles is chosen due to lack of real data of the new design from the vendor. The cone region at the bottom of the core is treated as filled with graphite balls.

To verify the results of the calculations, the reference design specifications are chosen to be the same as those quoted by Sikik (2003). The reference design for the calculations is the 268 MW_{th} PBMR design with a dynamic central column containing only graphite spheres. The core radius is 175 cm and a total height of 844 cm. The 6 cm diameter fuel spheres with low enriched (8%) uranium-oxide triso-coated particles and with a loading of 9 grams per fuel sphere is used. The reactor core is assumed to be at 300K with fresh fuel. Although the calculations are performed for many different fuel types, core geometry and temperatures, only the results for the reference design is presented in this work.

The thermal flux distributions for the design with central graphite pebbles are represented in Figure 5-5. The radial and axial flux distributions at different locations are also presented in Figure 5-6 and Figure 5-7 respectively. For all these figures, z = 0 cm represents the top of the reactor core. The effective criticality eigenvalue, k_{eff}, for the full core is 1.3278.

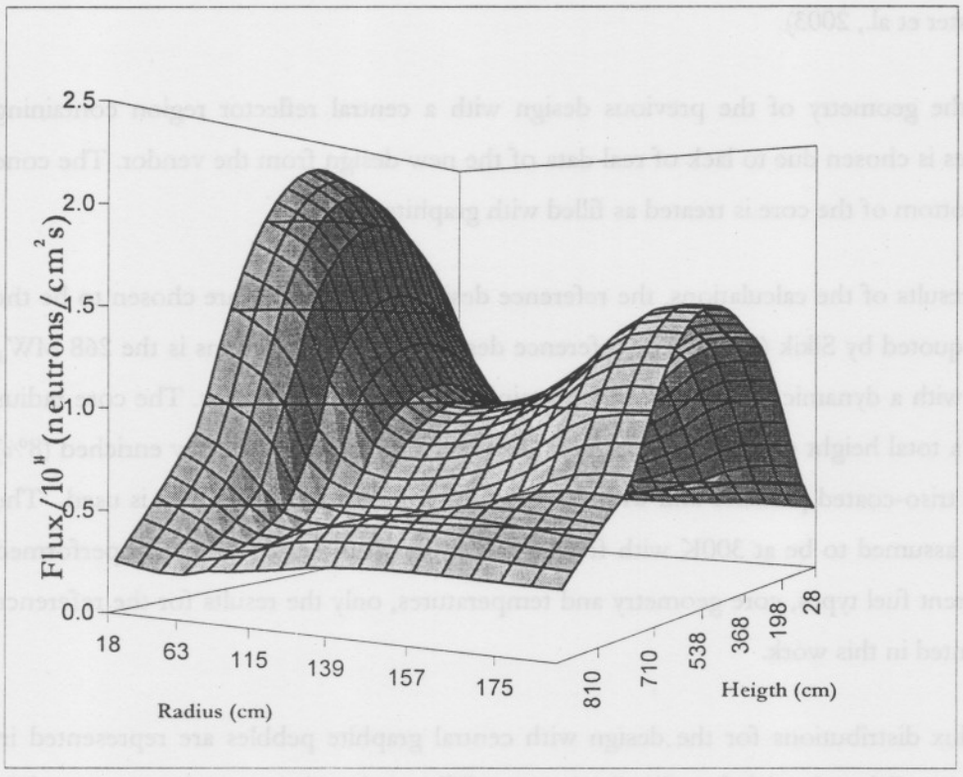

Figure 5-5: Thermal flux distribution in the core with graphite pebbles as central reflector.

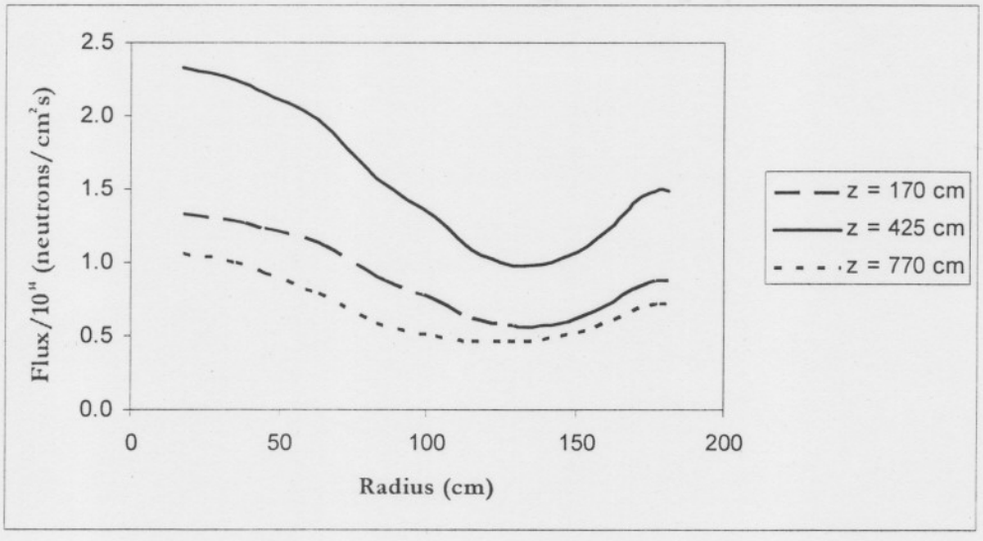

Figure 5-6: Radial thermal flux distribution.

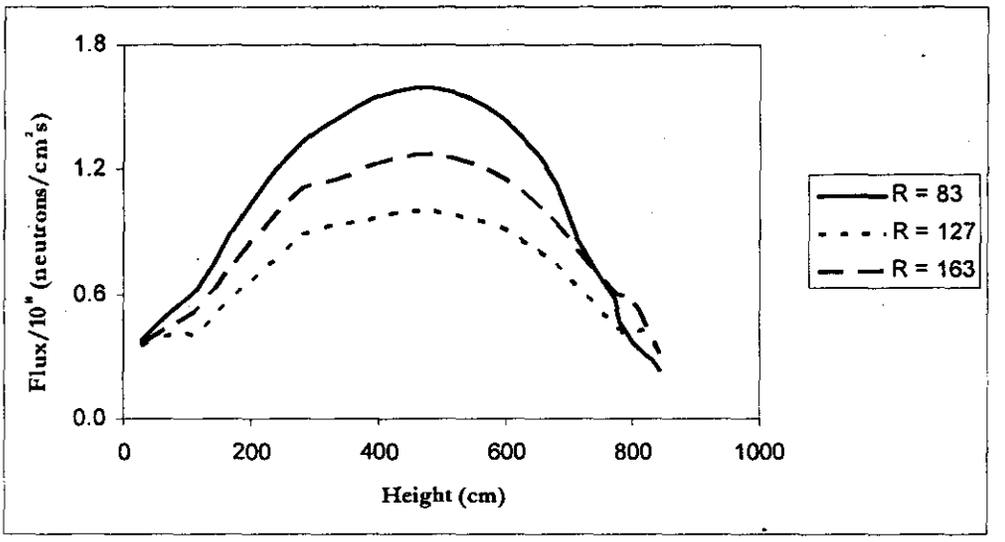

Figure 5-7: Axial thermal flux distribution.

In Figure 5-5 the regions in which flux values peak are the central and the side reflector zones. In the core with central graphite pebbles, there is a mixing zone of fuel and graphite pebbles between the graphite zone and the fuel zone. Mixing zone starts at 77 cm from the centre of core and finishes at 110 cm from the centre of the core. Fuel pebbles in the mixing zone are exposed to higher thermal flux than the pebbles in the fuel zone. Therefore, power generation in fuel pebbles in the mixing zone is higher than the power generation of pebbles in fuel zone which has a negative effect on the maximum fuel temperatures in a depressurization event.

5.4.1. Calculation of Group Neutron Fluxes

The calculation of the broad group neutron fluxes is performed with a four energy group structure. The energy boundaries calculated as described in previous chapters. The desired energy group boundaries are supplied as input and the actual group boundaries are calculated and used appropriate to the cross-section library group structure. The desired and actual used group structure is given in Table 4-4.

The 4th broad energy group flux distributions are presented above in figures Figure 5-5 to Figure 5-7, which range between 0 and 1.86 eV. For other 2 epithermal and fast groups, flux distributions are presented below, Figure 5-8 to Figure 5-13.

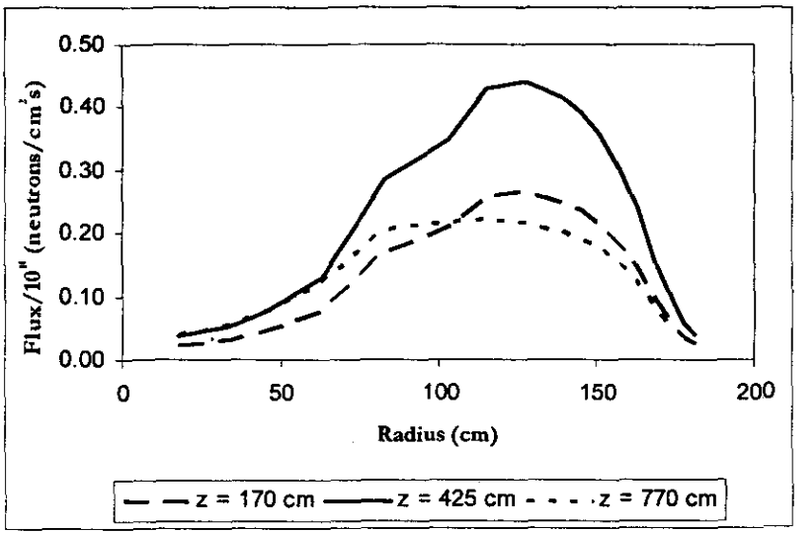

Figure 5-8: 1st group radial flux distribution.

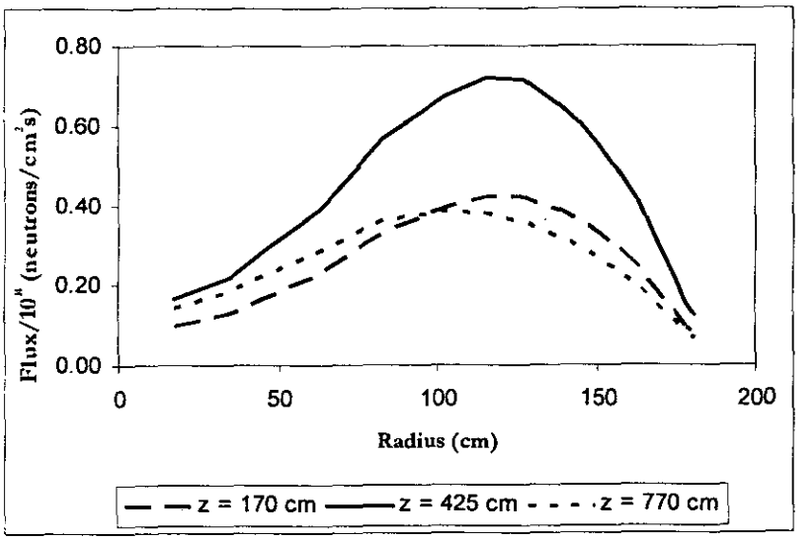

Figure 5-9: 2nd group radial flux distribution.

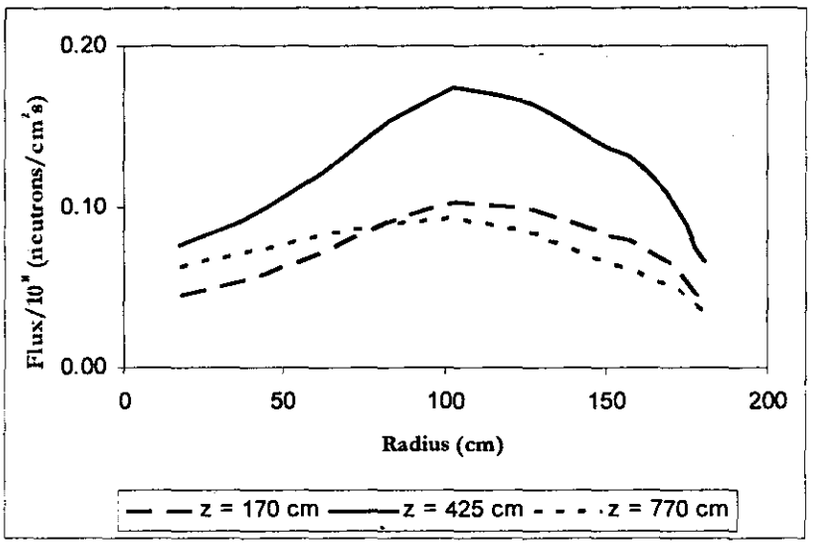

Figure 5-10: 3rd group radial flux distribution.

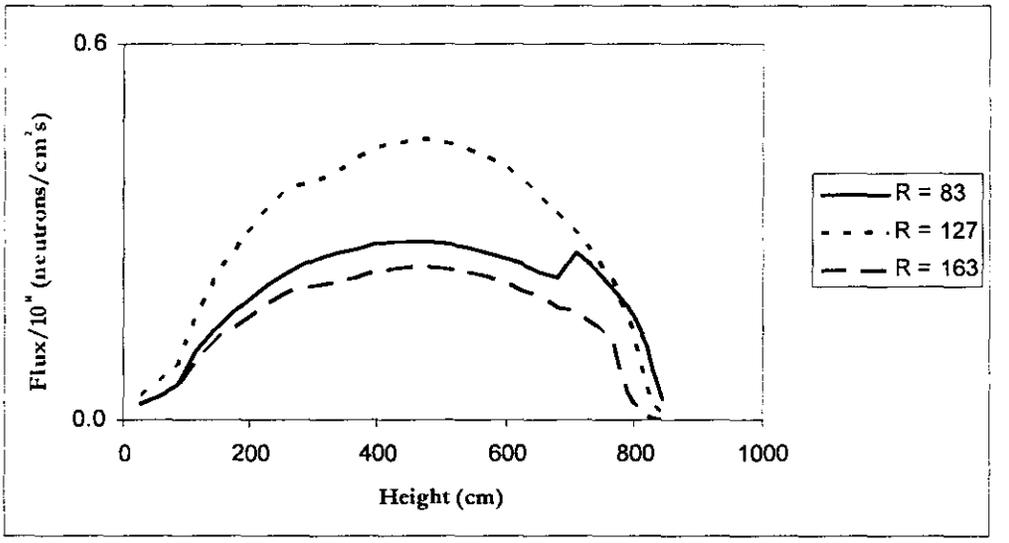

Figure 5-11: 1st group axial flux distribution.

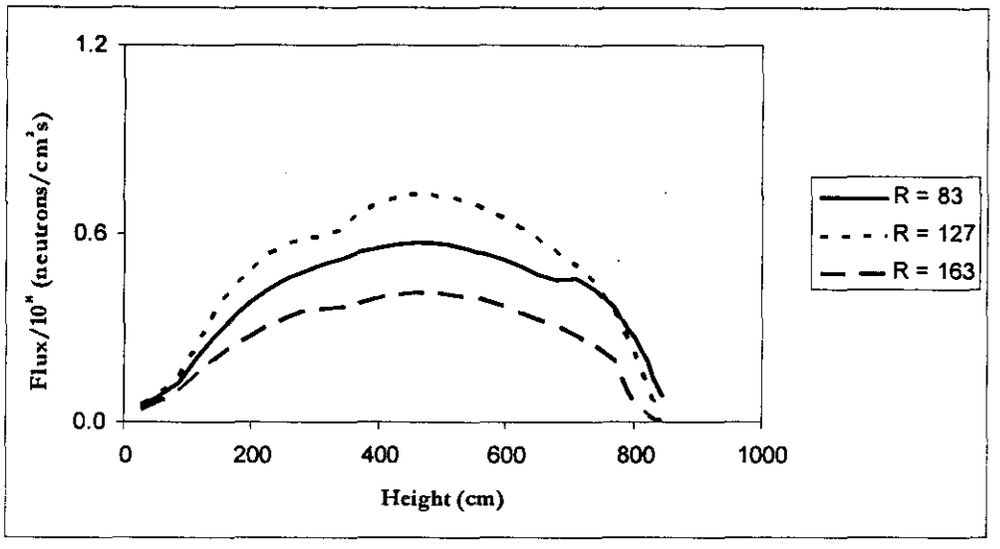

Figure 5-12: 2nd group axial flux distribution.

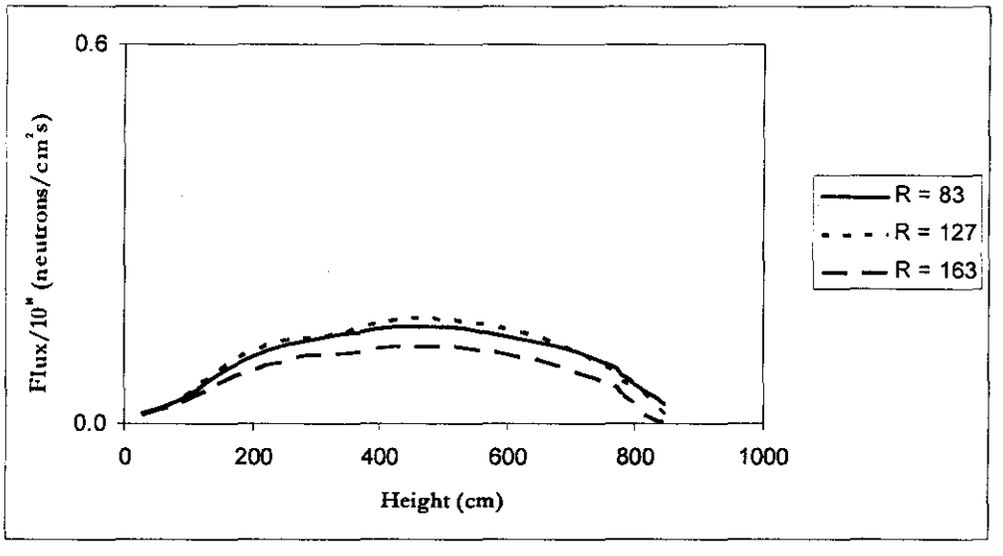

Figure 5-13: 3rd group axial flux distribution.

When the fast and thermal fluxes are compared, it is clear that fast flux reaches its highest value in the fuel region where the fission reaction takes place and neutrons are born. In reflector regions fast flux diminishes due to the fact that neutrons slow down to thermal energies in these regions. Therefore, thermal flux has its maximum value around the middle of the central reflector.

5.5. Calculation of the Power Distribution throughout the Core

The static calculations are usually based on a solution of the multigroup diffusion equations for the multiplication eigenvalue k_{eff} and multigroup fluxes $\phi_g(r)$ characterising a given core configuration. One can construct the corresponding core power distribution by calculating the local fission rate as

$$q'''(r) = \sum_i w_f^{(i)} N_i(r) \int_0^\infty dE \sigma_f^{(i)}(E) \phi(r, E). \tag{5.24}$$

Where the volumetric fission heat source is calculated by multiplying the fission reaction rate density for each isotope by w_f the recoverable energy released per fission event. The emitted and the recoverable energies for a fission event of U-235 are given below in Table 5-3. Of course, since the flux and number density of the fuel vary across the reactor core, there will be a corresponding variation in the fission heat source. The volumetric heat generation rate throughout the core is shown in Figure 5-14.

Table 5-3: Emitted and recoverable energies for fission of U-235 (Lamarsh, 1983).

Form	Emitted Energy, MeV	Recoverable Energy, MeV
Fission Fragments	168	168
Fission Product Decay		
- β-decay	8	8
- γ-rays	7	7
- neutrinos	12	-
Prompt γ-rays	7	7
Fission neutrons (kinetic energy)	5	5
Capture γ-rays	-	3-12
Total	207	198-207

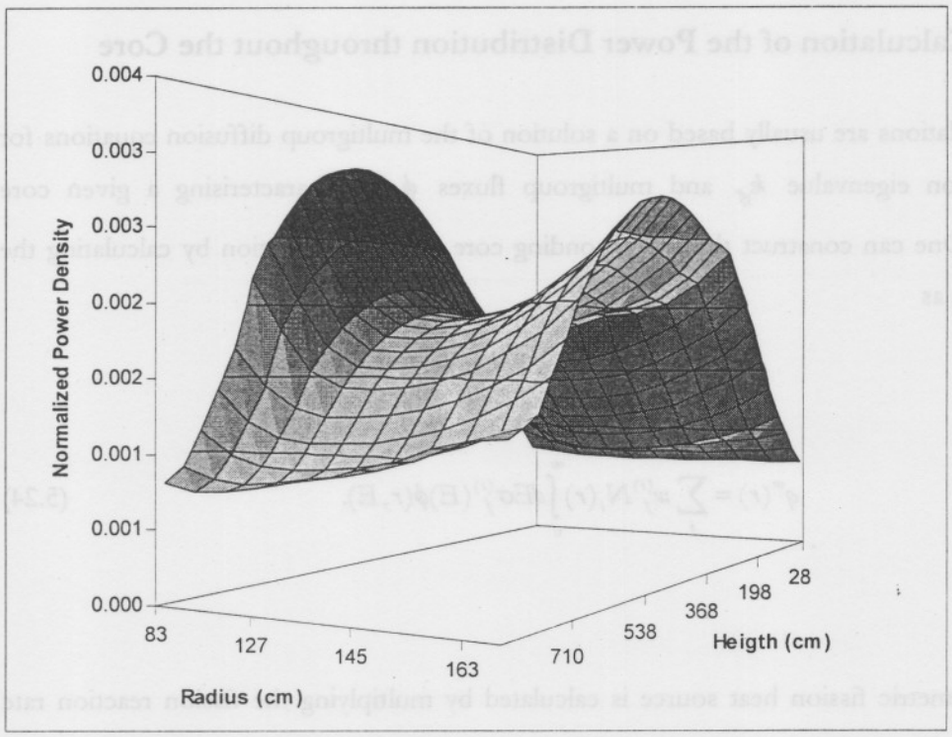

Figure 5-14: Power density distribution.

The static reactor flux and power distributions are also considerably important in reactor design. In particular, the power distribution is essential for the subsequent thermal hydraulic analysis of the core (Katz and Melese, 1984). For example, axial power profile determine how closely the core performance approaches thermal design limitations.

5.6. Verification of Results

Sikik (2003) gives the following figures as results obtained by V.S.O.P.'94 in his study. The thermal flux distribution throughout the reactor is illustrated in Figure 5-15, while the radial and axial thermal flux distributions are presented in Figure 5-16 and Figure 5-17 respectively.

VSOP'94 code is developed using the FORTRAN programming language. Although it uses the same cross-section libraries as used in our model, the leakage feedback to the spectrum calculations and the use of neutron streaming effects, which are not implemented in the model, are input options in VSOP code system. The treatment of the reflector regions is also different in two codes. The neutron flux throughout the reflector regions are not calculated in the model but the reflector-core boundaries are treated as reflected boundaries with a given efficiency as

input, i.e. albedo boundary condition.

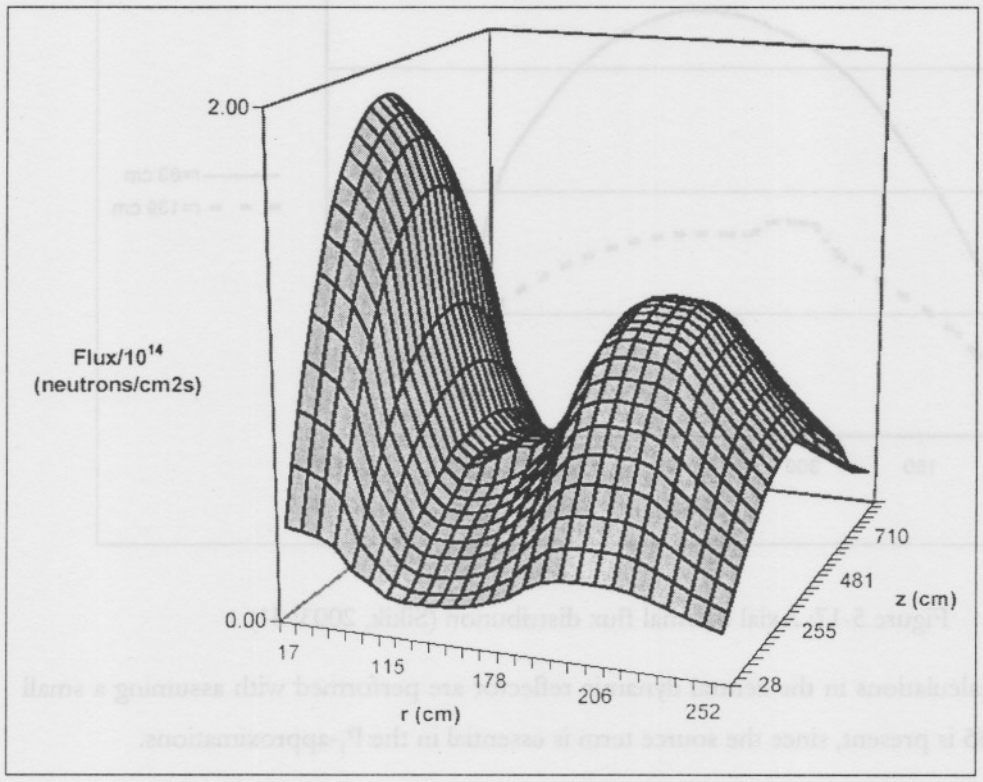

Figure 5-15: Thermal flux distribution in the reactor with graphite pebbles (Sikik, 2003: 29).

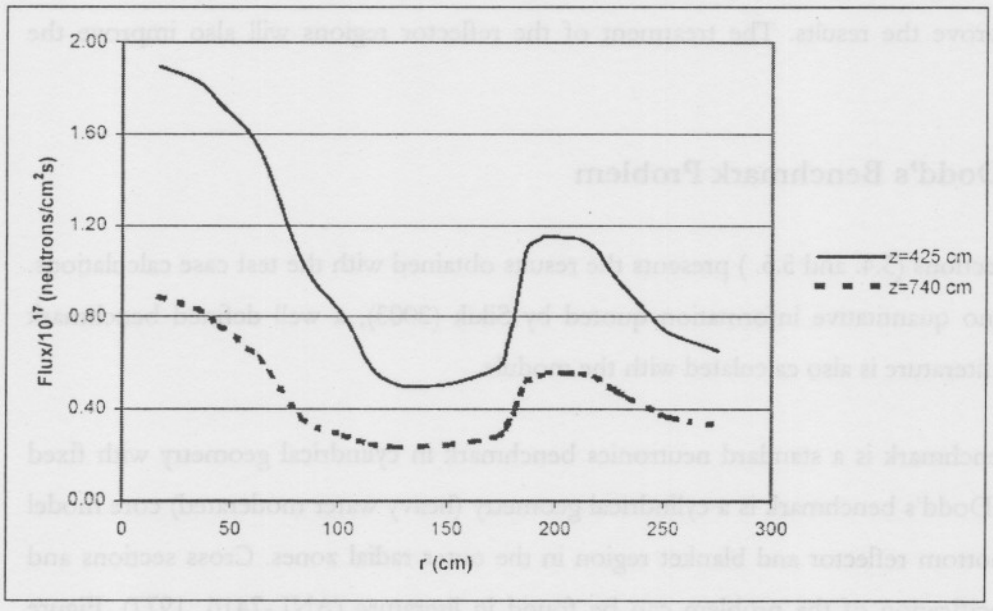

Figure 5-16: Radial thermal flux distribution (Sikik, 2003: 30).

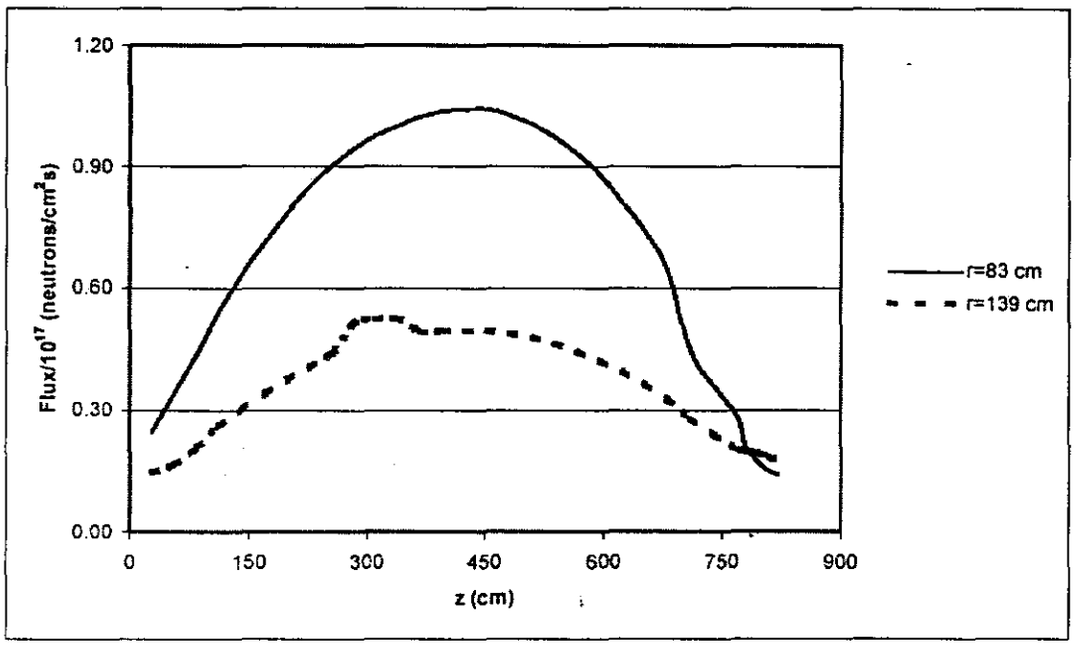

Figure 5-17: Axial thermal flux distribution (Sikik, 2003: 31).

The spectrum calculations in the central dynamic reflector are performed with assuming a small amount of U-235 is present, since the source term is essential in the P_1-approximations.

Noting the above mentioned differences between the two codes, the flux profile and the values are in fairly good agreement. Implementing the leakage and the neutron streaming effects to the model will improve the results. The treatment of the reflector regions will also improve the results.

5.7. Dodd's Benchmark Problem

The previous sections (5.4. and 5.5.) presents the results obtained with the test case calculations. Since there is no quantitative information quoted by Sikik (2003), a well defined benchmark problem in the literature is also calculated with the module.

The Dodd's benchmark is a standard neutronics benchmark in cylindrical geometry with fixed cross-sections. Dodd's benchmark is a cylindrical geometry (heavy water moderated) core model with top and bottom reflector and blanket region in the outer radial zones. Cross sections and the further specification of the problem can be found in literature (ANL-7416, 1977). Figure 5-18 illustrates the geometry specification used in the benchmark problem. Each number

represents a region with different cross section value. Only the steady-state core eigenvalue calculations that form part of the benchmark were considered.

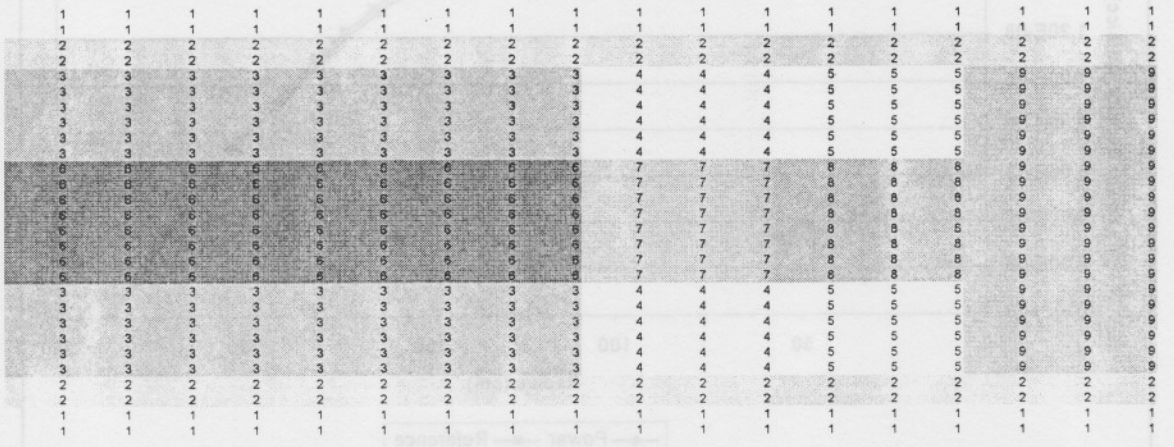

Figure 5-18: Dodd's Benchmark Geometry Description

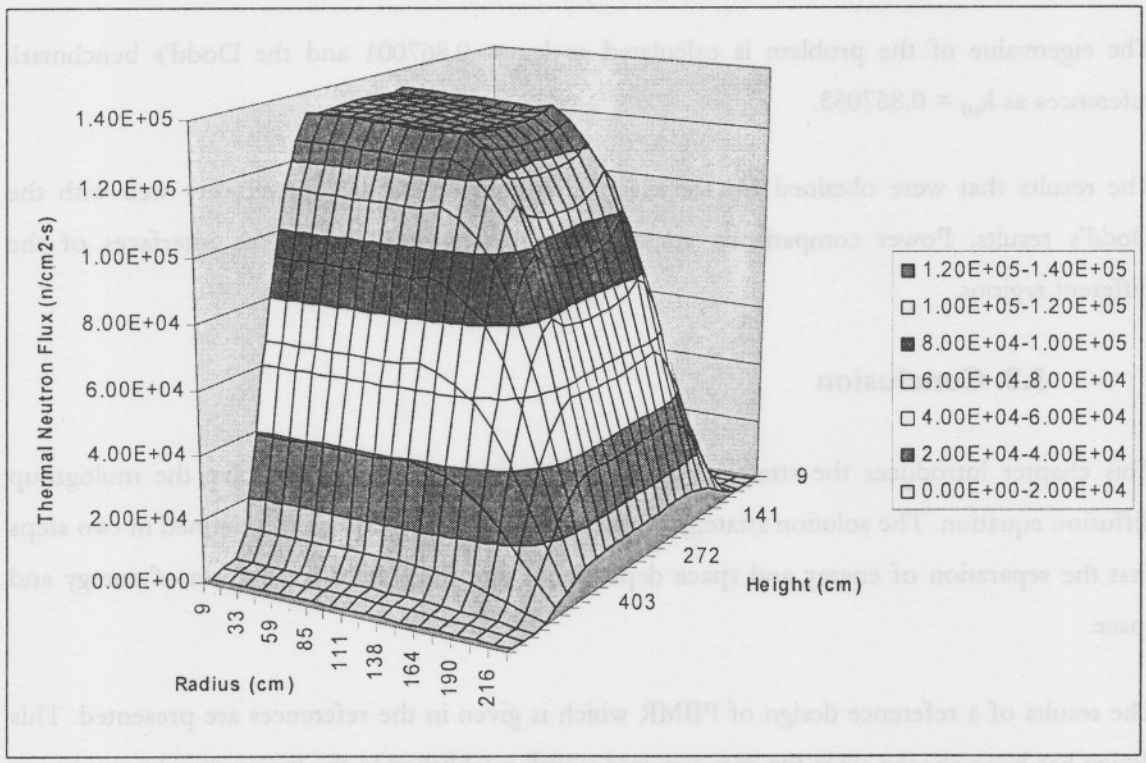

Figure 5-19: Thermal Flux Distribution (Dodd's benchmark)

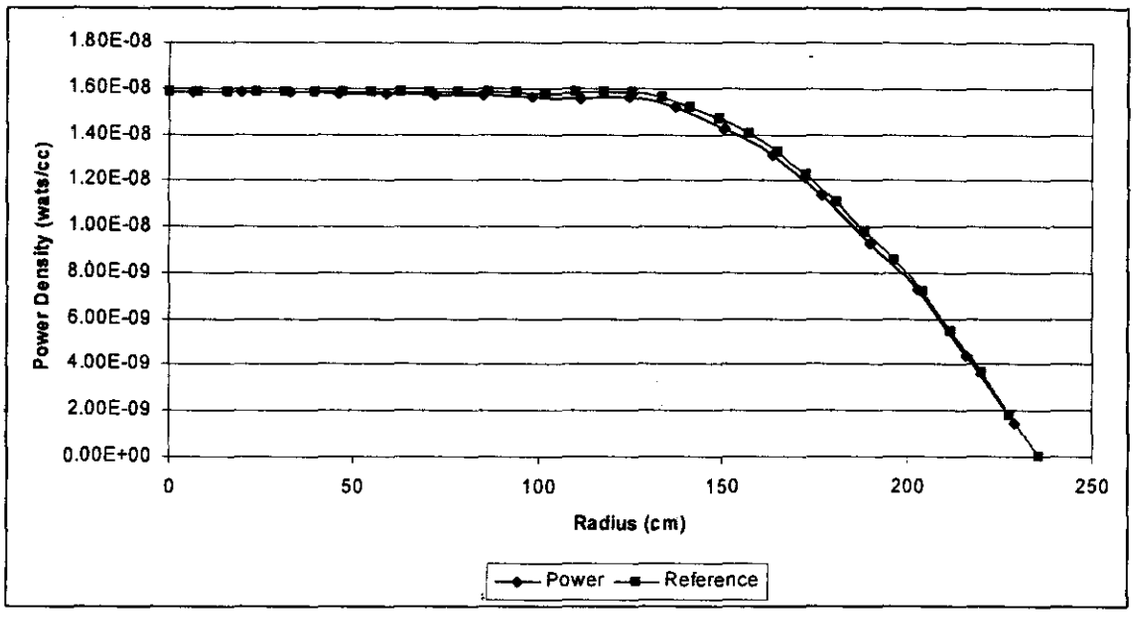

Figure 5-20: Axially averaged point power density for Dodd's benchmark

The eigenvalue of the problem is calculated as k_{eff} = 0.867001 and the Dodd's benchmark references as k_{eff} = 0.867053.

The results that were obtained for the eigenvalue comparison are agreed very well with the Dodd's results. Power comparisons are also agreed very well except the interfaces of the different regions.

5.8. Conclusion

This chapter introduces the strategies and techniques that are used to solve the multigroup diffusion equation. The solution strategy of multigroup diffusion equation is defined in two steps first the separation of energy and space dependence and then the discretisation of energy and space.

The results of a reference design of PBMR which is given in the references are presented. This design has been chosen since the data required is well established in the literature. The results are compared with the results of a previous study. It is seen that the results are compare relatively well.

The Dodd's benchmark has shown that the finite difference diffusion solution method in the

code produces correct results for a cylindrical geometry problem.

Chapter 6. Summary, Conclusion, Future Work

6.1. Summary

In this study, neutronics calculations are done for the Pebble Bed Modular Reactor. A new computer programme is developed for these calculations. One reference core is modelled which contains graphite pebbles as the central reflector.

The first core design of PBMR is modelled in this study due to the lack of the new design data from the provider. The new design contains a solid graphite column instead of the graphite pebbles as central reflector.

The reference design core has 77 cm of graphite pebbles at the centre and a 33 cm of mixing region of fuel and graphite pebbles and a 65 cm of pure fuel region. The core height is 844 cm. For this core type, fuel to moderator ratio is higher than the core with solid central reflector, thus the thermal flux for the reference core model is higher. In the mixing region of reactor with central graphite pebbles, fuel pebbles exposed to higher thermal flux than the pebbles in the pure fuel zone. This causes higher power generation in these pebbles.

It is possible to use different fuel compositions and different fuel loading strategies in the operation of PBMR. However, it is important to make sure that inherent safety features of the reactor are not jeopardised.

6.2. Conclusion

The development of the 2D static neutronics model of the PBMR core is presented. With the geometry and the material data provided, the programme which is presented can calculate the flux profile throughout the core and so the power distribution. With the code it is possible to study the effects of various fuel designs, geometry and temperature.

After implementing with FLOWNEX, more sophisticated analyses can be performed. The transients can be done in a quasi-static manner. The static analysis of the PBMR core can be made at one time-step with a known temperature field. Providing the power profile to FLOWNEX, FLOWNEX can calculate the resultant temperature field for the next time-step. With an additional module to the code it might be used to calculate the point kinetic parameters

at the beginning of a transient.

6.3. Recommendations for future work

As the 2D static neutronic model for PBMR core is developed and will be integrated to FLOWNEX, the most important future work is developing a dynamic model for PBMR core. The dynamic treatment of a nuclear reactor comprises a description of the changing nuclear characteristics due to the changed core composition, and the resultant temperature fields. The dynamic model consists of the modelling of:

- The progressing burn-up;
- The influence of strong absorber material close to the core, such as reactivity control systems and/or its movement;
- The change in concentration of short-lived strong absorbers, such as ^{135}Xe;
- The decay heat generation;
- The change in composition of the coolant could be considered together with the corrosion of the structural materials (such as, water ingress and the temperature-dependent graphite corrosion).

References

ANL-7416. *Argonne Code Center: Benchmark Problem Book.* ANL-7416, Suppl. 2, ANL(1977).

Cardoso, C.E.S., Martinez, A.S., da Silva, F.C., 1996. *Adjoint Neutron Spectrum Calculation for Heteregenous Cells.* J. Phys. D: Appl. Phys., 29 (1996), p. 2204 – 2208.

Clark, M. Jr, and Hansen, K.F. 1964. *Numerical Methods of Reactor Analysis.* Academic Press, New York and London.

Dodds, H.L., Jr, Honeck, H.C., Hostetler, D.E., 1975. *Carse-Mesh Method for Two-dimensional Mixed-lattice Diffusion Theory Calculations.* Transactions of the American Nuclear Society, vol. 21 (1975), p. 223 – 224.

Duderstadt, J.J., Hamilton, L.J. 1976. *Nuclear Reactor Analysis.* John Wiley & Sons.

Dunn, M. E., Greene, N.M. 2002. AMPX – 2000: A Cross – Section Processing System for Generating Nuclear Data for Criticality Safety Applications. Transactions of the American Nuclear Society, vol. 86 (2002), p. 118 – 119.

Drozdowicz, K., Gabariska, B., Krynicka, E., Woznicka, U. 2001. Influence of the grain size on the effective absorption cross-section of thermal neutrons in a medium containing highly absorbing centers. Annals of Nuclear Energy, vol. 28 (2001), p. 1485 – 1497.

ENDF-102 2001. *Data Formats and Procedures for the Evaluated Nuclear Data File. ENDF-6,* BNL-NCS-44945-01/04-Rev, Informal Report, edited by V. McLane, 2001. US National Nuclear Data Center, Brookhaven National Laboratory, Upton, NY, USA.

Gillette, V.H., Sbaffoni, M.M., Granada, J.R., Pepe, M.E. 1999. *Thermal neutron cross sections for moderator materials: comparison of a synthetic scattering function and NJOY results.* Annals of Nuclear Energy, vol. 26 (1999), p. 1167 – 1181.

Gregory, M.V., Honeck, H.C., 1976.*Control Algorithms in a Coarse-Mesh Rebalance Framework.* Nuclear Science and Engineering, vol. 61 (1976), p. 437 – 445.

Katz, R. and Melese, G. 1984. *Thermal and Flow Design of Helium Cooled Reactors.* American Nuclear

Society

Kazimi, M.S. and Todreas, N.E. 1993. *Nuclear Systems I.* Taylor and Francis.

Kiryushin, A.I., Kodochigov, N.G., Kouzowkov, N.G., Ponomarev- Stepnoi, N.N., Gloushkov, E.S., Grebennik, V.N., et al., 1997. *Project of the GT-MHR high-temperature helium reactor with gas turbine.* Nuclear Engineering and Design, vol. 173 (1997), p.119 - 129.

Knoll, G.F. 1979. *Radiation, Detection and Measurement.* New York, NY, Wiley.

Koster A., Matzner H.D., Nichols D.R., 2003. *PBMR Design for the Future.* Nuclear Engineering and Design (222), 2003.

Krane, K.S. 1998. *Introductory nuclear physics.* New York, NY, Wiley.

Kugeler, K., Alkan, Z., Poppe, N. 2003. *High Temperature Reactor Technology - HTR-Course notes.* Potchefstroom University for CHE, April 2003.

LA-12625-M 1997. MCNP- A General Monte Carlo N-Particle Transport Code. Manual, Version 4B.

Lamarsh, John R., 1983. *Introduction to Nuclear Engineering,* 2nd ed. Massachusetts, Addison – Wesley Publishing.

Lewis, E.E. 1977. *Nuclear Power Reactor Safety.* John Wiley and Sons.

MacFarlane, R. E. and Muir, D. W. 1994. *The NJOY Nuclear Data Processing System, Version 91.* Report LA-12740-M, October 1994.

Massimo, L. 1975. Physics of High – Temperature Reactors, Pergamon Press.

Mulder, E.J. 1999. *Pebble Bed Reactor with Equalized Core Power Distribution Inherently Safe and Simple.* Institut fur Sicherheitsforchung und Reaktortechnik, Jul-3632. Forschungszentrum, Julich.

Naito, Y., Tsuruta, S., Hayashi, M., 1981. *A New Mixed Method with Finite Difference and Finite Element Method for Neutron Diffusion Calculation.* Journal of Nuclear Science and Technology, 18(8), 1981, p. 571 – 580.

Nicholls, D.R. 1997. *The pebble-bed modular reactor.* Nuclear Engineer 38 (4), 1997, p. 105 – 107.

NUREG/CR-0200 1998. *SCALE4.4 Code System User Manual.* OAK RIDGE NATIONAL LABORATORY, September 1998.

PBMR 2003. *About the PBMR.* www.pbmr.co.za (last visited on December 2003)

Rousseau, P.G. 1999. Equations and input parameters for the PBMR pebble bed reactor simulation model. PBMR-0001-1999/A.

Sen, R.S., Colak, U. and Kadiroglu, O.K. 2003. *Nuclear Desalination with PBMR.* International Journal of Nuclear Desalination, vol 1 (2), 2003, p. 271 - 279.

Sikik, U.E., 2003. Neutronic and Thermalhydraulic Calculations of the Pebble Bed Modular Reactor. M. Eng Thesis, Hacettepe University, Turkey.

TECDOC-1198 2001. *Chapter 3: Review of the Pebble Bed Modular Reactor (PBMR).* International Atomic Energy Agency, Vienna.

Teuchert E., Haas K.A., Rütten H.J., Brockmann H., Gerwin H., Ohlig U., Scherer W. 1994. *V.S.O.P. [94] Computer Code System for Reactor Physics and Fuel Cycle Simulation Input Manual and Comments.* Institut für Sicheitsforschung und Reaktortechnik, Jülich.

Wolf, L., Scherer, W., Giesser, W., Feltes, W. 1990. *High Temperature Reactor Core Physics and Reactor Dynamics.* Nuclear Engineering and Design, vol. 121 (1990), p. 227 – 240.

Xu, Y. and Zuo, K. 2002. *Overview of the 10 MW High Temperature Gas Cooled Reactor-Test Module Project.* Nuclear Engineering and Design, vol. 218 (2002), p. 13 - 23.

Yamashita, K., et al. 1996. *Nuclear design of the hightemperature engineering test reactor (HTTR).* Nuclear Science and Engineering, vol. 122 (1996), p. 212 – 228.

Zhang, Z. and Yu, S. 2002. *Future HTGR developments in China after the criticality of the HTR-10.* Nuclear Engineering and Design, vol. 218 (2002), p. 249 - 257.

Appendix A. Cross-section Libraries

Table A-1: GAM Library (Teuchert et al., 1994).

No.	Id.-no.				No.	Id.-no			
1	1	H-1	Mat 1301	ENDFB-V	91	91	Cs-137	Mat 9669	ENDFB-V
2	2	H-2	Mat 4012	JEF-I	92	92	Ba-134	Mat 4564	JEF-I
3	3	Be-9	Mat 1289	ENDFB-IV	93	93	Ba-136	Mat 4566	JEF-I
4	4	B(nat)		JEF-I	94	94	Ba-137	Mat 4567	JEF-I
5	5	C	Mat 1306	ENDFB-V	95	95	Ba-138	Mat 4568	JEF-I
6	6	Th-232	Mat 4902	JEF-I	96	96	La-139	Mat 9707	ENDFB-V
7	7	Pa-233	Mat 1391	ENDFB-V	97	97	Ce-140	Mat 4580	JEF-I
8	8	U-233	Mat 4923	JEF-I	98	98	Ce-142	Mat 4582	JEF-I
9	9	U-234	Mat 4924	JEF-I	99	99	Pr-141	Mat 9742	ENDFB-V
10	10	U-235	Mat 4925	JEF-1	100	100	Nd-142	Mat 9763	ENDFB-V
11	11	U-236	Mat 4926	JEF-1	101	101	Nd-143	Mat 4603	JEF-I
12	12	U-238	Mat 4928	JEF-1	102	102	Nd-144	Mat 4604	JEF-I
13	13	Np-239	Mat 4939	JEF-1	103	103	Nd-145	Mat 9766	ENDFB-V
14	14	Pu-239	Mat 1264	ENDFB-IV	104	104	Nd-146	Mat 4606	JEF-I
15	15	Pu-240	Mat 4940	JEF-1	105	105	Nd-148	Mat 9769	ENDFB-V
16	16	Pu-241	Mat 4941	JEF-1	106	106	Nd-150	Mat 4600	JEF-I
17	17	Pu-242	Mat 1342	ENDFB-V	107	107	Pm-147	Mat 9783	ENDFB-V
18	18	Fission-Product			108	108	Sm-147	Mat 9806	ENDFB-V
19	19	Fiss.Prod. U-235		GAMJUL	109	109	Sm-148	Mat 9807	ENDFB-V
20	20	Fiss.Prod. U-233		GAMJUL	110	110	Sm-149	Mat 1318	ENDFB-V
21	21	Fiss.Prod. Pu-239		GAMJUL	111	111	Sm-150	Mat 9809	ENDFB-V
22	22	N-14	Mat 4074		112	112	Sm-151	Mat 4621	JEF-I
23	23	O-16	Mat 4086	JEF-1	113	113	Sm-152	Mat 9811	ENDFB-V
24	24	Mg	Mat 4120	JEF-1	114	114	Sm-154	Mat 9813	ENDFB-V
25	25	Al-27	Mat 4137	JEF-1	115	115	Eu-151	Mat 4631	JEF-I
26	26	Si	Mat 4140	JEF-1	116	116	Eu-153	Mat 4633	JEF-I
27	27	Cr	Mat 4240	JEF-1	117	117	Eu-154	Mat 4634	JEF-I
28	28	Mn-55	Mat 4255	JEF-1	118	118	Eu-155	Mat 9832	ENDFB-V
29	29	Fe(nat)	Mat 4260	JEF-1	119	119	Gd-154	Mat 4644	JEF-I
30	30	Co-59	Mat 4279	JEF-1	120	120	Gd-155	Mat 4645	JEF-I
31	31	Ni	Mat 4280	JEF-1	121	121	Gd-156	Mat4646	JEF-I
32	32	Cu	Mat 4290	JEF-1	122	122	Gd-157	Mat 4647	JEF-I
33	33	Sc-82	Mat 4342	JEF-1	123	123	Gd-158	Mat 4648	JEF-I
34	34	Br-81	Mat 4351	JEF-1	124	124	Tb-159	Mat 4659	JEF-I
35	35	Kr-83	Mat 4363	JEF-1	125	125	Au-197	Mat 4797	JEF-I
36	36	Kr-84	Mat 4364	JEF-1	126	126	Pb	Mat 4820	JEF-I
37	37	Kr-85	Mat 4365	JEF-1	127	127	Bi-209	Mat 4839	JEF-I
38	38	Kr-86	Mat 4366	JEF-1	128	128	Li-6	Mat 4036	JEF-I
39	39	Rb-85	Mat 4375	JEF-1	129	129	Li-7	Mat 4037	JEF-I
40	40	Rb-87	Mat 4377	JEF-1	130	130	B-10	Mat 4050	JEF-I
41	41	Sr-88	Mat 4388	JEF-1	131	131	Nitrogen-14		GAMEFB
42	42	Sr-90	Mat 4380	JEF-1	132	132	U-237	Mat 4927	JEF-I
43	43	Y-89	Mat 4399	JEF-1	133	133	Np-237	Mat 4937	JEF-I
44	44	Zr	Mat 4409	JEF-1	134	134	V mit Cr-Streumatrix		GER
45	45	Zr-90	Mat 4400	JEF-1	135	135	V	Mat 4230	JEF-I
46	46	Zr-91	Mat 4401	JEF-1	136	136	Nb mit Zr-Streumatrix		GER
47	47	Zr-92	Mat 4402	JEF-1	137	137	Ti	Mat 4220	JEF-I
48	48	Zr-93	Mat 4403	JEF-1	138	138	Zry=Zr		GAMJUL
49	49	Zr-94	Mat 4404	JEF-1	139	139	Ag-107	Mat 4477	JEF-I
50	50	Zr-96	Mat 4406	JEF-1	140	140	Nb-93	Mat 4413	JEF-I
51	51	Mo	Mat 4420	JEF-1	141	141	W(nat)		JEF-I
52	52	Mo-95	Mat 4425	JEF-1	142	142	Ru-105	Mat 4445	JEF-I
53	53	Mo-96	Mat 9283	ENDFB-V	143	143	Rh-105	Mat 4455	JEF-I
54	54	Mo-97	Mat 4427	JEF-I	144	144	Cs-134	Mat 4554	JEF-I
55	55	Mo-98	Mat 9285	ENDFB-V	145	145	Ce-144	Mat 4584	JEF-I
56	56	Mo-100	Mat 9287	ENDFB-V	146	146	Pr-142	Mat 4592	JEF-I
57	57	Tc-99	Mat 1308	ENDFB-V	147	147	Pm-148	Mat 4612	JEF-I
58	58	Ru-100	Mat 4440	JEF-I	148	148	Pm-148m	Mat 4613	JEF-I

No.	Id.-no.				No.	Id.-no			
59	59	Ru-101	Mat 4441	JEF-I	149	149	Zr-95	Mat 4405	JEF-I
60	60	Ru-102	Mat 4442	JEF-I	150	150	Poison in C Dummy		
61	61	Ru-104	Mat 4444	JEF-I	151	151	Ru-103	Mat 4443	JEF-I
62	62	Rh-103	Mat 1310	ENDFB-V	152	152	Xe-133	Mat 4547	JEF-I
63	63	Pd-104	Mat 4464	JEF-I	153	153	Ce-141	Mat 9725	ENDFB-V
64	64	Pd-105	Mat 4465	JEF-I	154	154	Pr-143	Mat 4593	JEF-I
65	65	Pd-106	Mat 4466	JEF-I	155	155	Pm-149	Mat 4614	JEF-I
66	66	Pd-107	Mat 4467	JEF-I	156	156	I-131	Mat 4536	JEF-I
67	67	Pd-108	Mat 9386	ENDFB-V	157	160	Fiss..Prod. U-235 Chain 44		
68	68	Pd-110	Mat 4460	JEF-I	158	161	Fiss..Prod. U-235 Chain 39		
69	69	Ag-109	Mat 1373	ENDFB-V	159	162	Fiss..Prod. U-235 Chain 34		
70	70	In-115	Mat 4495	JEF-I	160	163	Fiss..Prod. U-235 Chain 29		
71	71	Cd	Mat 4480	JEF-I	161	164	B-11	Mat 4051	JEF-I
72	72	Cd-110	Mat 4483	JEF-I	162	165	Hf-174	Mat 4724	JEF-I
73	73	Cd-111	Mat 4484	JEF-I	163	166	Hf-176	Mat 4726	JEF-I
74	74	Cd-112	Mat 4485	JEF-I	164	167	Hf-177	Mat 4727	JEF-I
75	75	Cd-113	Mat 4486	JEF-I	165	168	Hf-178	Mat 4728	JEF-I
76	76	Cd-114	Mat 4487	JEF-I	166	169	Hf-179	Mat 4729	JEF-I
77	77	Te-126	Mat 4525	JEF-I	167	170	Hf-180	Mat 4720	JEF-I
78	78	Te-128	Mat 4527	JEF-I	168	171	W-182	Mat 4742	JEF-I
79	79	Te-130	Mat 4529	JEF-I	169	172	W-183	Mat 4743	JEF-I
80	80	I-127	Mat 9606	ENDFB-V	170	173	W-184	Mat 4744	JEF-I
81	81	I-129	Mat 9608	ENDFB-V	171	174	W-186	Mat 4746	JEF-I
82	82	Xe-128	Mat 4542	JEF-I	172	175	Pm-151	Mat 4615	JEF-I
83	83	Xe-130	Mat 4544	JEF-I	173	176	U-232	Mat 8232	ENDFB-V
84	84	Xe-131	Mat 4545	JEF-I	174	177	Pu-238	Mat 1338	ENDFB-V
85	85	Xe-132	Mat 4546	JEF-I	175	178	Am-241	Mat 1361	ENDFB-V
86	86	Xe-134	Mat 4548	JEF-I	176	179	Am-242	Mat 8542	ENDFB-V
87	87	Xe-135	Mat 4549	JEF-I	177	180	Am-242m	Mat 1369	ENDFB-V
88	88	Xe-136	Mat 4551	JEF-I	178	181	Am-243	Mat 1363	ENDFB-V
89	89	Cs-133	Mat 4553	JEF-I	179	182	Cm-242	Mat 8642	ENDFB-V
90	90	Cs-135	Mat 4555	JEF-I	180	183	Cm-243	Mat 1343	ENDFB-V
					181	184	Cm-244	Mat 1344	ENDFB-V

Table A-2: THERMOS Library Part -1 (Teuchert et al., 1994).

Id.-no.	Absorber			Id.-no.	Absorber		
4	Baron (nat)	JEF-I	Mat 4050/51 (20% B-10 + 80% B-11)	95	Barium-138	JEF-I	Mat 4568
6	Thorium-232	JEF-I	Mat 4902	96	Lanthanum-139	ENDFB-V	Mat 9707
7	Protactinium-233	ENDFB-V	Mat1391	97	Cerium-140	JEF-I	Mat 4580
8	Uranium-233	JEF-I	Mat4923	98	Cerium-142	JEF-I	Mat 4582
9	Uranium-234	JEF-I	Mat 4924	99	Praseodymium-141	ENDFB-V	Mat 9742
10	Uranium-235	JEF-I	Mat 4925	100	Neodymium-142	JEF-I	Mat 4602
11	Uranium-236	JEF-I	Mat 4926	101	Neodymium-143	JEF-I	Mat 4603
12	Uranium-238	JEF-I	Mat 4928	102	Neodymium-144	ENDFB-V	Mat 9765
13	Neptunium-239	JEF-I	Mat 4939	103	Neodymium-145	ENDFB-V	Mat 9766
14	Plutonium-239	ENDFB-IV	Mat 1264	104	Neodymium-146	ENDFB-V	Mat 9767
15	Plutonium-240	JEF-I	Mat 4940	105	Neodymium-148	ENDFB-V	Mat 9769
16	Plutonium-241	JEF-I	Mat 4941	106	Neodymium-150	JEF-I	Mat 4600
17	Plutonium-242	ENDFB-V	Mat 1342	107	Promethium-147	ENDFB-V	Mat 9783
22	Nitrogen-14	JEF-I	Mat 4074	108	Samarium-147	ENDFB-V	Mat 9806
24	Magnesium (nat)	JEF-I	Mat 4120	109	Samarium-148	JEF-I	Mat 4628
25	Aluminium-27	JEF-I	Mat 4137	110	Samarium-149	ENDFB-V	Mat 1319
26	Silicon (nat)	JEF-I	Mat 4140	111	Samarium-150	JEF-I	Mat 4620
27	Chromium (nat)	ENDFB-IV	Mat 1191	112	Samarium-151	JEF-I	Mat 4621
28	Manganese-55	JEF-I	Mat 4255	113	Samarium-152	ENDFB-V	Mat 9811
29	Iron (nat)	JEF-I	Mat 4260	114	Samarium-154	JEF-I	Mat 4624
30	Cobalt-59	JEF-I	Mat 4279	115	Europium-151	JEF-I	Mat 4631
31	Nickel (nat)	JEF-I	Mat 4280	116	Europium-153	JEF-I	Mat 4633
32	Copper (nat)	JEF-I	Mat 4290	117	Europium-154	JEF-I	Mat 4634
33	Selenium-82	JEF-I	Mat 4342	118	Europium-155	ENDFB-V	Mat 9832
34	Bromine-81	JEF-I	Mat 4351	119	Gadolinium-154	JEF-I	Mat 4644
35	Krypton-83	JEF-I	Mat 4363	120	Gadolinium-155	JEF-I	Mat 4645
36	Krypton-84	JEF-I	Mat 4364	121	Gadolinium-156	JEF-I	Mat 4646
37	Krypton-85	JEF-I	Mat 4365	122	Gadolinium-157	JEF-I	Mat 4647
38	Krypton-86	JEF-I	Mat 4366	123	Gadolinium-158	JEF-I	Mat 4648
39	Rubidium-85	JEF-I	Mat 4375	124	Terbium-159	ENDFB-V	Mat 9857
40	Rubidium-87	JEF-I	Mat 4377	125	Gold-197	JEF-I	Mat 4797
41	Strontium-88	JEF-I	Mat 4388	126	Lead (nat)	JEF-I	Mat 4820
42	Strontium-90	JEF-I	Mat 4380	127	Bismuth-209	JEF-I	Mat 4839
43	Yttrium-89	JEF-I	Mat 4399	128	Lithium-6	JEF-I	Mat 4036
44	Zirconium (nat)	JEF-I	Mat 4409	129	Lithium-7	JEF-I	Mat 4037
45	Zirconium-90	JEF-I	Mat 4400	130	Boron-10	JEF-I	Mat 4050
46	Zirconium-91	JEF-I	Mat 4401	131	Nitrogen-14	ENDFB 68	XA=1.885*(VO/V) XS=10.2
47	Zirconium-92	JEF-I	Mat 4402	132	Uranium-237	JEF-I	Mat 4927
48	Zirconium-93	JEF-I	Mat 4403	133	Neptunium-237	JEF-I	Mat 4937
49	Zirconium-94	JEF-I	Mat 4404	135	Vanadium (nat)	JEF-I	Mat 4230
50	Zirconium-96	JEF-I	Mat 4406	137	Titanium (nat)	JEF-I	Mat 4220
51	Molybdenum (nat)	JEF-I	Mat 4420	138	Zircaloy-4	XA nach GEMP-346 zus.gest. XS con Zircon Teu III.68	
52	Molybdenum-95	JEF-I	Mat 4425	139	Silver-107	JEF-I	Mat 4477
53	Molybdenum-96	JEF-I	Mat 4426	140	Niobium-93	JEF-I	Mat 4413
54	Molybdenum-97	JEF-I	Mat 4427	141	Wolfram	nach Resonanzd. BNL-235 mit Genex % Ant. Nuklidk. 21.5.69 Bonka	
55	Molybdenum-98	ENDFB-V	Mat 9285	142	Ruthenium-105	JEF-I	Mat 4445
56	Molybdenum-100	ENDFB-V	Mat 9287	143	Rhodium-105	JEF-I	Mat 4455
57	Technetium-99	ENDFB-V	Mat 1308	144	Cesium-143	JEF-I	Mat 4554
58	Ruthenium-100	JEF-I	Mat 4440	145	Cerium-144	JEF-I	Mat 4584
59	Ruthenium-101	JEF-I	Mat 4441	146	Praseodymium-142	JEF-I	Mat 4592
60	Ruthenium-102	JEF-I	Mat 4442	147	Promethium-148	JEF-I	Mat 4612
61	Ruthenium-104	JEF-I	Mat 4444	148	Promethium-148m	JEF-I	Mat 4613
62	Rhodium-103	ENDFB-V	Mat 1310	149	Zirconium-95	JEF-I	Mat 4405
63	Palladium-104	JEF-I	Mat 4464	150	Poison in C	Nukem A3, A2-B. Teu. I.70 B,U,Al, Si,Cr, Mn,Fe,Co,Ni,Cu etc.	
64	Palladium-105	JEF-I	Mat 4465	151	Ruthenium-103	JEF-I	Mat 4443
65	Palladium106	JEF-I	Mat 4466	152	Xenon-133	JEF-I	Mat 4547
66	Palladium-107	JEF-I	Mat 4467	153	Cerium-141	ENDFB-V	Mat 9725
67	Palladium-108	ENDFB-V	Mat 9386	154	Praseodymium-143	JEF-I	Mat 4593
68	Palladium-110	ENDFB-V	Mat 9389	155	Promethium-149	JEF-I	Mat 4614
69	Silver-109	ENDFB-V	Mat 1373	156	Iodine-131	JEF-I	Mat 4536
70	Indium-115	JEF-I	Mat 4495	160	Fiss. Prod.U235 Chain 44		
71	Cadmium (nat)	JEF-I	Mat 4480	161	Fiss. Prod.U235 Chain 39		
72	Cadmium-110	JEF-I	Mat 4483	162	Fiss. Prod.U235 Chain 34		
73	Cadmium-111	JEF-I	Mat 4484	163	Fiss. Prod.U235 Chain 29		

Id.-no.	Absorber			Id.-no.	Absorber		
74	Cadmium-112	JEF-I	Mat 4485	164	Boron-11	JEF-I	Mat 4051
75	Cadmium-113	JEF-I	Mat 4486	165	Halfnium-174	JEF-I	Mat 4724
76	Cadmium-114	JEF-I	Mat 4487	166	Halfnium-176	JEF-I	Mat 4726
77	Tellurium-126	JEF-I	Mat 4525	167	Halfnium-177	JEF-I	Mat 4727
78	Tellurium-128	JEF-I	Mat 4527	168	Halfnium-178	JEF-I	Mat 4728
79	Tellurium-130	JEF-I	Mat 4529	169	Halfnium-179	JEF-I	Mat 4729
80	Iodine-127	ENDFB-V	Mat 9606	170	Halfnium-180	JEF-I	Mat 4720
81	Iodine-129	ENDFB-V	Mat 9608	171	Tungsten-182	JEF-I	Mat 4742
82	Xenon-128	JEF-I	Mat 4542	172	Tungsten-183	JEF-I	Mat 4743
83	Xenon-130	JEF-I	Mat 4544	173	Tungsten-184	JEF-I	Mat 4744
84	Xenon-131	JEF-I	Mat 4545	174	Tungsten-186	JEF-I	Mat 4746
85	Xenon-132	JEF-I	Mat 4546	175	Promethium-151	JEF-I	Mat 4615
86	Xenon-134	JEF-I	Mat 4548	176	Uranium-232	JEF-I	Mat 8232
87	Xenon-135	JEF-I	Mat 4549	177	Plutonium-238	JEF-I	Mat 1338
88	Xenon-136	JEF-I	Mat 4551	178	Americium-241	ENDFB-V	Mat 1361
89	Cesium-133	ENDFB-V	Mat 1355	179	Americium-242	ENDFB-V	Mat 8542
90	Cesium-135	JEF-I	Mat 4555	180	Americium-242m	ENDFB-V	Mat 1369
91	Cesium-137	ENDFB-V	Mat 9669	181	Americium-243	ENDFB-V	Mat 1363
92	Barium-134	JEF-I	Mat 4564	182	Curium-242	ENDFB-V	Mat 8642
93	Barium-136	JEF-I	Mat 4566	183	Curium-243	ENDFB-V	Mat 1343
94	Barium-137	JEF-I	Mat 4567	184	Curium-244	ENDFB-V	Mat 1344

Id.-no.	Scatterer	
1001	Carbon	300K P0 & P1 Summit to IeV & Gass 739.32K I/V 3.38mb
1002	Carbon	600K P0 & P1 Summit to IeV & Gass 890.98K I/V 3.38mb
1003	Carbon	900K P0 & P1 Summit to IeV & Gass 1110.51K I/V 3.38mb
1004	Carbon	1200K P0& P1 Summit to IeV & Gass 1363.14K I/V 3.38mb
1005	Carbon	1350K P0 & P1 Gas kernel I/V Absorption Sigma0 = 3.38mb
1006	Carbon	1500K P0 & P1 Gas kernel I/V Absorption Sigma0 = 3.38mb
1007	Hydrogen	300K P0 & P1 Gas kernel I/V Absorption Sigma0 = .332b
1008	Hydrogen in H2O	300K P0 & P1 Gaker to IeV & Gass 1153.26K I/V .332b
1009	Hydrogen	589K P0 & P1 Gas kernel 600F I/V .332b
1010	Hydrogen in H2O	589K P0 & P1 600F Gaker to IeV & Gass 1269.37K I/V .332b
1011	Hydrogen	1200K P0 & P1 Gas kernel I/V Sigma0=.332b
1012	Beryllium	980K P0 & P1 Gas kernel I/V Sigma0=10mb
1013	Beryllium	1366K P0 & P1 Gas kernel 2000F I/V Sigma0=10mb
1014	Beryllium	1422K P0 & P1 Gas kernel 2100F I/V Sigma0 =10mb
1015	Oxygen	589K P0 & P1 Gas kernel 600F
1016	Deuterium	Gas-Kern T = 293.4K Teuchert 18.5.1967
1017	Deuterium	Gas-Kern T = 493.4K Teuchert 18.5.1967
1018	Deuterium	Gas-Kern T = 593.4K Teuchert 18.5.1967
1019	Deuterium	Gas-Kern T = 693.4K Teuchert 18.5.1967
1020	Deuterium	593K *Gaker – Kira for Gr. I-55, 22-75 & Gas kernel Teu/Ha.67*
1021	Sauerstoff	Gas-Kern mit BASK bei T = 900K
1022	Beryllium in BeO	900K Summit-BeO-Matr. minus O-Matr. Rest von 101.2
1023	Berylliumoxyd	900K Summit-BeO-Matr. XA = 0.01/V XS = 9.69 S = S(O) & S(Be)
1101	Hydrogen	Nelkin-Kern (Gaker-Kira) 293.6K IX.68 Darvas
1102	Hydrogen	Nelkin-Kern (Gaker-Kira) 323.6K IX.68 Darvas
1103	Hydrogen	Nelkin-Kern (Gaker-Kira) 373.6K IX.68 Darvas
1104	Hydrogen	Nelkin-Kern (Gaker-Kira) 473.6K IX.68 Darvas
1105	Hydrogen	Nelkin-Kern (Gaker-Kira) 573.6K IX.68 Darvas
1111	Deuterium	Nelkin-Kern (Gaker-Kira) 293.6K IX.68 Darvas
1112	Deuterium	Nelkin-Kern (Gaker-Kira) 323.6K IX.68 Darvas
1113	Deuterium	Nelkin-Kern (Gaker-Kira) 373.6K IX.68 Darvas
1114	Deuterium	Nelkin-Kern (Gaker-Kira) 473.6K IX.68 Darvas
1115	Deuterium	Nelkin-Kern (Gaker-Kira) 573.6K IX.68 Darvas
1121	Oxygen	Brown-St-John-Freigas 293.6K IX.68 Teuchert
1122	Oxygen	Brown-St-John-Freigas 323.6K IX.68 Teuchert
1123	Oxygen	Brown-St-John-Freigas 373.6K IX.68 Teuchert
1124	Oxygen	Brown-St-John-Freigas 473.6K IX.68 Teuchert
1125	Oxygen	Brown-St-John-Freigas 573.6K IX.68 Teuchert
1126	Oxygen	Brown-St-John-Freigas 900.0K XII.70 Teuchert
1127	Oxygen	Brown-St-John-Freigas 1200.0K XII.70 Teuchert
1128	Oxygen	Brown-St-John-Freigas 1350.0K XII.70 Teuchert
1500	Weisser Riese	1000K Atomgewicht 1000000 22.XII.70
1600	Carbon	300K Young Phon.-Spektr. Colli Punktwerte 2eV Schroeder 4.7.70
1601	Carbon	400K Young Phon.-Spektr. Colli Punktwerte 2eV Schroeder 4.7.70
1602	Carbon	500K Young Phon.-Spektr. Colli Punktwerte 2eV Schroeder 4.7.70
1603	Carbon	600K Young Phon.-Spektr. Colli Punktwerte 2eV Schroeder 4.7.70
1604	Carbon	700K Young Phon.-Spektr. Colli Punktwerte 2eV Schroeder 4.7.70
1605	Carbon	800K Young Phon.-Spektr. Colli Punktwerte 2eV Schroeder 4.7.70
1606	Carbon	900K Young Phon.-Spektr. Colli Punktwerte 2eV Schroeder 4.7.70
1607	Carbon	1000K Young Phon.-Spektr. Colli Punktwerte 2eV Schroeder 4.7.70

1608	Carbon	1100K	Young Phon.-Spektr. Colli Punktwerte 2eV Schroeder 4.7.70
1609	Carbon	1200K	Young Phon.-Spektr. Colli Punktwerte 2eV Schroeder 4.7.70
1610	Carbon	1300K	Young Phon.-Spektr. Colli Punktwerte 2eV Schroeder 4.7.70
1611	Carbon	1350K	Young Phon.-Spektr. Colli Punktwerte 2eV Schroeder 4.7.70
1612	Carbon	1500K	Young Phon.-Spektr. Colli Punktwerte 2eV Schroeder 4.7.70

Table A-3: Fission Product Chains (Teuchert et al., 1994).

VSOP-Id.no.	Chain 44	GAM-Id.	Chain 39	GAM-Id.	Chain 34	GAM-Id.	Chain 29	GAM-Id.
14	^{135}Xe	87	^{135}Xe	87	^{135}Xe	87	^{135}Xe	87
15	FP-44	160	FP-39	161	FP-34	162	FP-29	163
16	^{136}Xe	88	^{83}Kr	35	^{83}Kr	35	^{99}Tc	57
17	^{83}Kr	35	^{95}Zr	149	^{95}Zr	149	^{103}Ru	151
18	^{95}Zr	149	^{95}Mo	52	^{95}Mo	52	^{103}Rh	62
19	^{95}Mo	52	^{99}Tc	57	^{99}Tc	57	^{105}Rh	143
20	^{97}Mo	54	^{101}Ru	59	^{101}Ru	59	^{131}Xe	84
21	^{99}Tc	57	^{103}Ru	151	^{103}Ru	151	^{133}Xe	152
22	^{101}Ru	59	^{103}Rh	62	^{103}Rh	62	^{133}Cs	89
23	^{103}Ru	151	^{105}Rh	143	^{105}Rh	143	^{134}Cs	144
24	^{103}Rh	62	^{105}Pd	64	^{131}I	156	^{143}Pr	154
25	^{105}Rh	143	^{108}Pd	67	^{131}Xe	84	^{143}Nd	101
26	^{105}Pd	64	^{109}Ag	69	^{133}Xe	152	^{144}Nd	102
27	^{108}Pd	67	^{131}I	156	^{133}Cs	89	^{145}Nd	103
28	^{109}Ag	69	^{131}Xe	84	^{134}Cs	144	^{146}Nd	104
29	^{113}Cd	75	^{133}Xe	152	^{143}Pr	154	^{147}Pm	107
30	^{131}I	156	^{133}Cs	89	^{143}Nd	101	^{148}Pm/m	148
31	^{131}Xe	84	^{134}Cs	144	^{144}Nd	102	^{148}Pm/g	147
32	^{133}Xe	152	^{141}Pr	99	^{145}Nd	103	^{147}Sm	108
33	^{133}Cs	89	^{143}Pr	154	^{146}Nd	104	^{148}Sm	109
34	^{134}Cs	144	^{143}Nd	101	^{147}Pm	107	^{149}Pm	155
35	^{141}Pr	99	^{144}Nd	102	^{148}Pm/m	148	^{149}Sm	110
36	^{143}Pr	154	^{145}Nd	103	^{148}Pm/g	147	^{150}Sm	111
37	^{143}Nd	101	^{146}Nd	104	^{147}Sm	108	^{151}Pm	175
38	^{144}Nd	102	^{147}Pm	107	^{148}Sm	109	^{151}Sm	112
39	^{145}Nd	103	^{148}Pm/m	148	^{149}Pm	155	^{152}Sm	113
40	^{146}Nd	104	^{148}Pm/g	147	^{149}Sm	110	^{153}Eu	116
41	^{147}Pm	107	^{147}Sm	108	^{150}Sm	111	^{154}Eu	117
42	^{148}Pm/m	148	^{148}Sm	109	^{151}Pm	175	^{155}Eu	118
43	^{148}Pm/g	147	^{149}Pm	155	^{151}Sm	112		
44	^{147}Sm	108	^{149}Sm	110	^{152}Sm	113		
45	^{148}Sm	109	^{150}Sm	111	^{153}Eu	116		
46	^{149}Pm	155	^{151}Pm	175	^{154}Eu	117		
47	^{149}Sm	110	^{151}Sm	112	^{155}Eu	118		
48	^{150}Sm	111	^{152}Sm	113				
49	^{151}Pm	175	^{153}Eu	116				
50	^{151}Sm	112	^{154}Eu	117				
51	^{152}Sm	113	^{155}Eu	118				
52	^{153}Eu	116	^{155}Gd	120				
53	^{154}Eu	117						
54	^{155}Eu	118						
55	^{155}Gd	120						
56	^{156}Gd	121						
57	^{157}Gd	122						

Appendix B. Neutron Transport Equation

B. 1. Introduction

This appendix gives the derivation of the Neutron Transport Equation and the definition of the terms that are used in this equation. This equation is used to solve the central problem of nuclear reactor theory, the determination of the distribution of neutrons in the reactor. To determine the distribution of neutrons in the reactor, it is necessary to investigate the process of neutron transport, that is, the motion of the neutrons as they stream about the reactor core, frequently scattering off of atomic nuclei and eventually either being absorbed or leaking out of the reactor.

B. 2. Introductory Concepts

B.2.1. Neutron Density and Flux

The neutron density $N(\underline{r},t)$ at any point $\underline{r}$ in the reactor core is defined by

$$N(\underline{r},E,t)\,d^3r dE \equiv \left[\begin{array}{l}\text{expected number of neutrons}\\ \text{in } d^3r \text{ about } \underline{r},\ \text{energies in } dE \text{ about } E\\ \text{at a time } t\end{array}\right]. \tag{B.1}$$

The neutron density is of importance because it allows calculating the rate at which nuclear reactions are occurring at any point in the reactor.

The reaction rate density $F(\underline{r},t)$ at any point in the system by multiplying the neutron density $N(\underline{r},t)$ by the interaction frequency $v\Sigma$

$$\begin{aligned} F(\underline{r},E,t)\,d^3r dE &\equiv v\Sigma(E)\,N(\underline{r},E,t)\,d^3r dE \\ &\equiv \left[\begin{array}{l}\text{expected rate at which interactions are}\\ \text{occuring in } d^3r \text{ about } \underline{r},\ \text{energies } dE \text{ about E}\\ \text{at time } t\end{array}\right], \end{aligned} \tag{B.2}$$

where v is the neutron speed and $\Sigma(E)$ is the macroscopic cross-section of the reaction.

The product $vN(\underline{r},E,t)$ in equation (B.2) is given a special name:

$$\phi(\underline{r},E,t) \equiv vN(\underline{r},E,t) \equiv \text{neutron flux } \left[\text{cm}^{-2}\text{s}^{-1}\right]. \tag{B.3}$$

The tradition in nuclear engineering is to refer this quantity as the neutron flux is very misleading since $\phi(\underline{r},E,t)$ is not all like the fluxes encountered in other engineering professions. The latter fluxes are vector quantities, whereas $\phi(\underline{r},E,t)$ is a scalar quantity.

B.2.2. Angular Neutron Density and Current

The characteristics that determine the state of an individual neutron as illustrated in Figure B-1 are:

- The neutron position, $\underline{r}$,
- energy E (or speed $v = (2E/m)^{1/2}$),
- the direction of motion, $\underline{\Omega} = \underline{v}/|\underline{v}|$,
- the time, t.

The above variables provide a sufficient description of the state of the neutron for reactor calculations. The angular neutron density function that depends on all of these variables, $n(\underline{r},E,\underline{\Omega},t)$ is defined as

$$n(\underline{r},E,\underline{\Omega},t)\,d^3r dE d\Omega = \left[\begin{array}{l}\text{the probable number of neutrons in } dr \text{ about } \underline{r},\\ \text{having energy within } dE \text{ about } E,\\ \text{travelling with direction in the solid angle } d\Omega \text{ about } \Omega,\\ \text{at time } t..\end{array}\right].$$

The angular neutron flux is defined in a similar manner as scalar neutron flux, simply by multiplying the angular neutron density by the neutron speed v:

$$\Psi(\underline{r},E,\underline{\Omega},t) \equiv vN(\underline{r},E,\underline{\Omega},t).$$

A related concept is the angular current density, defined by

$$J(\underline{r},E,\underline{\Omega},t) \equiv v\underline{\Omega}N(\underline{r},E,\underline{\Omega},t) = \underline{\Omega}\Psi(\underline{r},E,\underline{\Omega},t).$$

Since $\underline{\Omega}$ is a unit vector, the angular flux is the magnitude of the angular current density

$$\left|\underline{J}\right| = \left|\underline{\Omega}\right|\Psi = \Psi.$$

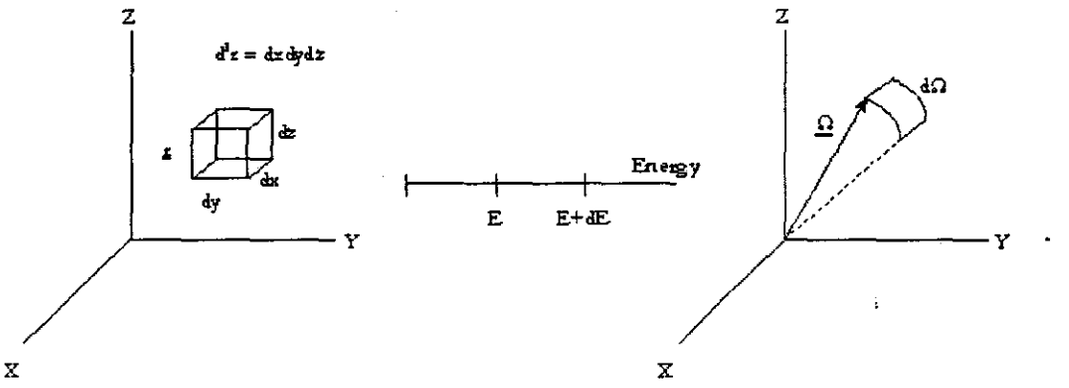

Figure B-1: The position, energy and direction variables characterising a neutron.

If D is some domain physical space, we have

$$\left[\int_D n(\underline{r},E,\underline{\Omega},t)\,d^3r\right]dEd\Omega = \begin{bmatrix}\text{the probable number of neutrons in } \underline{r},\\ \text{having energies within } dE \text{ about } E\\ \text{and directions } d\Omega \text{ about } \Omega, \text{ at time } t.\end{bmatrix},$$

and

$$\int_{4\pi}\int_{E_1}^{E_2}\int_D n(\underline{r},E,\underline{\Omega},t)d^3rdEd\Omega = \begin{bmatrix}\text{the total number of neutrons in } D,\\ \text{with energies between } E_1 \text{ and } E_2 \text{ at time } t.\end{bmatrix}.$$

Consider a surface as shown in Figure B-2 with an area increment dA and a unit normal vector $\underline{n}$ at the point $\underline{r}$:

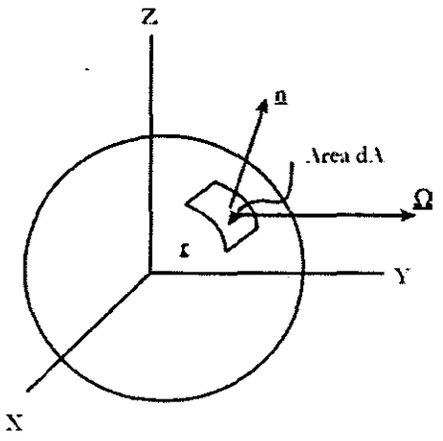

Figure B-2: Arbitrary surface with an area increment dA.

To compute the rate at which neutrons at $(\underline{r}, E, \underline{\Omega}, t)$ pass through dA, consider neutrons as shown in Figure B-3, at $\underline{r}$, travelling in the direction $\underline{\Omega}$, with energy E (or speed $v = (2E/m)^{1/2}$). In time dt the neutrons travel a distance $d\tau = v dt$.

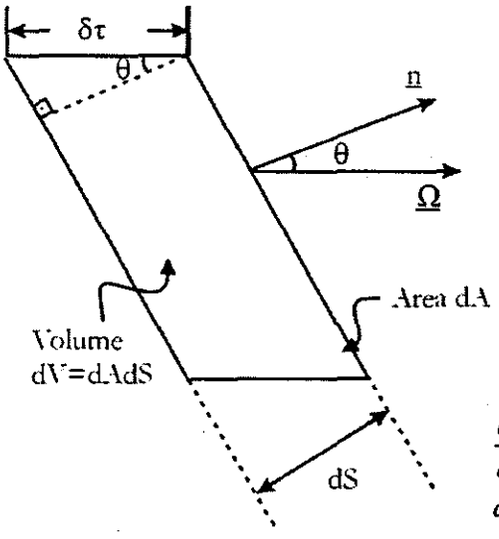

$$\frac{dS}{d\tau} = |\cos\theta| = |\underline{\Omega}\cdot\underline{n}|$$

$$dV = dA\,dS$$
$$= dA\,|\underline{\Omega}\cdot\underline{n}|\,d\tau$$
$$= dA\,|\underline{\Omega}\cdot\underline{n}|\,v\,dt.$$

Figure B-3: Neutrons incident on a differential element of area.

Since neutrons travel a distance $d\tau$, the every neutron in the volume dV at time t having direction $\underline{\Omega}$ and speed v, will exit through dA between t and $t + dt$. Therefore,

$$\begin{bmatrix}\text{number of neutrons that}\\ \text{pass through } dA \text{ in time } dt\end{bmatrix} = \begin{bmatrix}\text{number of neutrons initially in the volume}\\ \text{(and in } dE \text{ about } E,\ d\Omega \text{ about } \Omega)\end{bmatrix}$$
$$= \left(ndEd\underline{\Omega}\right)dV$$
$$= \left(ndEd\Omega\right)dA\left|\underline{\Omega}\cdot\underline{n}\right|vdt$$

and

$$v\left|\underline{\Omega}\cdot\underline{n}\right|n\left(\underline{r},E,\underline{\Omega},t\right)dEd\Omega dA = \begin{bmatrix}\text{the rate at which neutrons at } \underline{r}, \text{ within } dE \text{ about } E,\\ \text{within } d\Omega \text{ about } \Omega \text{ pass through } dA\end{bmatrix}.$$

Now, consider an arbitrary volume D with surface ∂D as shown in Figure B-4. At each point, $\underline{r} \in \partial D$. Let $\underline{n} = \underline{n}\left(\underline{r}\right)$ be the unit outer normal vector.

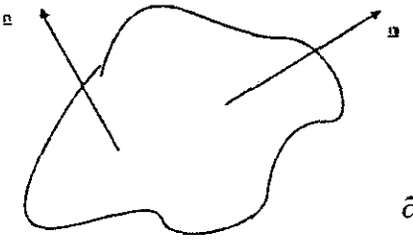

$\partial D^{\pm}$: that part of ∂D for which $\underline{\Omega}\cdot\underline{n} < 0$ or $\underline{\Omega}\cdot\underline{n} > 0$.

Figure B-4: An arbitrary volume D with surface ∂D.

Then for fixed $\underline{\Omega}, E$ and t,

$$\left[\int_{\partial D} v\underline{\Omega}\cdot\underline{n}n\left(\underline{r},E,\underline{\Omega},t\right)dA\right]dEd\Omega = \left[\int_{\partial D^{+}}^{\text{outflow } |\underline{\Omega}\cdot\underline{n}|>0} v\left|\underline{\Omega}\cdot\underline{n}\right|n\left(\underline{r},E,\underline{\Omega},t\right)dA\right]dEd\Omega$$
$$-\left[\int_{\partial D^{-}}^{\text{inflow } |\underline{\Omega}\cdot\underline{n}|<0} v\left|\underline{\Omega}\cdot\underline{n}\right|n\left(\underline{r},E,\underline{\Omega},t\right)dA\right]dEd\Omega \qquad \text{(B.4)}$$

$$\left[\int_{\partial D} v\underline{\Omega}\cdot\underline{n}n\left(\underline{r},E,\underline{\Omega},t\right)dA\right]dEd\Omega = \begin{bmatrix}\text{The rate at which neutrons within } dE \text{ about } E,\\ d\Omega \text{ about } \Omega \text{ flow out of } D\end{bmatrix}$$
$$-\begin{bmatrix}\text{The rate at which neutrons within } dE \text{ about } E,\\ d\Omega \text{ about } \Omega \text{ flow into } D\end{bmatrix}$$

or

$$\left[\int_{\partial D} v\underline{\Omega}\cdot\underline{n}n(\underline{r},E,\underline{\Omega},t)\,dA\right]dEd\Omega=\begin{bmatrix}\text{the net rate at which neutrons within } dE \text{ about } E,\\ \text{and } d\Omega \text{ about } \Omega \text{ leak out of } D\end{bmatrix}$$
$$=\text{the net leakage rate.}$$

This integral can be positive or negative. If it is positive, the rate of flow out of D is greater than the rate of flow in. if it is negative; then the rate of flow into D is greater tan the rate of flow out.

Similarly, if S is a surface with a continuously varying normal vector $\underline{n}(r)$ as shown as in Figure B-5, then

$$\left[\int_{S} v\underline{\Omega}\cdot\underline{n}n(\underline{r},E,\underline{\Omega},t)\,dA\right]dEd\Omega=\begin{bmatrix}\text{the net rate at which neutrons within } dE \text{ about } E \text{ and}\\ d\Omega \text{ about } \Omega \text{ flow through } S\end{bmatrix}.$$

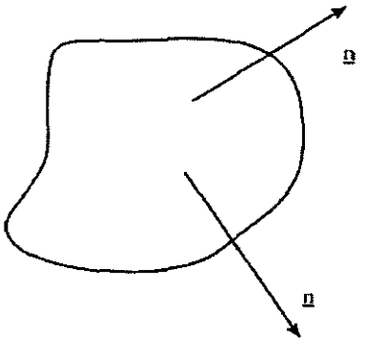

Figure B-5: An arbitrary surface S.

This integral can again be positive or negative. If it is positive, then the net neutron flow is in the direction of the normal vectors; otherwise it is in the opposite direction.

B. 3. Neutron Transport Equation

Using definitions defined in the previous section, it is possible to derive an equation for $n(\underline{r},E,\underline{\Omega},t)$. For any volume D and for fixed E and $\underline{\Omega}$ the general rate equation is given by

$$\begin{bmatrix}\text{Rate of change of}\\ \text{the neutron population for } r \in D,\\ \text{energies within } dE \text{ about } E\\ \text{and directions } d\Omega \text{ about } \Omega\end{bmatrix} = \begin{bmatrix}\text{rate of gain of neutrons in } r \in D,\\ \text{energies within } dE \text{ about } E\\ \text{and directions } d\Omega \text{ about } \Omega\end{bmatrix} - \begin{bmatrix}\text{rate of loss of neutrons in } r \in D,\\ \text{energies within } dE \text{ about } E \text{ and}\\ \text{directions } d\Omega \text{ about } \Omega\end{bmatrix}. \tag{B.5}$$

If the arbitrary volume D is chosen not to depend on time, the time differentiation can be brought inside the spatial integration

$$\begin{bmatrix}\text{Rate of change of}\\ \text{the neutron population for } r \in D,\\ \text{energies within } dE \text{ about } E \text{ and}\\ \text{directions } d\Omega \text{ about } \Omega\end{bmatrix} = \frac{d}{dt}\left[\int_D n(\underline{r},E,\underline{\Omega},t)\,d^3r\right]dEd\Omega = \left[\int_D \frac{\partial n(\underline{r},E,\underline{\Omega},t)}{\partial t}\,d^3r\right]dEd\Omega. \tag{B.6}$$

The loss mechanisms in volume D can be written as

$$\begin{bmatrix}\text{rate of loss of neutrons in}\\ \underline{r} \in D, \text{ energies within } dE \text{ about } E\\ \text{and directions } d\Omega \text{ about } \underline{\Omega}\end{bmatrix} = \begin{bmatrix}\text{rate at which neutrons in}\\ \underline{r} \in D, \text{ energies within } dE \text{ about } E\\ \text{and directions } d\Omega \text{ about } \underline{\Omega}\\ \text{undergo collisions}\end{bmatrix} + \begin{bmatrix}\text{leakage rate of neutrons in } \underline{r} \in D,\\ \text{energies within } dE \text{ about } E \text{ and}\\ \text{directions } d\Omega \text{ about } \underline{\Omega} \text{ out of } D\end{bmatrix} \tag{B.7}$$

$$= \left[\int_D v\Sigma_T(E)\,n(\underline{r},E,\underline{\Omega},t)\,d^3r\right]dEd\Omega + \left[\int_{\partial D} v\underline{\Omega}\cdot\underline{n}n(\underline{r},E,\underline{\Omega},t)\,d^3r\right]dEd\Omega$$

where $d^2r = dA, d^3r = dV$.

The divergence theorem (or Green's theorem) for a general vector function $\underline{F}(\underline{r})$ is

$$\int_{\partial D} \underline{n}\cdot\underline{F}(\underline{r})\,d^2r = \int_D \underline{\nabla}\cdot\underline{F}(\underline{r})\,d^3r$$

where the gradient operator is

$$\underline{\nabla} = \underline{i}\frac{\partial}{\partial x} + \underline{j}\frac{\partial}{\partial y} + \underline{k}\frac{\partial}{\partial z}.$$

Therefore

$$\int_{\partial D} \underline{n}\cdot\left[v\underline{\Omega}n\right]d^2r = \int_D \underline{\nabla}\cdot v\underline{\Omega}n\,d^3r = \int_D v\underline{\Omega}\cdot\underline{\nabla}n\,d^3r.$$

Thus, equation(B.7) can be written as

$$\begin{bmatrix}\text{rate of loss of neutrons in}\\ \underline{r}\in D,\ \text{energies within } dE \text{ about}\\ E \text{ and directions } d\Omega \text{ about } \underline{\Omega}\end{bmatrix} = \left\{\int_D\left[v\underline{\Omega}\cdot\underline{\nabla}n(\underline{r},E,\underline{\Omega},t) + v\Sigma_t(E)n(\underline{r},E,\underline{\Omega},t)\right]d^3r\right\}dEd\Omega. \tag{B.8}$$

Next, *the gain terms in the general rate equation are given as*

$$\begin{bmatrix}\text{rate of gain into}\\ \underline{r}\in D,\ \text{energies within } dE \text{ about}\\ E \text{ and directions } d\Omega \text{ about } \underline{\Omega}\end{bmatrix} = \begin{bmatrix}\text{rate of gain into}\\ \underline{r}\in D,\ \text{energies within } dE \text{ about}\\ E \text{ and directions } d\Omega \text{ about } \underline{\Omega} \text{ due to}\\ \textit{scottered neutrons}\end{bmatrix}$$
$$+\begin{bmatrix}\text{rate of gain into}\\ \underline{r}\in D,\ \text{energies within } dE \text{ about}\\ E \text{ and directions } d\Omega \text{ about } \underline{\Omega} \text{ due to}\\ \text{prompt fission neutrons}\end{bmatrix}$$
$$+\begin{bmatrix}\text{rate of gain into}\\ \underline{r}\in D,\ \text{energies within } dE \text{ about}\\ E \text{ and directions } d\Omega \text{ about } \underline{\Omega} \text{ due to}\\ \text{delayed fission neutrons}\end{bmatrix}$$
$$+\begin{bmatrix}\text{rate of gain into}\\ \underline{r}\in D,\ \text{energies within } dE \text{ about}\\ E \text{ and directions } d\Omega \text{ about } \underline{\Omega} \text{ due to}\\ \text{interiror sources}\end{bmatrix}. \tag{B.9}$$

The rate of gain due to the scattered and prompt fission neutrons is given as

$$\begin{bmatrix}\text{rate of gain due to}\\ \text{scattered neutrons}\end{bmatrix}=\left\{\iint_D\left[\int_{4\pi}\int_0^\infty \nu'\Sigma_s\left(E'\to E,\underline{\Omega}'\to\underline{\Omega}\right)n\left(\underline{r},E',\underline{\Omega}',t\right)dE'd\Omega'\right]d^3r\right\}dEd\Omega \qquad \text{(B.10)}$$

$$\begin{bmatrix}\text{rate of gain due to}\\ \text{prompt fission neutrons}\end{bmatrix}=\left\{\int_D\frac{\chi_p(E)}{4\pi}\right\}\left[\int_{4\pi}\int_0^\infty\left[1-\beta(E')\right]\nu(E')\nu'\Sigma_f(E')n\left(\underline{r},E',\underline{\Omega}',t\right)dE'd\Omega'\right]d^3Ed\Omega. \qquad \text{(B.11)}$$

The terms of the above equations are defined as:

- $\nu'\Sigma_f\left(E'\right)n\left(\underline{r},\underline{E}',\underline{\Omega}',t\right)dE'd\Omega'd^3r=\begin{bmatrix}\text{the fission rate in } dE' \text{ about } E',\\ d\Omega' \text{ about } \Omega' \text{ and } d^3r \text{ about } \underline{r}\end{bmatrix}$,
- $\nu(E')=\begin{bmatrix}\text{the total number of neutrons (promp \& delayed) produced}\\ \text{in a fission event that is caused by a neutron with energy } E'\end{bmatrix}$,
- $\beta(E')=\begin{bmatrix}\text{the function of neutrons in a fission event, caused by}\\ \text{a neutron with energy } E', \text{ that are delayed}\end{bmatrix}$,
- $\left[1-\beta(E')\right]\nu(E')\nu'\Sigma_f(E')n\left(\underline{r},E',\underline{\Omega}',t\right)dE'd\Omega'd^3r=\begin{bmatrix}\text{the rate at which}\\ \text{prompt fission neutrons}\\ \text{are created by neutrons}\\ \text{in } dE' \text{ about } E'd\Omega' \text{ about}\\ \Omega' \text{ and } d^3r \text{ about } \underline{r}\end{bmatrix}$.
- $\chi_p\geq(E)=\left[\text{prompt fission spectrum}\left[\int_0^\infty\chi_p(E)dE=1\right]\right]$,
- $\frac{\chi_p(E)}{4\pi}dEd\Omega=\begin{bmatrix}\text{probability that a prompt fission neutron is}\\ \text{emitted in } dE \text{ about } E \text{ and } d\Omega \text{ about } \Omega\end{bmatrix}$.

The rate of gain due to delayed fission neutrons and interior sources is given as

$$\begin{bmatrix}\text{Rate of gain due to}\\ \text{delayed fission neutrons}\end{bmatrix}=\left\{\int_D Qd\left(\underline{r},E,t\right)d^3r\right\}dEd\Omega \qquad \text{(B.12)}$$

and

$$\begin{bmatrix}\text{Rate of gain due to}\\ \text{interior sources}\end{bmatrix}=\left\{\frac{1}{4\pi}\int_D Q(r,E,t)\,d^3r\right\}dEd\Omega. \tag{B.13}$$

Interior sources are usually isotropic. The factor 4π is included as a normalisation factor so that

$$\int_{4\pi}\int_0^\infty\left\{\frac{1}{4\pi}\int_D Q(\underline{r},E,t)\,d^3r\right\}dEd\Omega=\int_0^\infty\int_D Q(\underline{r},E,t)\,d^3r dE$$
$$=\begin{bmatrix}\text{The total rate at which source}\\ \text{neutrons are introduced in } D\end{bmatrix}.$$

Combining equations (B.9) to(B.13), we have

$$\begin{bmatrix}\text{Rate of gain}\\ \text{into } \underline{r}\in D,\\ \text{energies within } dE\\ \text{about } E \text{ and}\\ \text{directions}\\ d\Omega \text{ about } \underline{\Omega}\end{bmatrix}=\left\{\int_D\left[\int\int\nu'\Sigma_s n dE'd\Omega'+\frac{\tau_p(E)}{4\pi}\int\int(1-\beta)\nu\Sigma_f\nu' n dEd\Omega'+Qd+\frac{1}{4\pi}Q\right]d^3r\right\}dEd\Omega. \tag{B.14}$$

Finally, combining equations(B.5), (B.6), (B.8) and (B.14), we obtain

$$\int_D\left[\frac{\partial n}{\partial t}+\nu\underline{\Omega}\cdot\underline{\nabla}n+\nu\Sigma_t n-\int\int\nu'\Sigma_s n dE'd\Omega'-\frac{\chi_p}{4\pi}\int\int(1-\beta)\nu\Sigma_f\nu' n dE'd\Omega'-Qd-\frac{Q}{4\pi}\right]d^3r=0.$$

Because D is arbitrary, the above integrand equals zero. Thus, introducing the angular neutron flux, we obtain

$$\frac{1}{\nu}\frac{\partial\Psi}{\partial t}+\underline{\Omega}\cdot\underline{\nabla}\Psi+\Sigma_t\Psi=\int\int\Sigma_s\Psi dE'd\Omega'$$
$$+\frac{\chi_p}{4\pi}\int\int(1-\beta)\nu\Sigma_f\Psi dE'd\Omega' \tag{B.15}$$
$$+Q_d+\frac{1}{4\pi}Q.$$

To derive an expression for Q_d, defining

$$Q_d(\underline{r},E,t)d^3rdEd\Omega = \begin{bmatrix}\text{the rate at which delayed neutrons are}\\ \text{outlined in } \underline{r}\in D,\ \text{energies within}\\ dE \text{ about } E \text{ and directions } d\Omega \text{ about } \underline{\Omega}\end{bmatrix}.$$

Recalling that neutrons arise from fissional nuclei that undergo spontaneous radioactive decay, the followings can be defined:

- $C_j(\underline{r},t)d^3r = \begin{bmatrix}\text{the probable number of fission nuclei in}\\ \text{preurser group } j, \text{ in } d^3r \text{ about } \underline{r} \text{ at time } t.\\ (\text{the decay constant for this nuclei is } \lambda_j)\end{bmatrix}$,
- $\chi_j(E) = \begin{bmatrix}\text{the spectrum of neutrons emitted from precursar}\\ \text{group } j.\ \left[\int_0^\infty \chi_j(E)dE = 1\right]\ [\text{j=1,2,.....,6}]\end{bmatrix}$,
- $\beta_j(\underline{r},E) = \begin{bmatrix}\text{the function of all fission neutrons,}\\ \text{caused by a neutron with energy } E,\\ \text{that are emitted from the } j-\text{th precursor group}\end{bmatrix}$,
- $\nu(\underline{r},E) = \begin{bmatrix}\text{expected total number of neutrons}\\ \text{emitted per fission at } \underline{r} \text{ caused by}\\ \text{a neutron at energy } E\end{bmatrix}$,
- $\beta_j(\underline{r},E)\nu(\underline{r},E) = \begin{bmatrix}\text{the expected number of neutrons that are emitted}\\ \text{by the } j\text{-th precursor group due to a fission event}\\ \text{at } \underline{r} \text{ caused by a neutron of energy E}\end{bmatrix}$,
- $\beta(E) = \sum_{j=1}^{6}\beta_j(E) = \begin{bmatrix}\text{the total function of delayed neutons in}\\ \text{a fission event caused by a neutron energy } E\end{bmatrix}$,
- $\frac{\chi_j(E)}{4\pi}dEd\Omega = \begin{bmatrix}\text{propability that a group } j \text{ delayed fission}\\ \text{neutron is emitted in } dE \text{ about } E \text{ and } d\Omega\\ \text{about } \Omega\ \left[\int_0^\infty\int_{4\pi}\frac{\chi_j}{4\pi}dEd\Omega = \int_0^\infty \chi_j dE = 1\right]\end{bmatrix}$.

Then, nuclei are introduced into the j-the precursor group in d^3r about $\underline{r}$ at the rate

$$\left[\int_0^\infty\int_{4\pi}\beta_j(E')\nu(E')\nu\Sigma_f(E')n(\underline{r},E',\underline{\Omega}',t)dE'd\Omega'\right]d^3r=\left[\int_0^\infty\int_{4\pi}\beta_j(E')\nu\Sigma_f(E')\Psi(\underline{r},E',\underline{\Omega}',t)dE'd\Omega'\right]d^3r.$$

Therefore

$$\frac{\partial}{\partial t}C_j(\underline{r},t)+\lambda_jC_j(\underline{r},t)=\int_0^\infty\int_{4\pi}\beta_j(E')\nu\Sigma_f(E')\Psi(\underline{r},E',\underline{\Omega}',t)d\Omega'dE'. \tag{B.16}$$

The rate at which precursor group j nuclei spontaneously decay is λ_jC_j , and hence this is the rate at which group j neutrons are produced. Since the spectrum for these neurons is $\lambda_j(E)$, then

$$\frac{\lambda_j(E)}{4\pi}\lambda_jC_j(\underline{r},t)d^3rdEd\Omega=\begin{bmatrix}\text{the rate at which delayed neutrons are emitted from}\\ \text{the } j\text{-th precursor group into } \underline{r}\in D,\ \text{energies within}\\ dE \text{ about } E \text{ and directions } d\Omega \text{ about } \underline{\Omega} \text{ at time } t\end{bmatrix}.$$

Hence

$$Q_d(\underline{r},E,t)=\sum_{j=1}^{6}\frac{\lambda_j(E)}{4\pi}\lambda_jC_j(\underline{r},t).$$

Equation (B.15) becomes

$$\begin{aligned}&\frac{1}{v}\frac{\partial}{\partial t}\Psi(\underline{r},E,\underline{\Omega},t)+\underline{\Omega}\cdot\underline{\nabla}\Psi(\underline{r},E,\underline{\Omega},t)+\Sigma_t(E)\Psi(\underline{r},E,\underline{\Omega},t)\\&=\int_0^\infty\int_{4\pi}\Sigma_s(E'\to E,\Omega'\cdot\Omega)\Psi(\underline{r},E',\underline{\Omega}',t)d\Omega'dE'\\&+\frac{\chi_p(E)}{4\pi}\int_0^\infty\int_{4\pi}\left[1-\beta(E')\right]\nu\Sigma_f(E')\Psi(\underline{r},E',\underline{\Omega}',t)d\Omega'dE'\\&+\sum_{j=1}^{6}\frac{\chi_j(E)}{4\pi}\lambda_jC_j(\underline{r},t)+\frac{1}{4\pi}Q(\underline{r},E,t).\end{aligned} \tag{B.17}$$

This is the full-time-dependent neutron transport equation with delayed neutrons; it is coupled with equation (B.16) which governs the precursor densities.

In some formulations of this equations, the 4π factors are absent, but the $\chi_p(E)$, $\chi_j(E)$ and

$Q(\underline{r},E,t)$ have different normalisations.

Physics which are emitted from these equations:

- certain quantum mechanics effects,
- motion of the host material,
- statistical fluctuations in the neutron density n,
- neutron-neutron and other rare interactions,
- forces (for example gravity) an neutrons,
- temperature feedback (C_i depends a temperature which depends on Ψ).

B.3.1. Initial and boundary conditions:

Equations (B.16) and (B.17) do not, by themselves, describe Ψ, initial and boundary conditions are also needed. Physically, it is expected that given all (interior and boundary) sources of neutrons, and the initial values of the angular flux and precursor densities, one should be able to determine Ψ and C_j uniquely. This expectation is correct and it gives the appropriate initial and boundary conditions.

- Interior source of neutrons:

$$\begin{aligned} &\frac{1}{4\pi}Q(\underline{r},E,t) \\ &\underline{r}\in D, \\ &0<E<\infty, \\ &t>0. \end{aligned} \tag{B.18}$$

- Initial source of neutrons:

$$\begin{aligned} &\Psi(\underline{r},E,\underline{\Omega},0)=\Psi^{i}(\underline{r},E,\Omega) \\ &\underline{r}\in D, \\ &0<E<\infty, \\ &|\underline{\Omega}|=1 \\ &\text{where } \Psi^{i} \text{ is known.} \end{aligned} \tag{B.19}$$

- Boundary source of neutrons:

$$\begin{aligned} \Psi(\underline{r},E,\Omega,t) &= \Psi^b(\underline{r},E,\Omega,t) \\ \underline{r} &\in \pi D, \\ 0 < E &< \infty, \\ \Omega \cdot \underline{n} &< 0, \\ t &> 0, \\ \text{where } \Psi^b &\text{ is known.} \end{aligned} \tag{B.20}$$

Note that since $\underline{n}$ is the unit outer normal, $\Omega \cdot \underline{n} < 0$ corresponds to all directions Ω pointing in to the spatial domain D. Therefore, one can prescribe the incoming or incident flux, corresponding to $\Omega \cdot \underline{n} < 0$, but the outgoing or existing flux, corresponding to $\Omega \cdot \underline{n} > 0$, cannot be prescribed.

- Initial values of the precursor densities

$$\begin{aligned} C_j(\underline{r},0) &= C_j'(\underline{r}) \\ \underline{r} &\in D, \\ 1 \le j &\le 6 \\ \text{where } C_j' &\text{ are all known.} \end{aligned} \tag{B.21}$$

Equations(B.16) , (B.17) and the initial and boundary conditions given above uniquely determine Ψ and C_j in a given physical system D. An assumption implicit in this formulation is that neutrons entering D through its outer boundary can be arbitrarily chosen and are independent of the existing fluxes. This is true if the boundary of D is convex, so that neutron transport problems are always solved in physical systems that are convex. Different properties of boundary of different surfaces are illustrated in Figure B-6.

In Figure B-6 the problem in (B) can be cured by enlarging the definition of D to include some exterior points as in (B'), so that the new boundary is convex.

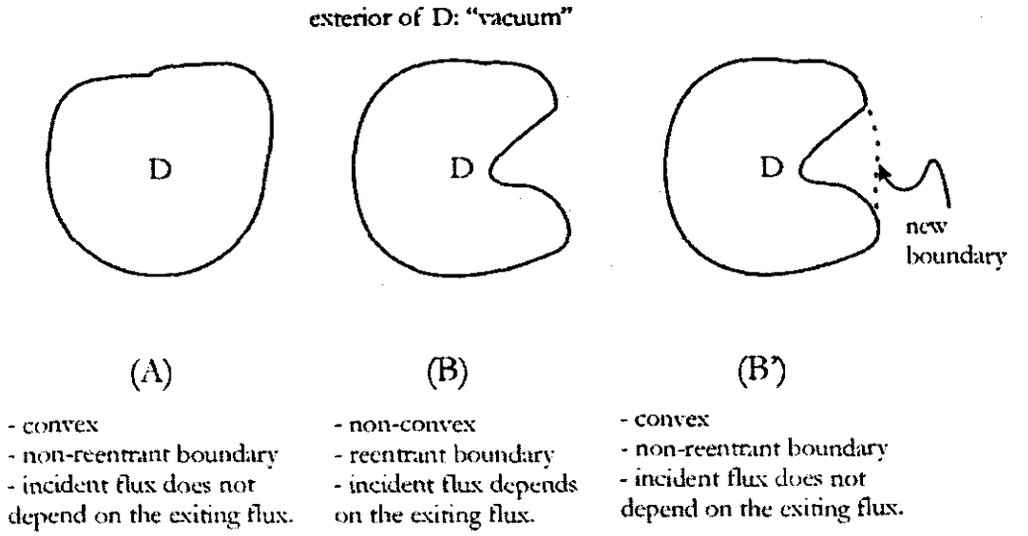

Figure B-6: Examples of re-entrant and non-re-entrant surfaces.

B. 4. Special forms of neutron transport equations

B.4.1.Transport Equation without Delayed Neutrons:

With setting $\beta_j = \beta = C_j = 0$, the Neutron transport equation becomes

$$\frac{1}{v}\frac{\partial \Psi}{\partial t} + \underline{\Omega}\cdot\underline{\nabla}\Psi + \Sigma_t \Psi = \int\int \Sigma_s \Psi d\Omega' dE' + \frac{\chi}{4\pi}\int\int \nu\Sigma_f \Psi d\Omega' dE' + \frac{1}{4\pi} Q. \tag{B.22}$$

The initial condition is given by equation (B.19) and boundary condition is given by equation(B.20).

B.4.2. Steady-state Transport Equation (Without Delayed Neutrons)

$$\underline{\Omega}\cdot\underline{\nabla}\Psi + \Sigma_t \Psi = \int\int \Sigma_s \Psi d\Omega' dE' + \frac{\chi}{4\pi}\int\int \nu\Sigma_f \Psi d\Omega' dE' + \frac{1}{4\pi} Q. \tag{B.23}$$

The corresponding boundary condition is given by equation(B.20).

B.4.3 Steady-state Transport Equation in a Purely Absorbing Medium

In a purely absorbing medium, meaning $\Sigma_s = \Sigma_f = 0$, the neutron transport equation becomes

$$\underline{\Omega}\underline{\nabla}\Psi + \Sigma_t \Psi = \frac{1}{4\pi} Q. \tag{B.24}$$

The corresponding boundary condition is given by equation(B.20).

B.4.4. Steady-state Transport Equation in a Vacuum

In a vacuum, the neutron transport equation is given by

$$\underline{\Omega}\underline{\nabla}\Psi = 0. \tag{B.25}$$

The corresponding boundary condition is given by equation(B.20).

Equations (B.24) and (B.25) can be explicitly solved because these equations do not couple angle or energy. Equation (B.23) couples angle and energy, and can be explicitly solved only in very special idealised cases.

Appendix C. Multigroup Diffusion Equations

The energy-dependent transport equation is given by

$$\begin{aligned}&\frac{1}{\upsilon}\frac{\partial \Psi}{\partial t}+\underline{\Omega}\cdot\underline{\nabla}\Psi+\Sigma_t(E)\Psi(\underline{r},E,\underline{\Omega},t)\\&=\frac{1}{4\pi}\int\int\left[\Sigma_{s0}(E'\to E)+3\underline{\Omega}'\cdot\underline{\Omega}\Sigma_{s1}(E'\to E)\right]\Psi(\underline{r},E',\underline{\Omega}',t)\,d\underline{\Omega}'dE'\\&+\frac{1}{4\pi}Q(\underline{r},E,t).\end{aligned}\tag{C.1}$$

This equation may be operated by $\int(.)\,d\Omega$ and $\int\underline{\Omega}(.)\,d\Omega$ to obtain exactly

$$\begin{aligned}\frac{1}{\upsilon}\frac{\partial \Phi}{\partial t}+\underline{\nabla}\cdot\underline{J}+\Sigma_t(E)\Phi&=\int\Sigma_{s0}(E'\to E)\Phi(\underline{r},E',t)\,dE'\\&+Q(\underline{r},E,t).\end{aligned}\tag{C.2}$$

and

$$\frac{1}{\upsilon}\frac{\partial}{\partial t}\underline{J}+\underline{\nabla}\cdot\int\underline{\Omega}\cdot\underline{\Omega}\Psi\,d\Omega+\Sigma_t(E)\underline{J}=\int\Sigma_{s1}(E'\to E)\underline{J}(\underline{r},E',t)\,dE',\tag{C.3}$$

by using approximations

$$\Psi(\underline{r},E,\underline{\Omega},t)\approx\frac{1}{4\pi}\left[\Phi(\underline{r},E,t)+3\underline{\Omega}\cdot\underline{J}(\underline{r},E,t)\right],\tag{C.4}$$

$$\underline{\nabla}\cdot\int\underline{\Omega}\cdot\underline{\Omega}\Psi\,d\Omega\approx\frac{1}{3}\underline{\nabla}\Phi,\tag{C.5}$$

yielding the energy-dependent P_1 equations as

$$\begin{aligned}&\frac{1}{\upsilon}\frac{\partial \Phi}{\partial t}(\underline{r},E,t)+\underline{\nabla}\cdot\underline{J}(\underline{r},E,t)+\Sigma_t(E)\Phi(\underline{r},E,t)\\&=\int\Sigma_{s0}(E'\to E)\Phi(\underline{r},E',t)\,dE'+Q(\underline{r},E,t),\end{aligned}\tag{C.6}$$

$$\frac{1}{\upsilon}\frac{\partial}{\partial t}\underline{J}(\underline{r},E,t)+\frac{1}{3}\underline{\nabla}\cdot\Phi(\underline{r},E,t)+\Sigma_t(E)\underline{J}(\underline{r},E,t) = \int\Sigma_{s1}(E'\to E)\underline{J}(\underline{r},E',t)\,dE'. \tag{C.7}$$

To proceed, approximations are introduced to terms $\frac{1}{\upsilon}\frac{\partial}{\partial t}\underline{J}(\underline{r},E,t)$ and $\int\Sigma_{s1}(E'\to E)\underline{J}(\underline{r},E',t)\,dE'$. For the first term as in the one-group case, it is customary to set $\frac{1}{\upsilon}\frac{\partial}{\partial t}\underline{J}\approx 0$ and for the second term to take

$$\Sigma_{s1}(E'\to E)\approx\Sigma_{s1}(E')\delta(E'\to E), \tag{C.8}$$

where

$$\Sigma_{s1}(E')=\int\Sigma_{s1}(E'\to E)\,dE. \tag{C.9}$$

Then the second term becomes

$$\int\Sigma_{s1}(E'\to E)\underline{J}(\underline{r},E',t)\,dE'\approx\int\Sigma_{s1}(E')\delta(E'\to E)\underline{J}(\underline{r},E',t)\,dE' = \Sigma_{s1}(E)\underline{J}(\underline{r},E,t). \tag{C.10}$$

Although this includes approximation the integral term of above equation is exact because of the equation(C.9). Equation (C.7) now becomes

$$\frac{1}{3}\underline{\nabla}\Phi+\Sigma_t\underline{J}=\Sigma_{s1}\underline{J}. \tag{C.11}$$

Obtaining Fick's law

$$\underline{J}(\underline{r},E,t)=-D(\underline{r},E)\underline{\nabla}\Phi(\underline{r},E,t), \tag{C.12}$$

$$D(\underline{r},E)=\frac{1}{3\left[\Sigma_t(\underline{r},E)-\Sigma_{s1}(\underline{r},E)\right]}, \tag{C.13}$$

and equation (C.6) becomes the standard time and energy dependent diffusion equation

$$\frac{1}{\upsilon}\frac{\partial}{\partial t}\Phi(\underline{r},E,t)-\underline{\nabla}\cdot D(\underline{r},E)\underline{\nabla}\Phi(\underline{r},E,t)+\Sigma_t(\underline{r},E)\Phi(\underline{r},E,t) = \int\Sigma_{s0}(\underline{r},E'\to E)\Phi(\underline{r},E',t)dE'+Q(\underline{r},E,t). \tag{C.14}$$

To derive the multigroup diffusion equations characterising the average behaviour of neutrons in each energy group, the equation for the energy dependent neutron flux, $\Phi(\underline{r},E,t)$, should be integrated (i.e. averaged) over a given group, $E_g < E < E_{g-1}$. It is assumed that this flux can adequately described by the energy dependent diffusion equation. If diffusion coefficient $D(\underline{r},E)$ and cross-sections $\Sigma_t(\underline{r},E)$ and $\Sigma_{s0}(\underline{r},E'\to E)$ are assumed to be constant over space, i.e. only depend on the neutron energy, equation (C.14) can be written as

$$\frac{1}{\upsilon}\frac{\partial\Phi}{\partial t}-\underline{\nabla}\cdot D(E)\underline{\nabla}\Phi(\underline{r},E,t)+\Sigma_t(E)\Phi(\underline{r},E,t) = \int\Sigma_s(E'\to E)\Phi(\underline{r},E',t)dE'+Q(\underline{r},E,t), \tag{C.15}$$

where the source term is defined as

$$Q(\underline{r},E,t)=\chi(E)\int\nu(E')\Sigma_f(E')\Phi(\underline{r},E',t)dE'+S_{ext}(\underline{r},E,t).$$

To eliminate the energy variable in the energy dependent diffusion equation, it should be integrated over the g-th energy group characterised by energies $E_g < E < E_{g-1}$:

$$\frac{\partial}{\partial t}\int_{E_g}^{E_{g-1}}dE\frac{1}{\upsilon}\Phi-\underline{\nabla}\cdot\int_{E_g}^{E_{g-1}}dED\underline{\nabla}\Phi+\int_{E_g}^{E_{g-1}}dE\Sigma_t\Phi = \int_{E_g}^{E_{g-1}}dE\int_0^{\infty}dE'\Sigma_s(E'\to E)\Phi(\underline{r},E',t)+\int_{E_g}^{E_{g-1}}dES. \tag{C.16}$$

The neutron flux in group g is defined as

$$\Phi_g(\underline{r},t)\equiv\int_{E_g}^{E_{g-1}}dE\Phi(\underline{r},E,t). \tag{C.17}$$

Next, the total cross-section for group g is defined as

$$\Sigma_{tg} \equiv \frac{1}{\Phi_g} \int_{E_g}^{E_{g-1}} dE \Sigma_t(E) \Phi(\underline{r}, E, t), \tag{C.18}$$

the diffusion coefficient for group g as

$$D_g \equiv \frac{\int_{E_g}^{E_{g-1}} dE D(E) \nabla_j \Phi(\underline{r}, E, t)}{\int_{E_g}^{E_{g-1}} dE \nabla_j \Phi(\underline{r}, E, t)}, \tag{C.19}$$

and the neutron speed characterising group g as

$$\frac{1}{\upsilon} \equiv \frac{1}{\Phi_g} \int_{E_g}^{E_{g-1}} dE \frac{1}{\upsilon} \Phi(\underline{r}, E, t). \tag{C.20}$$

To define the scattering term, the integral over E' is first broken up to write

$$\int_{E_g}^{E_{g-1}} dE \int_0^{\infty} dE' \Sigma_s(E' \to E) \Phi(\underline{r}, E, t) = \sum_{g'=1}^{G} \int_{E_g}^{E_{g-1}} dE \int_{E_{g'}}^{E_{g'-1}} dE' \Sigma_s(E' \to E) \Phi(\underline{r}, E', t), \tag{C.21}$$

then the group transfer scattering matrix is defined as

$$\Sigma_{g'g} \equiv \frac{1}{\Phi_{g'}} \int_{E_g}^{E_{g-1}} dE \int_{E_{g'}}^{E_{g'-1}} dE' \Sigma_s(E' \to E) \Phi(\underline{r}, E, t). \tag{C.22}$$

The fission cross-section for group is defined with a very similar manner by writing the fission term as

$$\int_{E_g}^{E_{g-1}} dE S_f(\underline{r}, E, t) = \int_{E_g}^{E_{g-1}} dE \chi(E) \left[\sum_{g'=1}^{G} \int_{E_{g'}}^{E_{g'-1}} dE' \nu(E') \Sigma_f(E') \Phi(\underline{r}, E', t) \right], \tag{C.23}$$

and the fission cross-section for group g is

$$\nu_{g'}\Sigma_{fg'} \equiv \frac{1}{\Phi_{g'}} \int_{E_{g'}}^{E_{g'-1}} dE'\nu(E')\Sigma_f(E')\Phi(\underline{r},E',t), \tag{C.24}$$

while defining

$$\chi_g \equiv \int_{E_g}^{E_{g-1}} dE\chi(E). \tag{3.25}$$

These purely formal definitions may now be used to write the multigroup diffusion equations as

$$\frac{1}{\upsilon_g}\frac{\partial\Phi_g}{\partial t} - \underline{\nabla}\cdot D_g\underline{\nabla}\Phi + \Sigma_{tg}\Phi_g(\underline{r},t) = \sum_{g'=1}^{G}\Sigma_{gg'}\Phi_{g'} + \chi_g\sum_{g'=1}^{G}\nu_{g'}\Sigma_{fg'}\Phi_{g'} + S_g, \tag{C.26}$$
$$g = 1,2,...,G.$$

The multigroup equations are still quite exact (within the diffusion approximation) but they are also quite formal in the sense that group constants are yet as undetermined. It is apparent that in order to calculate these group constants the flux $\Phi(\underline{r},E,t)$ should be known.

Appendix D. Solution Schemes of Multigroup Diffusion Equations

The multigroup diffusion equations are derived in Appendix C. , and are given by

$$\frac{1}{\upsilon_g}\frac{\partial \Phi_g}{\partial t} - \underline{\nabla}\cdot D_g \underline{\nabla}\Phi + \Sigma_{rg}\Phi_g(\underline{r},t) = \sum_{g'=1}^{G}\Sigma_{g'g}\Phi_{g'} + \chi_g\sum_{g'=1}^{G}\nu_{g'}\Sigma_{fg'}\Phi_{g'} + S_g, \qquad g = 1,2,...,G. \tag{D.1}$$

The procedure must be followed to solve this set of coupled differential equations can be summarised as:

- Determine the spectral function $\varphi(E)$ with fast and thermal neutron spectrum calculations.
- Determine the group structure.
- Determine the multigroup constants, with averaging the appropriate values over previously determined spectral function.
- Solve equation(D.1).

The above procedure can also used to perform a group collapse. The starting is not the energy-dependent diffusion equation, but rather a system of multigroup diffusion equations of the form equation (D.1) with a large number of groups, and the result is similar system of multigroup diffusion equations with fewer groups. There is a trade off in this group collapse: there is a loss in accuracy due to the reduction in the number of groups, but on the other hand the calculations required to solve the problem become less expensive.

Assuming that the discretisation in space and time is done, even for steady-state problems, multigroup diffusion equations are much more complicated than that is in one-speed approximation. Therefore it is not feasible to solve these equations by a direct method such as Gaussian elimination, and an iteration scheme must be used.

D. 1. Power Iteration Scheme for Fixed Source Problem

For steady-state problems multigroup diffusion equations can be written as

$$\begin{aligned}
-\nabla\cdot D_1\nabla\Phi_1+\Sigma_{r_1}\Phi_1&=\left(\chi_1F+\mathcal{Q}_1\right),\\
-\nabla\cdot D_2\nabla\Phi_2+\Sigma_{r_2}\Phi_2&=\left(\Sigma_{s_{12}}\Phi_1\right)+\left(\chi_2F+\mathcal{Q}_2\right),\\
&\vdots\\
-\nabla\cdot D_G\nabla\Phi_G+\Sigma_{r_G}\Phi_G&=\left(\sum_{g'=1}^{G}\Sigma_{s_{gG}}\Phi_{g'}\right)+\left(\chi_GF+\mathcal{Q}_G\right),
\end{aligned}\tag{D.2}$$

where fission source F is given by

$$F(r,t)=\sum_{g'=1}^{G}\nu\Sigma_{f_{g'}}\Phi_{g'}.\tag{D.3}$$

This suggests the iteration scheme

$$\begin{aligned}
-\nabla\cdot D_1\nabla\Phi_1^{(n+1)}+\Sigma_{r_1}\Phi_1^{(n+1)}&=\left(\chi_1F^{(n)}+\mathcal{Q}_1\right),\\
-\nabla\cdot D_2\nabla\Phi_2^{(n+1)}+\Sigma_{r_2}\Phi_2^{(n+1)}&=\left(\Sigma_{s_{12}}\Phi_2^{(n+1)}\right)+\left(\chi_2F^{(n)}+\mathcal{Q}_2\right),\\
&\vdots\\
-\nabla\cdot D_G\nabla\Phi_G^{(n+1)}+\Sigma_{r_G}\Phi_G^{(n+1)}&=\left(\sum_{g'=1}^{G}\Sigma_{s_{gG}}\Phi_G^{(n+1)}\right)+\left(\chi_GF^{(n)}+\mathcal{Q}_G\right),\\
F^{(n+1)}(r)&=\sum_{g'=1}^{G}\nu\Sigma_{f_{g'}}\Phi_{g'}^{(n+1)}(r).
\end{aligned}\tag{D.4}$$

The boundary condition for each of these equations is

$$\Phi_g(r)+2D_g(r)n(r)\cdot\nabla\Phi_g(r)=0\qquad r\in\partial D.\tag{D.5}$$

The iteration stops when the fission source is sufficiently converged, i.e. when

$$\max\left|F^{(n+1)}(r)-F^{(n)}(r)\right|_{r\in D}<\varepsilon,\tag{D.6}$$

where ε is pre-assigned convergence criteria, typically, $\varepsilon=10^{-5}$.

At each step in this scheme, one is only required to solve a one-group diffusion equation. In one-dimensional problems, each one-group diffusion problem can be solved directly by Gaussian elimination. However, in two- or three-dimensional problems, one must iterate to solve the

equations that hold within each group. These iterations are called inner iterations. A single sweep through equations (D.4) and (D.5)constitutes an outer iteration. Thus, a single outer iteration consists of possibly much inner iteration in each group.

D. 2. Inverse Power Iteration Scheme for Eigenvalue Problems

Multigroup k-eigenvalue problems typically have the form

$$-\underline{\nabla}\cdot D_g(r)\underline{\nabla}\Phi_g(r)+\Sigma_{rg}\Phi_g(r)=\sum_{g'=1}^{G}\Sigma_{g'g}\Phi_{g'}(r)+\frac{1}{k}\chi_g\sum_{g'=1}^{G}\nu_{g'}\Sigma_{fg'}\Phi_{g'}(r), \qquad g=1,2,...,G, \tag{D.7}$$

with boundary condition

$$\Phi_g(r)+2D_g(r)n(r)\cdot\nabla\Phi_g(r)=0 \qquad r\in\partial D.$$

If the function $\Phi_g(r)$ satisfies this problem, then $A\Phi_g(r)$ also satisfies it for any constant A. Therefore, the solution functions $\Phi_g(r)$ can be made unique by specifying normalisation such as

$$\int_D\left[\sum_{g'=1}^{G}\nu\Sigma_{f_{g'}}(r)\Phi_{g'}(r)\right]d^3r=\int_D F(r)d^3r=\int_D d^3r=V. \tag{D.8}$$

Physically this states that the average value of fission source $F(r)$ across the system is unity.

The inverse power iteration method is defined as follows. It begins with the (n+1)-st outer iteration with an eigenvalue estimate $k^{(n)}$ and a fission source estimate $F^{(n)}(r)$ satisfying

$$\frac{1}{V}\int_D F^{(n)}(r)d^3r=1. \tag{D.9}$$

The first step is to determine $\Phi_g^{\left(n+\frac{1}{2}\right)}$ by solving the following fixed source problem

$$-\nabla \cdot D_g \nabla \Phi_g^{\left(n+\frac{1}{2}\right)} + \Sigma_{r_g} \Phi_g^{\left(n+\frac{1}{2}\right)} = \sum_{g'=1}^{g-1} \Sigma_{s_{g'g}} \Phi_{g'}^{\left(n+\frac{1}{2}\right)} + \frac{\chi_g}{k^{(n)}} F^{(n)},$$
$$\Phi_g + 2D_g n \cdot \nabla \Phi_g = 0 \qquad r \in \partial D. \tag{D.10}$$

Next, the fission source term is defined as

$$F^{\left(n+\frac{1}{2}\right)}(r) = \sum_{g'=1}^{G} \nu \Sigma_{f_{g'}} \Phi_{g'}^{\left(n+\frac{1}{2}\right)}(r), \tag{D.11}$$

and then, equations (D.4) is summed up over g and $\sum \chi_g = 1$ is used

$$\sum_{g=1}^{G} \left[-\nabla \cdot D_g \nabla \Phi_g^{\left(n+\frac{1}{2}\right)} + \Sigma_{r_g} \Phi_g^{\left(n+\frac{1}{2}\right)} - \sum_{g'=1}^{g-1} \Sigma_{s_{g'g}} \Phi_{g'}^{\left(n+\frac{1}{2}\right)} \right] = \frac{1}{k^{(n)}} F^{(n)}. \tag{D.12}$$

Now, he above equation is integrated over spatial domain D and solved for $k^{(n)}$

$$k^{(n)} = \frac{\int_D F^{(n)}(r) d^3 r}{\int_D \sum_{g=1}^{G} \left[-\nabla \cdot D_g \nabla \Phi_g^{\left(n+\frac{1}{2}\right)} + \Sigma_{r_g} \Phi_g^{\left(n+\frac{1}{2}\right)} - \sum_{g'=1}^{g-1} \Sigma_{s_{g'g}} \Phi_{g'}^{\left(n+\frac{1}{2}\right)} \right] d^3 r}. \tag{D.13}$$

Using the most recent estimate for the scalar fluxes in this formula, define

$$k^{(n+1)} = \frac{\int_D F^{\left(n+\frac{1}{2}\right)}(r) d^3 r}{\int_D \sum_{g=1}^{G} \left[-\nabla \cdot D_g \nabla \Phi_g^{\left(n+\frac{1}{2}\right)} + \Sigma_{r_g} \Phi_g^{\left(n+\frac{1}{2}\right)} - \sum_{g'=1}^{g-1} \Sigma_{s_{g'g}} \Phi_{g'}^{\left(n+\frac{1}{2}\right)} \right] d^3 r}. \tag{D.14}$$

Dividing these last two equations, the simpler result is obtained

$$\frac{k^{(n+1)}}{k^{(n)}} = \frac{\int_D F^{\left(n+\frac{1}{2}\right)}(r) d^3 r}{\int_D F^{(n)}(r) d^3 r} = V, \tag{D.15}$$

or

$$k^{(n+1)} = k^{(n)} \left[\frac{1}{V} \int_D F^{\left(n+\frac{1}{2}\right)}(r) d^3 r \right]. \tag{D.16}$$

Finally, normalising $F^{\left(n+\frac{1}{2}\right)}(r)$, the following is obtained:

$$F^{(n+1)}(r) = \frac{F^{\left(n+\frac{1}{2}\right)}(r)}{\left[\frac{1}{V} \int_D F^{\left(n+\frac{1}{2}\right)}(r) d^3 r \right]}. \tag{D.17}$$

The inverse power iteration method is specified by equations (D.10)-(D.17). Iteration stops when

$$\left| k^{(n+1)} - k^{(n)} \right| < \varepsilon, \tag{D.18}$$

and

$$\max \left| F^{(n+1)}(r) - F^{(n)}(r) \right|_{r \in D} < \delta, \tag{D.19}$$

where ε and δ are pre-assigned convergence criteria, typically $\varepsilon = 10^{-5}$ and $\delta = 10^{-4}$.

Appendix E. Calculation of Geometric Escape Probability of Neutron in Double Heterogeneous Pebble Bed Media†

Suppose a neutron moderated in an absorber zone to the energy level E. The geometric escape probability for that neutron is the probability to escape and have its next interaction in the same or another absorber zone. Different possibilities for a neutron to experience its next interaction in a moderation zone are shown in Figure E-1. All these possibilities are embedded in the calculation of geometric escape probability. Neutron escape probability is evaluated by calculating partial escape probabilities W_i for each interaction that depends on the direction of flight of the neutron.

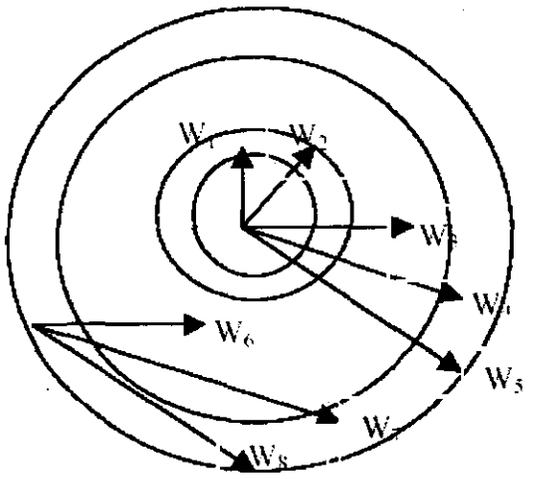

Figure E-1: Partial escape probabilities.

The partial escape probabilities have the following meanings:

W_1: The probability that a neutron born within the absorber zone of a coated particle will have its next interaction in the graphite region of the same coated particle. Apart from the graphite shell a portion of the matrix in between coated particles are included for consideration.

† Mulder, E.J., Power Performance of Inherently Safe High Temperature Reactors under Various Fuelling Schemes, University of Achen.

W_2: The probability that a neutron will leave a coated particle and adjoining graphite region without any collision.

W_3: The probability that a neutron, which has left a coated particle, has its next interaction in the graphite region of another coated particle within the same fuel sphere. An average value of all possible positions as to the originating coated particle is possible with this consideration.

W_4: The probability that a neutron as mentioned in W_3 has its next interaction within the fuel free zone of the fuel sphere.

W_5: The probability that a neutron leaves the fuel sphere without any collision.

W_6: The probability that a neutron coming from a neighbouring fuel sphere with random angular distribution of entry has an interaction in the graphite region of a coated particle of that fuel sphere.

W_7: The probability that a neutron as mentioned in W_6 has its interaction in the fuel free zone of the fuel sphere.

W_8: Probability that a neutron leaves the fuel sphere without any collision.

In fuel pin situations the escape probability is calculated due to Dancoff factors. If the pebble bed filled with a partial loading h of graphite spheres (blind spheres), then W_8 constitutes of the probabilities, W_{8a}, the portion of absorber spheres and, W_{8g}, the portion of graphite spheres. This is also valid for W_7 and W_6. Then

$$\begin{aligned} W_6 &= (1-h)W_{6a}, \\ W_7 &= (1-h)W_{7a} + hW_{7g}, \\ W_8 &= (1-h)W_{8a} + hW_{8g}. \end{aligned} \tag{E.1}$$

The probability to have an interaction within a coated particle bed is determined by the geometric layout of the coated particles in a sphere as long as the average free path length $1/\Sigma_t(E)$, within the coated particle kernel not considerably exceeds its inner radius r_i.

Homogenising over the sphere leads to incorrect interaction rates. It is necessary to drive substitute cross-sections in support of the calculated geometric escape probability $P(E)$.

Considering the following model for any particle bed:

A neutron path of flight is considered to enter the bed of coated particles with random angle of entry. The distance between any two particles touched by this line is set equal to the average distance L between the particle-cross-sectional areas perpendicular to the flight path within a particle bed of density N. These assumptions are equivalent to that of a neutron traversing any homogeneous medium for determining the probability of singular kernels being hit by that neutron. This consideration ignores any correlation to the location of neighbouring kernels.

The average length L is derived by considering the probability that the cross-section of a coated particle co-insides with a part dx of the line of flight of a neutron.

$$\frac{1}{L}dx = r_2^2\pi \cdot Ndx, \tag{E.2}$$

where r_2 is the outer radius of a coated particle. The number N of coated particles per cm^3 refers to the filling factor f given by

$$f = \frac{4\pi}{3}r_2^3 N, \tag{E.3}$$

thus $L = \frac{4r_2}{3f}$.

The probability that a neutron will travel the distance of its free path length L without any interaction is equal to the probability that a coated particle is crossed as well as a part in the graphite area in-between the coated particles. This probability is denoted as W_{8c} and given as

$$W_{8c} = e^{-\Sigma_3' L}, \tag{E.4}$$

where Σ_3' is an updated cross-section. The total probability of n pieces with length L flying through the bed without interactions subsequently defined by

$$W_{8cn} = e^{-\Sigma_3' nL}. \tag{E.5}$$

From this, Σ_3' is suitable for characterising the continuous medium in replacement of the heterogeneous bed. Within the range of the absorption resonances and for various reactor layouts, also in the thermal energy range, the total cross-sections of the core zone, Σ_1 and the coating Σ_2, are considerably different from one another. In these cases Σ_3' deviates considerably from an average cross-section Σ_3, this will result in treating the particle bed as a homogenised medium.

The probability W_{8c} can be strictly calculated. Similarly, the probability W_{71c}, which is denoting an interaction within the core zone of a particle due to a randomly penetrating neutron, and W_{72c} denoting an interaction in the graphite region, can be calculated. For these interactions the following is valid:

$$W_{8c} + W_{71c} + W_{72c} = 1. \tag{E.6}$$

Then $1 - W_{8c}$ is the probability that an interaction will occur during flight of a neutron.

This interaction is taking place within the core zone with probability of $\frac{W_{71c}}{1 - W_{8c}}$, while $\frac{W_{72c}}{1 - W_{8c}}$ will be the probability of interaction within the graphite zone. Based on these probabilities adapted cross-sections for the interactions within the core zone and graphite material are defined as

$$\begin{aligned} \Sigma_{31}' &= \frac{W_{71c}}{1 - W_{8c}} \Sigma_3', \\ \Sigma_{32}' &= \frac{W_{72c}}{1 - W_{8c}} \Sigma_3'. \end{aligned} \tag{E.7}$$

The calculation of interactions is explained by the lengths which depict the neutron path of flight through the individual material zones with angle of entry ϑ, as represented in Figure E-2. If $\sin^2 \vartheta = u$, then the following relationships hold:

$$
\begin{aligned}
l_1 &= r_2\left[\sqrt{1-u}-\sqrt{\left(\frac{r_1}{r_2}\right)^2-u}\right],\\
l_2-l_1 &= 2r_2\sqrt{\left(\frac{r_1}{r_2}\right)^2-u},\\
l_3 &= 2r_2\sqrt{1-u},\\
\lambda-l_0 &= r_2\left[\frac{2}{3f}-\sqrt{1-u}\right], and\\
\sin^2\vartheta = u_0 &= \left(\frac{r_1}{r_2}\right)^2.
\end{aligned}
\tag{E.8}
$$

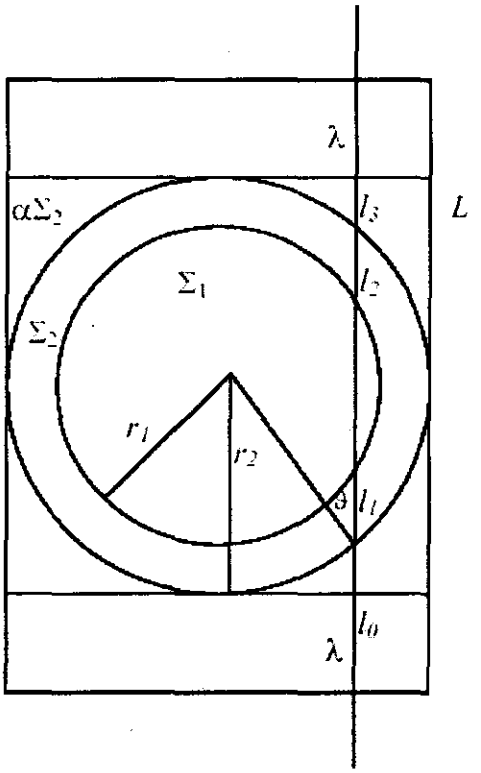

Figure E-2: W_i Calculation Model.

Now the interactions W_i can be written as:

$$W_{8c} = \int_{\vartheta=0\ldots\vartheta_0} \frac{\cos\vartheta}{\pi} d\Omega \cdot e^{-2\alpha\Sigma_2(\lambda-l_0)} \cdot e^{-2\Sigma_2 l_1} \cdot e^{-\Sigma_1(l_2-l_1)} + \int_{\vartheta=\vartheta_0\ldots\frac{\pi}{2}} \frac{\cos\vartheta}{\pi} d\Omega \cdot e^{-2\alpha\Sigma_2(\lambda-l_0)} \cdot e^{-2\Sigma_2 l_1},$$
$$W_{71c} = \int_{\vartheta=0\ldots\vartheta_0} \frac{\cos\vartheta}{\pi} d\Omega \cdot e^{-\alpha\Sigma_2(\lambda-l_0)-\Sigma_2 l_1}\left[1-e^{-\Sigma_1(l_2-l_1)}\right]. \quad \text{(E.9)}$$

Here, $\frac{\cos\vartheta}{\pi} d\Omega$ is the probability that any neutron entering the sphere with $d\vartheta$ the angle of entry. The other factors represent the penetrating probabilities through the single zones.

Then the W_i model becomes

$$W_3 \frac{1-W_{8c}}{W_{72c}} + W_4 + W_5 = 1,$$
$$W_{6a} \frac{1-W_{8c}}{W_{72c}} + W_{7a} + W_{8a} = 1, \quad \text{(E.10)}$$
$$W_{7b} + W_{8b} = 1.$$

According to above relations, the geometric escape probability is formulated as follows:

$$P(E) = W_1 + W_2\left(W_3 + W_4\right) + W_2 W_5 \frac{W_6 + W_7}{1-W_8}. \quad \text{(E.11)}$$

Here the first sum refers to interaction in the originating kernel, while second refers to the originating sphere, the third is the probability that the neutron leaves the sphere $\left(W_2 W_5\right)$, the none or more spheres are penetrated without an interaction $\left(\sum_{n=0}^{\infty} W_8^n = \frac{1}{1-W_8}\right)$ and finally in a sphere an interaction occurs in the graphite region $\left(W_6 + W_7\right)$.

Appendix F. P_N (Spherical Harmonics) Approximation to Transport Theory

The direct numerical solution of transport equation starts with converting the transport equation into a system of algebraic equations. This is accomplished by "discretising" each of the variables in the transport equations, that is, by replacing functions of continuous variables by a discrete set of points. The derivatives and integrals appearing in the transport equation must also be replaced by a corresponding discrete representation.

The discretisation of transport equation can be accomplished by using either the method of discrete ordinates or function expansions. Suppose an equation for a function, $f(x)$, which contains derivatives and integrals

$$F\left(f(x), \frac{df}{dx}, \frac{d^2 f}{dx^2}, ..., \int dx' f(x'), ...\right) = 0. \tag{F.1}$$

In the discrete ordinate approach, one begins with representing the unknown $f(x)$ only by its values at a discrete set of points x_i of the independent variable x. That is the domain is first discretised of variation of x into a mesh of discrete points, each of which is labelled by a subscript i. Then $f(x)$ is replaced by its value at each of these mesh points

$$f(x) \to f(x_i) \equiv f_i, \quad i = 1, 2, ..., N. \tag{F.2}$$

What has actually done, was to replace a function $f(x)$ by a column vector $\underline{f}$

$$f(x) \to \underline{f} = col(f_1, f_2, ..., f_N). \tag{F.3}$$

In this sense, the system of algebraic equations for the unknown components of $\underline{f}$ can be written as a matrix equation.

Next the various operations in the original equation must be replaced by their discretised counterparts. For example, for derivatives finite-difference formulas such as,

$$\left.\frac{df}{dx}\right|_{x=x_i} \cong \frac{f(x_i)-f(x_{i-1})}{x_i-x_{i-1}} = \frac{f_i-f_{i-1}}{x_i-x_{i-1}} \equiv \frac{\Delta f_i}{\Delta x_i}. \tag{F.4}$$

Integrals would be presented as sums or numerical quadrature formulas such as

$$\int_a^b dx f(x) \cong \sum_{i=1}^{N} w_i f(x_i) = \sum_{i=1}^{N} w_i f_i, \tag{F.5}$$

where the w_i is known as the quadrature weights.

An alternative way to arrive at a discrete representation of an equation is to write the unknown functions as an expansion in a finite number of known functions (frequently polynomials). If these expansion functions are presented by $p_l(x)$, then

$$f(x) \cong \sum_{l=1}^{N} f_l p_l(x). \tag{F.6}$$

Hence, once again the function $f(x)$ is represented by a vector $\underline{f}$; the components of the vector are just the unknown expansion coefficients f_l. When the dependent variable ranges between -1 and +1, a very convenient choice of expansion functions are the Legendre polynomials (Clark and Hansen, 1964):

$$P_0(x)=1, P_1(x)=x, P_2(x)=\frac{(3-x^2)}{2},\ldots \tag{F.7}$$

This choice of expansion is frequently used to represent the angular dependence of the neutron flux in one-dimensional problems in which $\mu=\cos\theta$ is the natural independent variable(Duderstadt, 1976):

$$\phi(x,\mu,E,t) = \sum_{l=1}^{N} \phi_l(x,E,t) P_l(\mu). \tag{F.8}$$

F. 1. The P_N Approximation

The basic equation of neutron conservation is the linear Boltzmann equation. For

monoenergetic neutrons this equation is

$$\underline{\Omega}\cdot\underline{\nabla}\phi(\underline{r},\underline{\Omega})+\sigma_t(\underline{r})\phi(\underline{r},\underline{\Omega})=\int_{\Omega}d\underline{\Omega}'\sigma_s(\underline{r},\underline{\Omega}'\rightarrow\underline{\Omega})\phi(\underline{r},\underline{\Omega}')+S(\underline{r},\underline{\Omega}), \qquad (F.9)$$

where $\phi(\underline{r},\underline{\Omega})$ is the number of neutrons crossing a unit surface at $\underline{r}$ per unit time going in a unit solid angle centred in the direction $\underline{\Omega}$, $\sigma_t(\underline{r})$ is the total neutron cross-section at $\underline{r}$, $\sigma_s(\underline{r},\underline{\Omega}'\rightarrow\underline{\Omega})$ is the probability per unit length that a neutron at $\underline{r}$ and going in the direction $\underline{\Omega}'$ will undergo a collision and emerge going in a unit solid angle centred at $\underline{\Omega}$, and $S(\underline{r},\underline{\Omega})$ is the number of neutrons created per unit volume at $\underline{r}$ going in unit solid angle centred at $\underline{\Omega}$.

A particularly useful approximation to the Boltzmann equation is so-called P_N or spherical harmonics approximation. The basis of the approximation is the expansion of all functions of the angular variable in terms of the spherical harmonics.

The Legendre polynomials suffice for one-dimensional problems. The Legendre polynomials given by equation (F.7) are an orthogonal set of functions and the flux in the equation (F.9) may be expanded with these Legendre polynomials. Resulting set of equations separates into an infinite set of coupled differential equations. The spherical harmonic approximation is introduced by truncating the infinite set of differential equations at some order and treating them either analytic or numerical methods.

The derivation for one-dimensional plane geometry starts with expanding the scattering cross-section, directional flux and the source in equation(F.9). For an isotropic medium the scattering cross-section is a function of only the angle between the vectors $\underline{\Omega}$ and $\underline{\Omega}'$, say θ_0. It is convenient to consider the variable $\cos\theta_0=\mu_0$, rather than θ_0 itself. The scattering function can then be expanded in terms of the Legendre polynomials $P_n(\mu_0)$. Thus

$$\sigma_s(\underline{r},\underline{\Omega}'\rightarrow\underline{\Omega})=\frac{1}{2\pi}\sum\frac{2m+1}{2}\sigma_m(\underline{r})P_m(\mu_0), \qquad (F.10)$$

the factor $\frac{2m+1}{4\pi}$ is inserted for later convenience. From the orthogonality of Legendre polynomials,

$$\sigma_{sn}(\underline{r}) = 2\pi \int_{-1}^{+1} d\mu_0 \sigma_s(\underline{r}, \underline{\Omega}' \to \underline{\Omega}) P_n(\mu_0). \tag{F.11}$$

in slab geometry the flux $\phi(x, \underline{\Omega})$ is a function of position x and, since the medium is assumed isotropic, the angle between the x-axis and $\underline{\Omega}$, say θ. The directional flux is expanded in the form

$$\phi(x, \underline{\Omega}) = \sum_n \frac{2n+1}{2} \phi_n(x) P_n(\mu), \tag{F.12}$$

with

$$\phi_n(x) = \int_{-1}^{+1} d\mu \phi(x, \mu) P_n(\mu). \tag{F.13}$$

In a similar manner, for the source

$$S(x, \underline{\Omega}) = \sum_n \frac{2n+1}{2} S_n(x) P_n(\mu), \tag{F.14}$$

with

$$S_n(x) = \int_{-1}^{+1} d\mu S(x, \mu) P_n(\mu). \tag{F.15}$$

the expansions for the flux and source are functions of μ, whereas the scattering function is a function of μ_0. It is evident geometrically that μ and μ_0 are related as shown by Figure F-1. The angles θ, φ refer to the coordinates of $\underline{\Omega}$ whereas θ', φ' refers to the vector $\underline{\Omega}'$.

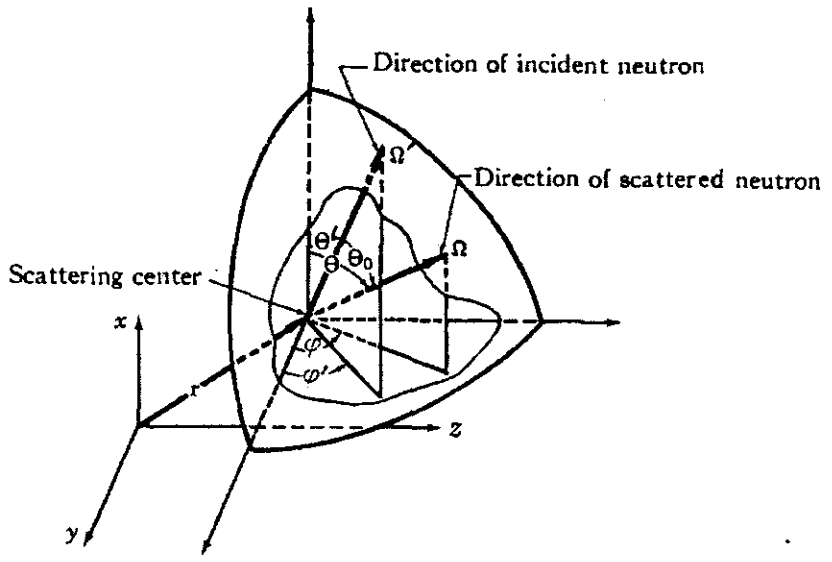

Figure F-1: Geometry of a scattering event (Clark and Hansen, 1964).

The unit vectors $\underline{\Omega}$ and $\underline{\Omega}'$ may be written in terms of the unit coordinate vectors as

$$\underline{\Omega} = \cos\theta\,\underline{i} + \sin\theta\cos\varphi\,\underline{j} + \sin\theta\sin\varphi\,\underline{k},$$

and

$$\underline{\Omega}' = \cos\theta'\,\underline{i} + \sin\theta'\cos\varphi'\,\underline{j} + \sin\theta'\sin\varphi'\,\underline{k}.$$

The cosine of the angle θ_0 is then

$$\cos\theta_0 = \mu_0 = \cos\theta\cos\theta' + \sin\theta\sin\theta'\left(\cos\varphi\cos\varphi' + \sin\varphi\sin\varphi'\right), \tag{F.16}$$

or

$$\mu_0 = \mu\mu' + \sqrt{1-\mu^2}\sqrt{1-\mu'^2}\cos\left(\varphi-\varphi'\right). \tag{F.17}$$

The Legendre polynomial satisfies the following so-called addition theorem (Clark and Hansen, 1964)

$$P_n\left(\mu_0\right) = \sum\frac{(n-\beta)!}{(n+\beta)!}P_n^{\beta}\left(\mu\right)P_n^{\beta}\left(\mu'\right)e^{i\beta(\varphi-\varphi')}, \tag{F.18}$$

where $\mu_0, \mu, \mu', \varphi$ and φ' are related to each other by equation(F.17), and $P_n^\beta(\mu)$ is the associated Legendre polynomial of order β and degree n. The associated Legendre polynomials are defined by

$$P_n^\beta(\mu) = (1-\mu^2)^{\beta/2} \frac{d^\beta}{d\mu^\beta}[P_n(\mu)]. \tag{F.19}$$

The scattering integral in the Boltzmann equation may be reduced to a function of x, μ only. The expansions defined by equations (F.10) and(F.12), and the addition theorem may be used in the integrand of the integral in equation(F.9). Only the term $\beta = 0$ in the sum over β, which arises from the use of addition theorem, contributed to the integral over φ'. Furthermore, in the integration over μ', only the combination $m = n$ provides a non-vanishing contribution. By use of the expansion defined by equations (F.12)and(F.14) in the remaining three terms of the Boltzmann equation

$$\begin{aligned} &\sum_n \frac{2n+1}{2}\left[\mu P_n(\mu)\frac{d}{dx}\phi_n(x) + \sigma_t P_n(\mu)\phi_n(x)\right] \\ &= \sum_n \frac{2n+1}{2}\left[\sigma_{s,n}(x) P_n(\mu)\phi_n(x) + S_n(x) P_n(\mu)\right] \end{aligned} \tag{F.20}$$

To derive the equation for each harmonic, equation (F.20) should be multiplied by $P_n(\mu)$ and integrated over μ. The term in $\mu P_n(\mu)$ is eliminated by use of the recurrence relation for the Legendre polynomials

$$(n-\beta+1)P_{n+1}^\beta(\mu) - (2n+1)\mu P_n^\beta(\mu) + (n+\beta)P_{n-1}^\beta(\mu) = 0. \tag{F.21}$$

After some algebra one gets an infinite set of coupled differential equations for the harmonics of the flux as

$$\begin{aligned} &\frac{n+1}{2n+1}\frac{d}{dx}\phi_{n+1}(x) + \frac{n}{2n+1}\frac{d}{dx}\phi_{n-1}(x) + \sigma_t\phi_n(x) = \sigma_{s,n}\phi_n(x) + S_n(x), \\ &n = 0, 1, \ldots \end{aligned} \tag{F.22}$$

Various order approximations are obtained by truncating the series at some fixed N. The

truncation to order N consists of assuming all quantities within index $N+1$ are zero. The first $N+1$ equations are then used. The resulting set of equations is known as P_N equations. The P_1 equations are

$$\begin{aligned} &\frac{d}{dx}\phi_1(x)+\sigma_t\phi_0(x)=\sigma_{s,0}\phi_0(x)+S_0(x), \\ &\frac{1}{3}\frac{d}{dx}\phi_0(x)+\sigma_t\phi_1(x)=\sigma_{s,1}\phi_1(x)+S_1(x). \end{aligned} \tag{F.23}$$

F. 2. Some Useful Definitions

- Slowing-down Density

Slowing-down density, $q(\underline{r},E)$, is defined as

$$\begin{aligned} q(\underline{r},E) &= \int_E^{E_0} S(E')\,dE' - \int_E^{E_0} \Sigma_a(E')\phi(E')\,dE', \\ &= \left[\begin{array}{l}\text{the rate at which source neutrons are}\\ \text{produced at energies > E}\end{array}\right] \\ &\quad - \left[\begin{array}{l}\text{the rate at which neutrons having}\\ \text{energies > E are absorbed}\end{array}\right]. \end{aligned} \tag{F.24}$$

This is a balance or conservation law, which must hold in a steady-state situation.

- Neutron Lethargy

Lethargy is a variable that is often used in slowing down calculations in place of the neutron energy variable since the slowing down equations become somewhat simpler. To define lethargy, let E_0 be the maximum neutron energy in a system, then lethargy of neutron with energy E is given by

$$u = \ln\frac{E_0}{E}. \tag{F.25}$$

Lethargy is always greater than zero, and as energy approaches zero, lethargy becomes infinity. Also note that, as a neutron loses energy in a collision, it means it gains lethargy and the changes

in lethargy are due to a collision is independent of the maximum neutron energy, E_0. In many applications, u is a more convenient variable than E, because the mathematical form of the slowing-down equation becomes simpler.

- Elastic Scattering Probability Function

The probability that a neutron, undergoing a scattering reaction at energy E', has final energy within dE about E is defined by,

$$P(E' \to E)\,dE = \begin{cases} \dfrac{1}{(1-\alpha)E'}, & \alpha E' < E < E', \\ 0, & \text{otherwise.} \end{cases} \tag{F.26}$$

Equation (F.26) is defined in terms of the lethargy variable as

$$p(u' \to u)|du| = P(E' \to E)\,dE. \tag{F.27}$$

Thus, for $\alpha E' < E < E'$

$$\begin{aligned} p(u' \to u) &= P(E' \to E)\left|\frac{dE}{du}\right|, \\ &= \frac{E}{(1-\alpha)E'}, \\ &= \frac{E_0 e^{-u}}{(1-\alpha)E_0 e^{-u'}}, \\ &= \frac{e^{u'-u}}{1-\alpha}. \end{aligned} \tag{F.28}$$

After rewriting the domain boundary conditions, $\alpha E' < E < E'$, in terms of the lethargy variable

$$p(u' \to u) = \begin{cases} \dfrac{e^{u'-u}}{1-\alpha}, & u' < u < u' + \ln\dfrac{1}{\alpha} \\ 0, & \text{otherwise.} \end{cases} \tag{F.29}$$

- Mean Lethargy Gain per Collision

Let a neutron with initial energy E' scatter off an atom with mass number A, and let the neutron have final energy E. Then the change in the lethargy of the neutron is

$$\begin{aligned} u-u' &= \ln\frac{E_0}{E}-\ln\frac{E_0}{E'}, \\ &= \left(\ln E_0-\ln E\right)-\left(\ln E_0-\ln E'\right), \\ &= \ln\frac{E'}{E}, \\ &= \Delta u. \end{aligned} \tag{F.30}$$

Now, define mean lethargy gain as

$$\begin{aligned} \xi &= \langle \Delta u \rangle, \\ &= \int_{u'}^{\infty}(u-u')\,p(u'\to u)\,du, \\ &= \int_{u'}^{u'+\ln\frac{1}{\alpha}}(u-u')\frac{e^{-(u-u')}}{1-\alpha}\,du, \\ &= \frac{1}{1-\alpha}\int_{0}^{\ln\frac{1}{\alpha}} te^{-t}\,dt, \qquad t=u-u', \\ &= \frac{1}{1-\alpha}\left[-(1+t)e^{-t}\right]_0^{\ln\frac{1}{\alpha}}, \\ \xi &= 1+\alpha\left(\frac{\ln\alpha}{1-\alpha}\right), \qquad \alpha=\left(\frac{A-1}{A+1}\right)^2. \end{aligned} \tag{F.31}$$

- Number of Collisions to Thermalise

If a neutron has initial energy E_i and (after one or more collisions), a final energy E_f, then by equation (F.30)

$$\ln\frac{E_i}{E_f} = u_f-u_i = N\langle \Delta u\rangle = N\xi. \tag{F.32}$$

Hence

$$N = \frac{1}{\xi} \ln \frac{E_i}{E_f}, \tag{F.33}$$

where ξ is a function of A, the mass number of the nucleus.

- Moderating Power and Moderating Ratio

The number of scattering collisions necessary to slow a neutron to thermal energies is inversely proportional to ξ. The probability of a scattering collision is small if scattering cross-section Σ_s is small. So, a good moderator is characterised by a large value of Σ_s. Hence, a more appropriate measure of the moderating or slowing down power is the product of ξ and Σ_s. Then

$$\text{Moderating Power} \equiv \xi\Sigma_s. \tag{F.34}$$

A good moderator has to be a weak absorber as well. Then the moderating power itself will not be sufficient to describe the effectiveness of a material for neutron moderation. Then

$$\text{Moderating Ratio} \equiv \frac{\xi\Sigma_s}{\Sigma_a}. \tag{F.35}$$

Therefore, a good moderator has large Σ_s, large ξ and small Σ_a. The moderating power and ratio are given for several materials of interest in Table F-1.

Table F-1: Slowing down parameters of typical moderators (Duderstadt, 1976:324).

Moderator	A	α	ξ	$\rho\left[g/cm^3\right]$	Number of collisions from 2MeV to 1eV	$\xi\Sigma_s\left[cm^{-1}\right]$	$\frac{\xi\Sigma_s}{\Sigma_a}$
H	1	0	1	Gas	14	-	-
D	2	0.111	0.725	Gas	20	-	-
H_2O	-	-	0.920	1.0	16	1.35	71
D_2O	-	-	0.509	1.1	29	0.176	5670
He	4	0.360	0.425	Gas	43	1.6×10^{-5}	83
Be	9	0.640	0.209	1.85	69	0.158	143
C	12	0.716	0.158	1.60	91	0.060	192
^{238}U	238	0.983	0.008	19.1	1730	0.003	0.0092

F. 3. Lethargy Dependent P_1 Equations

To derive lethargy dependent P_1 equations, it necessary to write the lethargy dependent transport equation

$$\begin{aligned}&\mu\frac{\partial}{\partial x}\psi(x,\mu,u)+\Sigma_t(u)\psi(x,\mu,u)\\&=\frac{1}{2}\int_0^{u}\int_{-1}^{+1}\left[\Sigma_{s0}(u'\to u)+3\mu\mu'\Sigma_{s1}(u'\to u)\psi(x,\mu',u')\right]d\mu'du'+\frac{1}{2}S_0(x,u).\end{aligned} \tag{F.36}$$

Setting the scalar flux, $\phi(x,u)$ and current, $J(x,u)$

$$\begin{aligned}\phi(x,u)&=\int_{-1}^{+1}\psi(x,\mu',u)\,d\mu',\\J(x,u)&=\int_{-1}^{+1}\mu'\psi(x,\mu',u)\,d\mu',\end{aligned} \tag{F.37}$$

results with

$$\begin{aligned}\mu\frac{\partial\psi}{\partial x}+\Sigma_t\psi=&\frac{1}{2}\int_0^{u}\Sigma_{s0}(u'\to u)\phi(x,u')\,du'\\&+\frac{3\mu}{2}\int_0^{u}\Sigma_{s1}(u'\to u)J(x,u')\,du'+\frac{1}{2}S_0(x,u).\end{aligned} \tag{F.38}$$

Now, setting

$$\psi\approx\frac{1}{2}\left[\phi(x,u)+3\mu J(x,u)\right], \tag{F.39}$$

and operating by $\int_{-1}^{+1}(.)d\mu$ and $\int_{-1}^{+1}\mu(.)d\mu$, the following is obtained:

$$\begin{aligned}\frac{d}{dx}J(x,u)+\Sigma_t(u)\phi(x,u)&=\int_0^{u}\Sigma_{s0}(u'\to u)\phi(x,u')\,du'+S_0(x,u),\\\frac{1}{3}\frac{d}{dx}\phi(x,u)+\Sigma_t(u)J(x,u)&=\int_0^{u}\Sigma_{s1}(u'\to u)J(x,u')\,du'.\end{aligned} \tag{F.40}$$

These are the lethargy dependant P_1 equations with

$$\Sigma_{s0}(u' \to u) = \begin{cases} \dfrac{\Sigma_s(u')e^{u'-u}}{1-\alpha}, & u' < u < u' - \ln(1/\alpha), \\ 0, & otherwise, \end{cases}$$
$$\Sigma_{s1}(u' \to u) = \Sigma_{s0}(u' \to u)\left[\frac{A+1}{2}e^{\frac{u'-u}{2}} - \frac{A-1}{2}e^{\frac{u'-u}{2}}\right]. \tag{F.41}$$

Equation (F.40) is approximated only because of the angular approximation made in the application of P_1 method. Because the scattering integrals in these equations are somewhat complicated, a rewriting of these integrals (for A=1) or an approximation to these integrals (for A >> 1) is usually performed. To do this, defining the slowing down densities

$$q_0(x,u) = \int_{u'=0}^{u}\int_{u''=u}^{\infty} \Sigma_{s0}(u' \to u'')\phi(x,u')\,du''du',$$
$$q_1(x,u) = \int_{u'=0}^{u}\int_{u''=u}^{\infty} \bar{\mu}_0\Sigma_{s1}(u' \to u'')J(x,u')\,du''du'. \tag{F.42}$$

Differentiating the above equations and using the appropriate definition of equation (F.41) yields

$$\frac{d}{du}q_0 = \Sigma_s(u)\phi(x,u) - \int_0^u \Sigma_{s0}(u' \to u)\phi(x,u')\,du',$$
$$\frac{d}{du}q_1 = \bar{\mu}_0\Sigma_{s0}(u)J(x,u) - \int_0^u \Sigma_{s1}(u' \to u)J(x,u')\,du'. \tag{F.43}$$

Introducing above equations into equation(F.40) gives

$$\frac{d}{dx}J(x,u) + \Sigma_t(u)\phi(x,u) = \Sigma_s(u)\phi(x,u) - \frac{d}{du}q_0 + S_0(x,u),$$
$$\frac{1}{3}\frac{d}{dx}\phi(x,u) + \Sigma_t(u)J(x,u) = \bar{\mu}_0\Sigma_s(u)J(x,u) - \frac{d}{du}q_1. \tag{F.44}$$

or defining the non-elastic cross-section, $\Sigma_{ne}(u)$ and transport cross-section, $\Sigma_{tr}(u)$

$$\begin{aligned} &\frac{d}{dx}J(x,u)+\Sigma_{re}(u)\phi(x,u)=-\frac{d}{du}q_0+S_0(x,u),\\ &\frac{1}{3}\frac{d}{dx}\phi(x,u)+\Sigma_{tr}(u)J(x,u)=-\frac{d}{du}q_1. \end{aligned} \tag{F.45}$$

This gives two equations with four unknowns. Equation (F.42) yields two other equations. However, the integral terms in these equations are too complicated, so some special cases (for A=1) or approximations (for A >> 1) are usually applied to these equations. Details of such approximation can be found in many textbooks (Duderstadt, 1976; Massimo, 1975). A summary can be given of these various approximate treatments of neutron slowing down by writing P_1 equations as

$$\begin{aligned} &\frac{\partial J}{\partial x}+\Sigma_{re}(u)\phi(x,u)=-\frac{\partial q_0^H}{\partial u}-\sum_i\frac{\partial q_0^{NH_i}}{\partial u}+S_0(x,u),\\ &\frac{1}{3}\frac{\partial \phi}{\partial x}+\Sigma_{tr}(u)J(x,u)=-\frac{\partial q_1^H}{\partial u}-\sum_i\frac{\partial q_1^{NH_i}}{\partial u}. \end{aligned} \tag{F.46}$$

where slowing-down densities superscripted with H represent the hydrogenous while NH represents non-hydrogenous medium.

The effects of inelastic scattering and fission are including in the source term as

$$\begin{aligned} S_0(x,u)=&\sum_{i=1}^{N}\int_0^u du'\Sigma_{in}^i(u'\to u)\phi(x,u')\\ &+\sum_{i=1}^{N}\chi_i(u)\int_0^\infty du'\nu_i\Sigma_f^i(u')\phi(x,u')+S_{ext}(x,u). \end{aligned} \tag{F.47}$$

The slowing down densities are given by

$$\begin{aligned} &\frac{\partial q_0^H}{\partial u}+q_0^H(x,u)=\Sigma_s^H\phi(x,u),\\ &\frac{2}{3}\frac{\partial q_1^H}{\partial u}+q_1^H(x,u)=\frac{4}{9}\Sigma_s^H J(x,u),\quad \begin{pmatrix}\text{exact treatment of}\\ \text{Hydrogenous medium}\end{pmatrix},\\ &\lambda_{0i}\frac{\partial q_0^{NH_i}}{\partial u}+q_0^{NH_i}(x,u)=\beta_{0i}\phi(x,u),\\ &\lambda_{1i}\frac{\partial q_0^{NH_i}}{\partial u}+q_1^{NH_i}(x,u)=\beta_{1i}J(x,u),\quad \begin{pmatrix}\text{approximate treatment of}\\ \text{non-Hydrogenous medium}\end{pmatrix}. \end{aligned} \tag{F.48}$$

The various approximations can then be characterised by the appropriate choice of the coefficients $\lambda_{0i}, \lambda_{1i}, \beta_{0i}$ and β_{1i}, which are summarised in Table F-2, and for Greuling-Goertzel (s-wave scattering) approximation these coefficients are given as

$$\lambda_{0i} \equiv \frac{1-\alpha_i\left(1+\ln\frac{1}{\alpha_i}+\frac{1}{2}\ln^2\frac{1}{\alpha_i}\right)}{1-\alpha_i\left(1+\ln\frac{1}{\alpha_i}\right)}, \tag{F.49}$$

$$\lambda_{1i} \equiv -\left\{\begin{array}{l}\frac{(1+\gamma_i)^2}{4\gamma_i}\left\{\frac{(1+\gamma_i)}{3}\left[\frac{8}{9}-\alpha_i^{3/2}\left(\ln^2\frac{1}{\alpha_i}-\frac{4}{3}\ln\frac{1}{\alpha_i}+\frac{8}{9}\right)\right]\right\} \\ -(1-\gamma_i)\left[8-\alpha_i^{1/2}\left(\ln^2\frac{1}{\alpha_i}-4\ln\frac{1}{\alpha_i}+8\right)\right]\end{array}\right\}\varsigma^{-1}, \tag{F.50}$$

where

$$\varsigma_i \equiv \frac{(1+\gamma_i)^2}{\gamma_i^2}\left\{\frac{1+\gamma_i}{9}\left(1-\alpha_i^{3/2}\left(\frac{3}{2}\ln\frac{1}{\alpha_i}+1\right)\right)-(1-\gamma_i)\left(1-\alpha_i^{1/2}\left(\frac{1}{2}\ln\frac{1}{\alpha_i}+1\right)\right)\right\}, \tag{F.51}$$

$$\gamma_i \equiv A_i^{-1}.$$

Table F-2: Parameters for continuous slowing down models (Duderstadt, 1976).

Model	λ_{0i}	λ_{1i}	β_{0i}	β_{1i}
Age approximation Selengut-Goertzel	0	0	$\xi_i\Sigma_s^i$	0
Consistent Age approximation	0	0	$\xi_i\Sigma_s^i$	$\varsigma_i\Sigma_s^i$
Greuling-Goertzel (s-wave scattering)	Eqn. (F.49)	Eqn. (F.50)	$\xi_i\Sigma_s^i$	$\varsigma_i\Sigma_s^i$

F. 4. Treatment of Spatial Dependence in the P_1 Slowing Down Equations

To conclude the discussion of this chapter, three ways of including the effects of spatial dependence in fast spectrum calculations will be described. All these three methods assume a homogeneous spatial medium. These methods are:

- Age-diffusion theory, which combines diffusion theory in space with age theory in

lethargy u.

- Muft-Gam calculations, which use a buckling approximation in space applied to lethargy dependant P_1 equations.
- The B_1 method, which uses a buckling approximation in space applied to the lethargy dependant transport equation.

F.4.1. Age-Diffusion Theory

Age diffusion theory is also known as *age*, *Fermi age*, *inconsistent age* or *continuous slowing down theory*. The starting point for this method is the lethargy dependant diffusion equation with a delta function (in u) source

$$-D(u)\frac{\partial^2}{\partial x^2}\phi(x,u)+\Sigma_{ne}(x,u)\phi(x,u)=-\frac{\partial}{\partial u}q_0(x,u)+S_0(x)\delta(u),$$
$$q_0(x,u)=\xi\Sigma_s(u)\phi(x,u). \tag{F.52}$$

Eliminating $\phi(x,u)$ from equation (F.52) results in

$$\frac{\partial}{\partial u}q_0(x,u)+\frac{\Sigma_{ne}(u)}{\xi\Sigma_s(u)}q_0(x,u)=\frac{D(u)}{\xi\Sigma_s(u)}\frac{\partial^2}{\partial x^2}q_0(x,u)+S_0(x)\delta(u). \tag{F.53}$$

Now, giving the definitions for $q_0(x,u)$ and Fermi age τ as

$$q_0(x,u)=\hat{q}(x,u)\exp\left(-\int_0^u\frac{\Sigma_{ne}(u')}{\xi\Sigma_s(u')}du'\right), \tag{F.54}$$

$$\tau=\int_0^u\frac{D(u')}{\xi\Sigma_s(u')}du',$$
$$\frac{d\tau}{du}=\frac{D(u)}{\xi\Sigma_s(u)}, \tag{F.55}$$

and also defining

$$\hat{q}(x,u)=\tilde{q}(x,\tau),$$
$$\frac{d\tilde{q}}{d\tau}=\frac{d\hat{q}}{du}\frac{du}{d\tau}=\frac{d\hat{q}}{d\tau}\frac{\xi\Sigma_s(u)}{D(u)}. \tag{F.56}$$

and substituting $\hat{q}(x,u)$ into equation(F.53), give

$$\frac{\xi\Sigma_s(u)}{D(u)}\frac{\partial\hat{q}}{\partial u}=\frac{\partial^2}{\partial x^2}\hat{q}+\left[\frac{\xi\Sigma_s(0)}{D(0)}\right]S_0(x)\delta(u). \tag{F.57}$$

Using the new independent variable τ

$$\frac{\partial}{\partial\tau}\tilde{q}(x,\tau)=\frac{\partial^2}{\partial x^2}\tilde{q}(x,\tau)+\left[\frac{\xi\Sigma_s(0)}{D(0)}\right]S_0(x)\delta(u). \tag{F.58}$$

However, for $\tau\cong 0$ and $u\cong 0$, equation (F.55) gives

$$\tau\approx u\frac{D(0)}{\xi\Sigma_s(0)}=au\Rightarrow u\approx\frac{1}{a}\tau,$$
$$\delta(u)=\delta\left(\frac{\tau}{a}\right)=a\delta(\tau)=\frac{D(0)}{\xi\Sigma_s(0)}\delta(\tau). \tag{F.59}$$

Therefore, equations (F.58) and (F.59) yield

$$\frac{\partial}{\partial\tau}\tilde{q}(x,\tau)=\frac{\partial^2}{\partial x^2}\tilde{q}(x,\tau)+S_0(x)\delta(\tau). \tag{F.60}$$

By equations (F.55) and (F.56), $u<0$ implies $\tau<0$, and since $q_0(u)=0$ for $u<0$, $\tilde{q}(u)=0$ for $\tau<0$. Operating equation (F.60) by $\int_{-\varepsilon}^{+\varepsilon}(.)\,du$ results in

$$\tilde{q}(x,\varepsilon)=\int_0^{\varepsilon}\frac{\partial^2\tilde{q}}{\partial x^2}d\tau+S_0(x), \tag{F.61}$$

and letting $\varepsilon \to 0$

$$\tilde{q}(x,0^+) = S_0(x). \tag{F.62}$$

Therefore equation (F.60) can be replaced by

$$\frac{\partial}{\partial \tau}\tilde{q}(x,\tau) = \frac{\partial^2}{\partial x^2}\tilde{q}(x,\tau), \tag{F.63}$$

which is valid for $\tau > 0$ and subject to initial condition, $\tilde{q}(x,0) = S_0(x)$. Equation (F.63) is the Fermi Age Equation. It has the form of the standard time-dependent diffusion equation with τ playing the role of time.

F.4.2. Muft-Gam Method

In this method one consistently solves equation (F.46) but with an assumed separable form for the spatial dependence

$$\begin{aligned}
\phi(x,u) &= \phi(u)e^{iBx}, \\
J(x,u) &= iJ(u)e^{iBx}, \\
q_0(x,u) &= q_0(u)e^{iBx}, \\
q_1(x,u) &= iq_1(u)e^{iBx}, \\
S_0(x,u) &= S_0(u)e^{iBx},
\end{aligned} \tag{F.64}$$

where B is the geometric buckling. The idea is that $f(x) = e^{iBx}$ satisfies the equation

$$\frac{d^2}{dx^2}f(x) + B^2 f(x) = 0,$$

which approximately describes the spatial dependence of the angular flux.

The resulting P_1 equations is

$$\begin{aligned} iBJ(u)+\Sigma_{ne}(u)\phi(u) &= -\frac{\partial q_0^H}{\partial u}-\sum_i \frac{\partial q_0^{NH_i}}{\partial u}+S_0(u), \\ \frac{iB}{3}\phi(u)+\Sigma_{tr}(u)J(u) &= -\frac{\partial q_1^H}{\partial u}-\sum_i \frac{\partial q_1^{NH_i}}{\partial u} \end{aligned} \tag{F.65}$$

augmented by the set

$$\begin{aligned} \frac{\partial q_0^H}{\partial u}+q_0^H(u) &= \Sigma_s^H \phi(u), \\ \frac{2}{3}\frac{\partial q_1^H}{\partial u}+q_1^H(u) &= \frac{4}{9}\Sigma_s^H J(u), \end{aligned} \tag{F.66}$$

and

$$\begin{aligned} \lambda_{0i}\frac{\partial q_0^{NH_i}}{\partial u}+q_0^{NH_i}(u) &= \beta_{0i}\phi(u), \\ \lambda_{1i}\frac{\partial q_0^{NH_i}}{\partial u}+q_1^{NH_i}(u) &= \beta_{1i}J(u). \end{aligned} \tag{F.67}$$

the inelastic scattering and fission have been included in the source term by

$$S_0(u)=\sum_{i=1}^{N}\int_0^u du'\Sigma_{in}^i(u'\to u)\phi(u')+\sum_{i=1}^{N}\chi_i(u)\int_0^\infty du'\nu_i\Sigma_f^i(u')\phi(u')+S_{ext}(u). \tag{F.68}$$

F.4.3. B_1 Method

The same separable spatial approximation as in the Muft-Gam method is used but here the starting point is the lethargy dependent transport equation as below, rather than the lethargy dependent P_1 equations.

$$\begin{aligned} \mu\frac{\partial}{\partial x}\psi(x,\mu,u)+\Sigma_t(u)\psi(x,\mu,u) &= \frac{1}{2}\int_0^\infty \Sigma_{s0}(u'\to u)\phi(x,u')du' \\ &\quad +\frac{3\mu}{2}\int_0^\infty \Sigma_{s1}(u'\to u)J(x,u')du' \\ &\quad +\frac{1}{2}S_0(x,u), \end{aligned} \tag{F.69}$$

where

$$\phi(x,u)=\int_{-1}^{+1}\psi(x,\mu',u)\,d\mu',$$
$$J(x,u)=\int_{-1}^{+1}\mu'\psi(x,\mu',u)\,d\mu'.$$

Using equation(F.43), equation (F.69) becomes

$$\begin{aligned}\mu\frac{\partial}{\partial x}\psi(x,\mu,u)+\Sigma_t(u)\psi(x,\mu,u)=&\frac{1}{2}\left[\Sigma_s(u)\phi(x,u)-\frac{\partial}{\partial u}q_0(x,u)\right]\\&+\frac{3\mu}{2}\left[\bar{\mu}_0\Sigma_s(u)J(x,u)-\frac{\partial}{\partial u}q_1(x,u)\right]\\&+\frac{1}{2}S_0(x,u).\end{aligned}\qquad\text{(F.70)}$$

Also, q_0 and q_1 are approximated same as in equation (F.48). Introducing the same assumed separable form shown below for the spatial variation into equation (F.70) gives the basis equations of the B_1 method.

$$\begin{aligned}\psi(x,\mu,u)&=\phi(\mu,u)e^{iBx},\\ \phi(x,u)&=\phi(u)e^{iBx},\\ J(x,u)&=iJ(u)e^{iBx},\\ q_0(x,u)&=q_0(u)e^{iBx},\\ q_1(x,u)&=iq_1(u)e^{iBx},\\ S_0(x,u)&=S_0(u)e^{iBx}.\end{aligned}\qquad\text{(F.71)}$$

After some rearranging these equations can be written as

$$\begin{aligned}BJ(u)+\Sigma_m(u)\phi(u)&=-\frac{d}{du}q_0(u)+S_0(u),\\ \frac{B}{3}\phi(u)+\gamma(u)\Sigma_t(u)J(u)&=-\frac{d}{du}q_1(u),\\ \lambda_0\frac{d}{du}q_0(u)+q_0(u)&=\beta_0\phi(u),\\ \lambda_1\frac{d}{du}q_1(u)+q_1(u)&=\beta_1J(u),\end{aligned}\qquad\text{(F.72)}$$

where

$$\gamma(u)=\frac{\left(\frac{B}{\Sigma_t}\right)^2 \tan^{-1}\left(\frac{B}{\Sigma_t}\right)}{3\left[\frac{B}{\Sigma_t}-\tan^{-1}\left(\frac{B}{\Sigma_t}\right)\right]} \cong 1+\frac{4}{15}\left(\frac{B}{\Sigma_t}\right).$$

Appendix G. Narrow Resonance Approximations

The effective resonance integral for capture for a single resonance at energy E_0 is defined as

$$I_\gamma = \int_{E_0} \sigma_\gamma^F(E)\phi_F(E)dE, \tag{G.1}$$

where σ_γ^F is the Doppler broadened microscopic capture cross-section of the absorber and $\phi_F(E)$ is the energy dependent flux in the fuel. In order to calculate effective resonance integral, first, σ_γ^F and after that the flux, $\phi_F(E)$ should be evaluated.

G. 1. The Doppler Broadened Resonance

Bethe-Plazcek formula is widely used for the Doppler broadened resonance cross-section. It is a convolution of the Maxwellian energy distribution of the resonance absorbers and the resonance cross-section that is a function of the neutron energy in the centre of mass system of the neutron and target nucleus described by the Breit-Wigner formula.

The Bethe-Plazcek resonance cross-section for capture (Duderstadt, 1976) is given as

$$\sigma_\gamma = \sigma_0 \frac{\Gamma_\gamma}{\Gamma}\psi(\zeta, x), \tag{G.2}$$

where Γ_γ is the natural line width and σ_0 is the total cross-section at the resonance energy for the unbroadened cross-section defined as

$$\sigma_0 = 2.608\times 10^6 \left(\frac{A+1}{A}\right)^2 \frac{1}{E_0}\frac{\Gamma_n}{\Gamma} g,$$

where A is the mass number of the absorber, Γ_n is the natural line width for resonance scattering and g is the statistical spin factor, which is equal to unity for the $l = 0$ resonances which are of primary interest in nuclear reactor calculations.

The Bethe-Plazcek function $\psi(\zeta, x)$ is given by (Duderstadt, 1976) as follows:

$$\psi(\zeta,x)=\frac{\zeta}{2\sqrt{\pi}}\int_{-\infty}^{+\infty}\frac{\exp\left(-\frac{1}{4}\zeta^2(x-y)^2\right)}{1+y^2}dy,$$
$$x=\frac{2(E-E_0)}{\Gamma},\qquad (G.3)$$
$$\zeta=\frac{\Gamma}{\Gamma_D}=\frac{\Gamma}{\sqrt{\frac{4E_0k_BT}{A}}}=\sqrt{\frac{A\Gamma^2}{4E_0k_BT}},$$

where Γ_D is the Doppler width of the resonance and k_BT is the temperature in eV. The exact value of the function ψ at the resonance energy is

$$\psi(\zeta,0)=\frac{\sqrt{\pi}}{2}\zeta\exp\left(\frac{1}{4}\zeta^2\right)erfc\left(\frac{\zeta}{2}\right).\qquad (G.4)$$

G. 2. The Energy Dependent Flux

The energy dependent flux $\phi_F(E)$ can be obtained by solving the slowing down equations for a two region unit-cell. Two approximate solutions exist namely narrow resonance (NR) and narrow resonance infinite mass (NRIM). In the NR the practical width of the resonance is small compared to the energy loss of a neutron suffered in a collision with an absorber nucleus. NRIM is valid for the opposite situation (Duderstadt, 1976). This means that for NRIM

$$\Delta E|_A=\left(\frac{1-\alpha_A}{2}\right)E_0 \square\ \Gamma_P,$$
$$\Gamma_P=\sqrt{\frac{\sigma_0}{\sigma_P^F}\Gamma},\qquad (G.5)$$

where σ_P^F is the potential scattering cross-section of the absorber and $\alpha_A=\left(\frac{A-1}{A+1}\right)^2$.

In the NRIM the absorber nucleus mass is taken to be infinite, which implies that absorber does not contribute to the slowing down process of the neutron.

G. 3. The Effective Resonance Integral

Inserting both the flux and the broadened cross-section in equation (G.1) results in

$$
\begin{aligned}
I_i &= \frac{\sigma_0 \Gamma_\gamma}{E_0}\left[\beta J(\zeta,\beta)+L(\zeta,\beta)\right], \\
J(\zeta,\beta) &= \int_{-\infty}^{+\infty} \frac{\psi(\zeta,x)}{\psi(\zeta,x)+\beta}\,dx, \\
L(\zeta,\beta) &= \int_{0}^{+\infty} \frac{P_{FO}(\xi,\beta,x)\psi^2(\zeta,x)}{\psi(\zeta,x)+\beta}\,dx, \\
\beta_{NR} &= \frac{\sigma_P^{NR}}{\sigma_0}, \\
\beta_{NRIM} &= \frac{\sigma_P^{NRIM}}{\sigma_0}\frac{\Gamma}{\Gamma_\gamma}, \\
\sigma_P^{NR} &= \frac{\sigma_{SM}^F N_M^F}{N_A}+\sigma_P, \\
\sigma_P^{NRIM} &= \frac{\sigma_{SM}^F N_M^F}{N_A},
\end{aligned}
\qquad \text{(G.6)}
$$

where

$\sigma_P^{NR(IM)}$: potential scattering cross-section per absorber nuclide in the fuel,

σ_P : potential scattering cross-section of the absorber nuclide,

N_M^F : the nuclide density of the moderator admixed in the fuel,

σ_{SM}^F : the microscopic scattering cross-section of the moderator admixed in the fuel.

G. 4. Application of the Wigner's Rational Approximation

A considerable simplification is achieved when Wigner's rational approximation for P_{FO} is inserted into the effective resonance integral expression (equation(G.6)).

For the NR case:

$$\begin{aligned} P_{FO}(\zeta,\beta,x) &= \left[1+\Sigma_t^F \bar{l}_F'\right]^{-1}, \\ &= \left[1+\left(\sigma_P^{NR}+\sigma_0\psi(\zeta,x)\right)N_A\bar{l}_F'\right]^{-1}, \\ &= \left[1+\left(\beta_{NR}+\psi(\zeta,x)\right)\sigma_0 N_A\bar{l}_F'\right]^{-1}. \end{aligned} \tag{G.7}$$

For the NRIM case:

$$\begin{aligned} P_{FO}^{NRIM}(\zeta,\beta,x) &= \left[1+\left(\Sigma_t^F - N_A\sigma_{SA}^F\right)\bar{l}_F'\right]^{-1}, \\ &= \left[1+\left(\sigma_P+\sigma_\gamma^F+\frac{N_M^F}{N_A}\sigma_{SM}^F\right)N_A\bar{l}_F'\right]^{-1}, \\ &= \left[1+\left(\beta_{NRIM}+\psi(\zeta,x)\right)\frac{\sigma_0\Gamma_\gamma}{\Gamma}N_A\bar{l}_F'\right]^{-1}. \end{aligned} \tag{G.8}$$

Inserting these equations for the first flight escape probability in equation(G.6), a simple expression for the individual effective resonance integral is achieved.

$$\begin{aligned} I^{NR(IM)} &= \frac{\sigma_0\Gamma_\gamma}{E_0}\beta'_{NR(IM)}J\left(\zeta,\beta'_{NR(IM)}\right), \\ \beta'_{NR} &= \frac{\sigma_P^{NR}+\sigma_e}{\sigma_0}, \\ \beta'_{NRIM} &= \frac{\sigma_P^{NRIM}+\sigma_e}{\sigma_0}\frac{\Gamma}{\Gamma_\gamma}, \\ \sigma_e &= \frac{1}{N_A\bar{l}_F'}, \end{aligned} \tag{G.9}$$

whee σ_e is defined as the escape cross-section.

Table G-1 gives the resonance parameters characterising several of the lower lying resonances of ^{238}U.

Table G-1: Low-lying resonance data for U-238 (Duderstadt, 1976:335).

$E_0(eV)$	$\Gamma_n(eV)$	$\Gamma_\gamma(eV)$	$\sigma_0(b)$	$\Gamma_p(eV)$	$\frac{1}{2}(1-\alpha_A)E_0(eV)$
6.67	0.00152	0.026	2.16×10^5	1.26	0.055
20.90	0.0087	0.025	3.19×10^4	1.95	0.174
36.80	0.032	0.025	3.98×10^4	3.65	0.306
66.54	0.026	0.022	2.14×10^4	2.26	0.554
102.47	0.070	0.026	1.86×10^4	3.98	0.850
116.85	0.030	0.022	1.30×10^4	1.32	0.966
165.27	0.0032	0.018	2.41×10^3	0.98	1.370
208.46	0.053	0.022	8.86×10^3	2.63	1.730

Appendix H. Approximate Models of Neutron Thermalisation

Neutrons having energies less than several eV are considered as thermal neutrons. Such neutrons are approximately in thermal equilibrium with the reactor, and on the average they neither gain nor lose energy in colliding with reactor nuclei. Thermal neutron scattering is more complicated than the fast neutron scattering because:

- Kinetic energy of a neutron is approximately equal to the thermal energy of atomic motion. Hence,
- upscattering is as important as down scattering, and
- the microscopic cross-section must be averaged over the thermal distribution of nuclear speeds (nuclei must be regarded as at rest).
- Kinetic energy of a neutron is approximately equal to the binding energy in molecular or crystalline materials. Therefore, neutrons can interact with aggregates of nuclei.
- Inelastic scattering can be important.
- Diffraction effects can be important.

H. 1. The Proton Gas (Wigner-Wilkins) Model

This model is exact under the following conditions:

- The proton gas is in thermal equilibrium at temperature T.
- The microscopic scattering cross-section σ_s^H is independent of the relative velocity v_r between a neutron and a hydrogen atom.
- The absorption cross-section behaves as $\sigma_a^H = \frac{\gamma}{v_r}$.
- There is no direct contribution from fission neutrons in the thermal energy range. Thus $\chi(E) = 0$ for thermal energies.

The Wigner-Wilkins equation is defined as (Duderstadt, 1976)

$$-\frac{d}{dx}\left\{\frac{1}{P(x)}\frac{d}{dx}[V(x)+\Gamma]\psi(x)\right\}+\left\{W(x)[V(x)+\Gamma]-\frac{4}{\sqrt{\pi}}\right\}\psi(x)=0,$$

$$W(x)=\frac{x^2}{P(x)}-\frac{e^{-x^2}}{P^2(x)},\quad x\equiv\left(\frac{E}{kT}\right)^{1/2},\qquad (H.1)$$

$$P(x)=e^{-x^2}+\sqrt{\pi}x\,erf(x),$$

$$\Gamma=\frac{\Sigma_a(kT)}{\Sigma_{fr}^H}=\frac{N_A\gamma}{\upsilon_T N_H\sigma_s^H},$$

where Σ_{fr}^H is the free atom scattering cross-section for hydrogen atom, kT is the temperature in eV. The boundary conditions are that the flux variable vanishes as $x\to 0[E\to 0]$ and be normalised to the slowing down source for $x\gg 1[E\gg kT]$.

H. 2. The Heavy Gas Model

Obviously the proton gas model is of limited value in analysing neutron thermalisation in non-hydrogenous moderators such as graphite. The simplest thermalisation model is based on expanding the cross-section for a free gas of arbitrary mass number A in powers of 1/A, hence arriving at an approximation which should be valid for large mass numbers.

The differential cross-section for a free gas can be derived in a straightforward consideration of two-body kinematics (Duderstadt, 1976). This cross-section can be written as

$$\Sigma_s(E'\to E)=\frac{\Sigma_{fr}\theta^2}{2E'}e^{-(\varepsilon-\varepsilon')}\left\{\begin{array}{l}\left[erf\left(\theta\sqrt{\varepsilon'}-\rho\sqrt{\varepsilon}\right)\pm erf\left(\theta\sqrt{\varepsilon'}+\rho\sqrt{\varepsilon}\right)\right]\\ +erf\left(\theta\sqrt{\varepsilon'}-\rho\sqrt{\varepsilon}\right)\mp erf\left(\theta\sqrt{\varepsilon'}+\rho\sqrt{\varepsilon}\right)\end{array}\right\},\qquad (H.2)$$

where

$$\theta=\frac{(A+1)}{2\sqrt{A}},\quad \rho=\frac{(A-1)}{2\sqrt{A}},\quad \varepsilon=\frac{E}{kT}.$$

Expanding in inverse mass number A^{-1} and retain only lowest order term results with the heavy gas model of the scattering kernel

$$\Sigma_s(E' \to E) = \Sigma_{fr}\left(\frac{E}{E'}\right)^{\frac{1}{2}}\left\{\delta(E-E') + \frac{(E+E')}{A}\left[\delta'(E-E') + kT\delta''(E-E')\right]\right\}''. \quad \text{(H.3)}$$

Here δ' and δ'' "refers to the first and second derivatives of the Dirac δ-function. The corresponding total scattering cross-section for this model is

$$\Sigma_s(E) = \Sigma_{fr}\left(1 + \frac{kT}{2AE}\right). \quad \text{(H.4)}$$

After substituting this rather singular scattering kernel into differential scattering cross-section equation, one finds

$$\Sigma_a(E)\phi(E) = \xi\Sigma_{fr}\left[EkT\frac{d^2\phi}{dE^2} + E\frac{d\phi}{dE} + \phi(E)\right]. \quad \text{(H.5)}$$

This simple differential equation is known as the heavy gas equation. The heavy gas model is far less effective at predicting thermal spectra in graphite moderated reactors than is the proton gas model for the LWR because of the significance of chemical binding effects.

H. 3. Synthetic Scattering Kernel Models

The scattering kernel $\Sigma_s(E' \to E)$ is of such a form that the integral form of the infinite medium spectrum equation could easily be transformed into a differential equation by some models. One such a model is generalised heavy gas or primary model in which the scattering terms in infinite medium spectrum equation are modelled by a differential equation similar to the heavy gas model (Duderstadt, 1976):

$$\int_0^\infty dE'\Sigma_s(E' \to E)\phi(E') - \Sigma_s(E)\phi(E) \cong \xi\Sigma_{fr}\frac{d}{dE}\left\{f(E)\left[EkT\frac{d\phi}{dE} + (E-kT)\phi\right]\right\}. \quad \text{(H.6)}$$

Here $f(E)$ is an arbitrary function that must be determined either by fitting to experimental spectrum measurements or by a fit to an integral of the scattering kernel itself $\Sigma_s(E' \to E)$.

The primary model satisfies the detailed balance condition and includes some accounting for the chemical binding effects. Unfortunately, it fails to yields satisfactory results when a strong

absorption is present. For this reason a slightly more elaborate approximation, known as the *secondary model*, containing two free functions is developed.

The scattering kernel can be written as a product of two free functions $\upsilon(E)$ and $\nu(E)$ such that

$$M(E)\Sigma_s(E \to E') \cong \begin{cases} \upsilon(E)\nu(E'), & E > E' \\ \upsilon(E')\nu(E), & E < E'. \end{cases} \tag{H.7}$$

Then the infinite medium spectrum equation can be written as the coupled set of differential equations

$$\begin{aligned} \Sigma_a(E)\phi(E) &= \frac{dq}{dE} + S(E), \\ \frac{d}{dE}\left[\frac{\phi(E)}{M(E)}\right] &= j(E)q(E) - \frac{d}{dE}\left[k(E)\frac{dq}{dE}\right], \end{aligned} \tag{H.8}$$

where $j(E)$ and $k(E)$ are given in terms of free functions, $\upsilon(E)$ and $\nu(E)$, as

$$\begin{gathered} j(E) = \frac{1}{\nu_1(E)}\frac{d}{dE}\left[\nu(E)k(E)\right], \qquad \nu_1(E) \equiv \int_0^E dE'\nu(E'), \\ k(E) = \left[M(E)\Sigma_s(E)\right]^{-1}. \end{gathered} \tag{H.9}$$

With proper choices of $\upsilon(E)$ and $\nu(E)$ this model will reduce to several other models, including the proton gas model, the heavy gas model, the Fermi age model, and the Greuling-Goertzel model. Hence the secondary model is evidently capable of bracketing the thermalisation properties of the true scattering kernel.